POLITECNICO DI MILANO
School of Engineering - Ingegneria dei Sistemi
Master Degree in Biomedical Engineering

EFFECTS OF AIRWAY OBSTRUCTION ON RESPIRATORY SYSTEM MECHANICS DURING HIGH FREQUENCY JET VENTILATION

Supervisor: Prof. Andrea Aliverti

Co-Supervisors: Ing. Antonella Lo Mauro
M.D., Ph.D. Peter Frykholm
M.D. Robert Leiter

Presented by:
Stefano Gandolfi - 768313

Academic Year 2011 - 2012

A mio padre e mia madre
per il loro continuo e indispensabile supporto.

Contents

Abstract

Mechanical ventilation is a very important tool in many clinical applications, during surgery or in Intensive Care Units (ICUs), therefore the research and the development of new technologies to improve performances is a central point for many researchers. Usually mechanical ventilation is applied by means of positive pressure ventilators, either pressure-, volume- or flow-controlled, creating a close system with the patient throughout an endoscope and a cuff.

These systems have some disadvantages, for example they cannot be employed during either upper airway or vocal cords surgery, since the endoscope does not permit the access of the surgeon's instruments and laser surgery can be performed only if the endoscope's material is compatible with the laser beam. Mainly for these reasons, about forty years ago researchers introduced an alternative mechanical ventilation method called jet ventilation. During jet ventilation, gas is delivered through a thin metallic cannula placed either above or below the glottis. In this way, the surgeon has free access to both airway and vocal cords and there are no problems related to the interaction with a laser beam. Recently, cannulas have been integrated in a metallic endoscope, improving gas transport towards the lungs without impairing the access for the surgeon.

The working principle of jet ventilation is based on Venturi's effect. The cannula is integrated in the endoscope, forming an open system: the high velocity jet is delivered by the cannula in the endoscope where impacts with the larger and relatively immobile mass of gas that is filling the endoscope itself. The kinetic energy of the high velocity jet is transferred to this mass of gas (which can be also a special gas mixture if an external source is present) that is recruited and contributes to increase tidal volume moving towards the lungs.

Jet ventilation can be performed in three modalities:

- High Frequency Jet Ventilation (HFJV) if respiratory rate is greater than 1-2 Hz;
- Low Frequency Jet Ventilation (LFJV) if respiratory rate is similar to the physiological rate (16 bpm);
- Superimposed High Frequency Jet Ventilation (SHFJV) if HFJV and LFJV are

applied together.

Since its debut, many studies have been published reporting that HFJV is equivalent to the conventional mechanical ventilation, and in some applications is even superior, as in case of fistulas or during upper airway surgery. In other cases, like in presence of stenosis or pulmonary over-distension, the characteristics of this technique led researchers to have doubts on its applicability because high end expiratory positive pressures (PEEP) and hyper-inflation may occur due to the short expiration time imposed by the jet ventilator. Moreover, at high ventilation rates, carbon dioxide washout is compromised causing hypercapnic condition.

These problems led to the introduction of SHFJV that, combining the positive effects of the application of HFJV (the PEEP effect) and of LFJV (carbon dioxide removal), would permit to benefit from all the advantages related to the application of jet ventilation.

The main problem of all previous studies on jet ventilation was the difficult measurement of ventilation-related volumes and particularly of the tidal volume (V_T), since, being the jet ventilator-patient an open system, the presence of a pneumotachograph would have affected the Venturi's effect and thus the complete ventilation. Furthermore, practical problems related to the positioning and the correct calibration made impossible these kinds of measurement.

Recently, an innovative technique that measures ventilation through the measurement of the chest-wall displacements has been proposed and validated by many studies, avoiding any interference with both the ventilation system and the mobility of the patient. This technique, called Optoelectronic Plethysmography (OEP) uses CCDs cameras to detect the three-dimensional coordinates of passive markers placed on the patient's chest-wall, properly illuminated by flashing infra-red diodes. Detected keypoints are then interpolated according to a geometrical model in order to obtain a close surface from which, by means of the application of Gauss' theorem, enclosed volume is computed. This volume corresponds to the chest-wall's volume, and its variations represent the tidal volume.

The aim of this thesis is the evaluation of the effects of HFJV and SHFJV in animals characterized by several grades of tracheal stenosis through parameters concerning the respiratory system mechanics, namely operating volumes and volume changes, pressures at different sites, ventilatory parameters and mechanical properties, varying both obstruction grade and ventilation rate..

Experiments took place at the Clinical Physiology Laboratory of the Uppsala University Hospital over a population of ten pigs. The protocol followed for each pig has been chosen in order to allow the randomized application of both ventilation mode

and obstruction grade, always having the same initial conditions in order to confront correctly detected data.

HFJV has been performed at 50, 100, 150, 200, 300, 400 and 600 bpm, and a LF signal at 16 bpm has been superposed to obtain SHFJV. Stent with inner diameter of 2, 4, 6 and 8 mm have been placed in trachea to simulate the obstruction.

Data about three-dimensional displacement of the chest-wall have been detected by means of an OEP system, while flow, upstream pressure and downstream pressure have been measured by analog sensors properly connected to the OEP system in order to get a packet containing all information synchronized. The following data processing represents the central core of this thesis' work, in fact several software have been developed in order to perform semi-automatically all those steps necessary to get numeric results starting from original data, which are labeling, tracking, volume computation and the extraction of the parameters. The need of developing software born because of the huge amount of data, having more than one thousand files to process.

The first part of the data processing refers to labeling and tracking of the tracks detected by the OEP system: developed software permit to rotate the cloud of key-points detected by the OEP according to a known reference system giving a single manually-labelled file as input. Then, geometric considerations are applied in order to identify any single track, classifying it according to pre-determined model and following it for the entire acquisition. During the development of these software, many problems have been taken in count: for example, the presence of outliers, the possible loss of information during the acquisition and the different geometry of the pigs.

This step is necessary to ensure the correct interpolation of the key-point, building the close surface representing the chest-wall of the pig and allowing the computation of the enclosed volume. The need to have a close surface represents a further problem, since only the anterior chest-wall is accessible by the OEP cameras; therefore, another Matlab software has been developed to generate a plain representing the posterior chest-wall surface.

At this point the geometric model, which represents the rules determining the interpolation of the key-point, has been applied: the points are connected forming a surface composed by triangles, whose vertexes are the tracks themselves, and the chest-wall is divided in two compartments, that are the thorax and the abdomen. The last step is thus the application of Gauss' theorem and the computation of the volume enclosed by the close surface described above.

Completing these 3D-data with data coming from analog sensors (pressures and flow), the time-dependent curves related to each data during each phase of the protocol have been obtained. More in detail, information are related to:

- Flow
- Pressure above and below the obstruction
- Volume of Rib Cage, Abdomen and Chest-Wall.

Some parameters have been identified in order to determine the effects of each ventilation mode: end expiratory volume (EEV), tidal volume (V_T), driving pressure (DP) and peak expiratory pressure (PEP). To consider only the steady-state behaviour, these parameters have been evaluated only in the last thirty seconds of each ventilation mode.

A semi-automatic selection of the points corresponding to the end-expirations and end-inspirations has been performed on the pressure and volume curves, and a Matlab software provided the parameters' values for each pig. The following computation of mean values and standard deviation for each parameter over the entire population grouped by ventilation mode and obstruction grade has generated all the results reported in the third chapter of this thesis.

In this study we evaluated also the influence of a tracheal stenosis on the mechanical parameters characterizing the respiratory system, that is Resistance and Compliance, on which frequency response and the general behaviour of the system depend.

The respiratory system, in fact, can be modelled by several models describing its functioning through a set of mechanical or electric components, whose characteristics, for example the frequency response, are well-known and, by assigning proper values, are used to simulate the behaviour of any respiratory system.

Referring to mechanical models, there are several degrees of complexity, starting from single-compartment linear model up to multi-compartmental non-linear model. Some of them are described in the first chapter of this thesis, and in particular the viscoelastic model will be deeply analysed, even if some approximations were necessary because of practical reasons. This model is preferred to the others because its relationship between flow, pressure and volume in not only time-dependent, but depends on their history as well.

Increasing the obstruction grade, also the resistance value should increase, while the compliance should not change. To verify and quantify these variations, flow-, pressure- and volume-data have been considered during conventional mechanical ventilation, since during jet ventilation the pneumotachograph was working in an open system and did not provide any reliable information about the flow.

For each pig the standard CMV breath has been computed, providing all the parameters necessary to compute resistance and compliance. The results, obtained as the mean of the single pigs-related results, show an average resistance of 86.06 cmH_2O with the 2 mm ID stent in place, which is reduced to 0.48 cmH_2O with the 8 mm

ID. The trend of the resistance vs. caliber curve is reflected in all the curves related to downstream parameters (tidal volume and driving pressure), confirming the direct dependence between airway resistance and pulmonary ventilation.

With the most severe obstruction, the lower part of the respiratory system can be considered uncoupled from the upper airways, and consequently HFJV is not able to provide adequate ventilation even at 50 bpm, while during SHFJV the obstruction blocks even a fraction of the LF-related ventilation. Furthermore, in this condition the resistance value has been dramatically increased, causing such a great increase of the physiological expiratory time constant to cause hyper-inflation and inadvertent PEEP effect already at 16 bpm.

Enlarging the tracheal ID, HFJV provides relevant V_T and DP only up to 150 bpm, whereas SHFJV produces much better results that get even better with a further decrease of the obstruction grade, thanks to the LF component-related effects.

The first chapter of this thesis contains an introduction in order to give all the notions to fully understand the carried out work and the obtained results. Thus, initially the mechanical models of the respiratory system are shown, then I will discuss about the effect of the interaction with a mechanical ventilator and the different techniques of mechanical ventilation, with a particular examination of the jet ventilation. In the end I will discuss the methods to measure lung volumes and the need to introduce new technologies as the Optoelectronic Plethysmography.

The second chapter describes the experiment, the instrumentation and the work that was necessary to process data and to compute the results, explaining in detail how the main developed software work. The first part refers to the computation of the more clinical parameters, that is pressures and volumes within the respiratory system, while the second part explains how mechanical parameters have been calculated, characterizing the respiratory system and its behavior from an engineering point of view.

The third chapter reports all obtained results, resumed in graphs with the related detailed description. The results about mechanical parameters are reported in the first pages, on which depend all the following results. Subsequently, in fact, all the results about volume (VT and EEV) and pressure (DP and PEP) during both HFJV and SHFJV for each obstruction grade are reported.

Sommario

La ventilazione meccanica è un aspetto molto importante in molte applicazioni cliniche, sia durante gli interventi chirurgici, sia nelle *Intensive Care Units* (ICUs), pertanto lo sviluppo e lo studio di nuove tecnologie che possano migliorare i risultati è un punto centrale per molti ricercatori. Solitamente la ventilazione meccanica viene applicata utilizzando sistemi a pressione positiva comandati in pressione, volume o flusso che creano un sistema chiuso con il paziente tramite un endoscopio e una cosiddetta *cuff*. Questi sistemi presentano però lo svantaggio di non poter essere utilizzati durante interventi chirurgici alle vie aeree superiori o alle corde vocali, in quanto l'endoscopio ne ostruisce l'accesso, inoltre, la chirurgia laser può essere eseguita solo se è disponibile un endoscopio il cui materiale sia compatibile con il fascio laser.

Per questi motivi circa quaranta anni fa i ricercatori hanno introdotto una modalità di ventilazione meccanica alternativa, chiamata *jet ventilation*. Questa tecnologia prevede l'erogazione del gas tramite una sottile cannula di metallo, che può essere posta sia sopra che sotto la glottide. In questo modo, l'accesso alle vie aeree o alle corde vocali non presenta problemi e l'interazione con il fascio laser non è pericolosa. Recentemente le cannule di emissione del gas sono state integrate in un endoscopio di metallo, migliorando il trasporto del gas verso i polmoni senza compromettere l'accessibilità per il chirurgo.

Il principio di funzionamento della jet ventilation è basato sull'effetto Venturi. La canula di emissione è accorpata nel laringoscopio, formando un *sistema aperto*: il getto di gas ad alta velocità viene emesso dalla canula nel laringoscopio in cui impatta con una massa di gas ferma molto più grande, costituita dall'aria contenuta nel laringoscopio. Per effetto Venturi, l'energia cinetica del getto ad alta velocità viene trasferita all'aria ambiente (o gas se è presente una sorgente esterna), che viene reclutata e concorre ad aumentare il volume corrente che si muove verso i polmoni.

Esistono diverse modalità con cui la jet ventilation è applicata:

- High Frequency Jet Ventilation (HFJV) se la frequenza è maggiore di 1-2 Hz;
- Low Frequency Jet Ventilation (LFJV) se la frequenza è quella fisiologica (16 bpm);

- Superimposed High Frequency Jet Ventilation (SHFJV) quando le due modalità precedenti sono applicate congiuntamente.

Nel corso degli anni sono stati pubblicati molti studi dai quali emerge che la HFJV è equivalente alla convenzionale ventilazione meccanica, e in alcune applicazione cliniche come nel caso di fistole o interventi alle vie aeree superiori è addirittura superiore. In altri casi, invece le caratterstiche di questa tecnologia hanno portato i ricercatori ad esprimere dubbi sulla sua applicabilità, come nel caso di stenosi o di sovradistensibilità polmonare, in quanto ci sarebbe il rischio di elevate pressioni di fine espirazione (PEEP) e di iper-insufflazione dovute ad un tempo di rilassamento fisiologico superiore al tempo di espirazione imposto dal ventilatore. Inoltre, a frequenze molto alte, è stato rilevato che l'eliminazione dell'anidride carbonica si riduce molto portando talvolta a condizioni di ipercapnia.

Questi problemi stanno alla base dell'introduzione della SHFJV, che, combinando gli effetti positivi dell'applicazione della HFJV (effetto PEEP) e della LFJV (rimozione della CO_2), permetterebbe di poter sfruttare tutti i vantaggi della jet ventilation senza dover giungere ad alcun compromesso.

Il problema principale di tutti gli studi effettuati sino ad ora era la diffcoltà di misura dei volumi e soprattutto del volume corrente (V_T), in quanto, essendo un sistema aperto, la presenza di un pneumotacografo o di un flussimetro interferiva con l'effetto Venturi e quindi con il funzionamento dell'apparecchiatura, oltre a presentare problemi di tipo pratico come la corretta calibrazione e il posizionamento.

Recentemente è stata proposta e validata da numerosi studi una tecnologia innovativa che permette di misurare la ventilazione mediante misure riguardanti gli spostamenti della parete toraco-addominale, in modo da non interferire nè con il sistema di ventilazione, nè con la mobilità del soggetto. Questa tecnica, nota come Pletismografia Optoelettronica (OEP) rileva tramite delle telecamere CCDs le coordinate tridimensionali di marker passivi posti sulla parete toraco-addominale del soggetto, opportunamente illuminati tramite flash luminosi emessi da corone di LED operanti nell'infrarosso. I punti rilevati vengono poi interpolati secondo un apposito modello geometrico, ottenendo così una superficie chiusa che, tramite l'applicazione del teorema della divergenza o di Gauss, permette il calcolo del volume racchiuso dalla superficie stessa, corrispondente al volume toraco-addominale del soggetto, le cui variazioni corrispondono al volume corrente respiratorio.

Lo scopo di questa tesi è la valutazione degli effetti della ventilazione tramite HFJV e SHFJV in animali caratterizzati da diversi gradi di stenosi tracheale tramite parametri ventilatori e relativi alla meccanica respiratoria come il volume polmonare e le sue variazioni, le pressioni in diversi punti e le propietà meccaniche al variare sia dell'ostruzione

sia della frequenza di ventilazione.

Gli esperimenti sono stati effettuati su una popolazione di dieci maiali presso il Laboratorio di Fisiologia Clinica dell'Uppsala University Hospital. Per ogni maiale è stato seguito un protocollo che consentisse l'applicazione randomizzata sia della modalità di ventilazione, sia del grado di ostruzione, consentendo però anche di avere condizioni iniziali comuni che permettessero di confrontare correttamente i dati raccolti.

La HFJV è stata applicata a 50, 100, 150, 200, 300, 400 e 600 bpm, a cui è stato sovrapposto un segnale LF a 16 bpm per ottenere la SHFJV. Le ostruzioni artificiali impiantate in trachea sono state scelte in modo da lasciare un lume di 2, 4, 6 e 8 mm.

I dati relativi ai movimenti tridimensionali della parete toraco-addominale sono stati rilevati tramite un sistema OEP, mentre i dati relativi al flusso e alle pressioni a monte e a valle dell'ostruzione sono stati raccolti tramite sensori analogici opportunamente interfacciati con il sistema OEP, in modo che esso integrasse tutti i diversi segnali in un unico pacchetto contente tutte le informazioni.

La successiva elaborazione dei dati rappresenta la parte centrale del lavoro di tesi, in quanto sono stati sviluppati diversi software che eseguissero in modo semi-automatico tutti i passi necessari per ottenere dei risultati numerici partendo dai dati grezzi: state quindi implementate le funzioni di labeling, tracking, computazione dei volumi e estrazione dei parametri. La necessità di sviluppare dei software è nata per via della enorme mole di dati a disposizione, basti pensare che il numero di file grezzi superava il migliaio.

La prima parte del lavoro riguarda la fase di *labeling* e di *tracking* delle tracce rilevate tramite il sistema OEP, per la quale è stata sviluppata una serie di software in Matlab che permettessero, a partire da un file etichettato manualmente, di ruotare la nuvola di punti rilevata dal sistema OEP secondo un sistema di riferimento noto per poi applicare una serie di considerazioni geometriche che permettessero di identificare univocamente ciascuna traccia e *inseguirla* per tutta la durata dell'acquisizione, classificandola secondo un ordinamento predeterminato. Durante lo sviluppo di questi software si è dovuto tenere conto di diverse problematiche, quali la possibile presenza di outliers, la possibile perdita di informazioni relative a qualche traccia utile e la diversa geometria dei maiali in esame.

Questo primo step è necessario per assicurare una corretta interpolazione dei punti, processo che ha come obiettivo la costruzione della superficie chiusa entro la quale si vuole calcolare il volume racchiuso. Proprio il bisogno di avere una superficie chiusa rappresenta un'ulteriore problematica, in quanto solo la parte anteriore della parete toraco-addominale del maiale è visibile dalle telecamere; per cui, tramite un software Matlab si è generato un piano fittizio che rappresentasse la parte posteriore del maiale.

A questo punto è stato applicato il modello geometrico, ovvero l'insieme delle regole con cui viene implementata l'interpolazione: i punti vengono connessi formando una superficie composta da triangoli, i cui vertici sono rappresentati dalle tracce stesse, e la parete toraco-addominale viene suddivisa in due compartimenti, ossia il torace e l'addome. L'ultimo step è appunto l'applicazione del teorema di Gauss e la conseguente computazione del volume racchiuso dalla sopradescritta superficie.

Integrando questi dati tridimensionali con i dati proveniente dalla sensoristica analogica (pressione e flusso), si ottengono le curve tempo-varianti relative a ciascun dato durante ciascuna fase del protocollo. Più precisamente, si avranno informazioni relative a:

- flusso
- pressione a monte e a valle dell'ostruzione
- volume addominale, toracico e complessivo.

Per determinare gli effetti di ciascuna modalità di ventilazione, sono stati individuati alcuni parametri quali il volume di fine espirazione (EEV), il volume corrente (V_T), la driving pressure (DP) e la pressione di picco espiratoria (PEP), che sono stati valutati considerando solo gli ultimi trenta secondi di ogni modalità di ventilazione, in modo da considerare solo il comportamento a regime e non i transitori.

Selezionando semi-automaticamente i punti corrispondenti a fine inspirazione e fine espirazione dai tracciati di volume e pressione si ottengono tutte i dati necessari per il calcolo dei parametri appena elencati relativi ad ogni maiale, e calcolando media e deviazione standard di ciascun parametro sulla popolazione divisa in gruppi omogenei per modalità di ventilazione e grado di ostruzione, si ottengono i risultati presentati nel terzo capitolo di questa tesi.

In questo studio è stata valutata anche l'influenza di una stenosi tracheale sui parametri meccanici che caratterizzano il sistema respiratorio, ossia Resistenza e Compliance, dai quale dipendono risposta in frequenza e comportamento del sistema respiratorio stesso.

Il sistema respiratorio, infatti, può essere modellizzato tramite diversi modelli che ne descrivono il funzionamento attraverso un insieme di componenti elettrici o meccanici, dei quali sono note tutte le caratteristiche come per esempio la risposta in frequenza e che, assumendo opportuni valori, simulano il comportamento di qualsiasi sistema respiratorio.

Riferendosi ai modelli meccanici, esistono modellizzazioni di diversa complessità, a partire dai modelli lineari a singolo compartimento, fino ad arrivare a quelli non lineari

a più compartimenti. Alcuni di questi sono descritti nel primo capitolo di questa tesi, e più precisamente ci si riferirà al modello viscoelastico, sebbene con qualche approssimazione dovuta a motivi pratici. Questo modello è preferito agli altri poichè la relazione tra flusso, pressione e volume è dipendente non solo dal tempo, ma anche dalla loro storia.

Aumentando il grado di stenosi tracheale, ci si aspetta un conseguente aumento di resistenza, mentre la compliance dovrebbe rimanere costante. Per verificare e quantificare queste variazioni, si sono presi in considerazione i dati di flusso, pressione e volume durante la ventilazione convenzionale, dato che ovviamente durante la jet ventilation non si ha nessuna informazione relativa al flusso, essendo un sistema aperto.

Per ogni maiale è stato calcolato un respiro standard dovuto alla ventilazione convenzionale e da esso sono stati estratti tutti i parametri necessari per il calcolo di resistenza e compliance. I risultati, ottenuti mediando i risultati ottenuti sui singoli maiali, evidenziano una resistenza media di 86.06 cmH_2O nel caso di lume tracheale ridotto a 2 mm, che si riduce a 0.48 cmH_2O quando il calibro della trachea è 8 mm.

Il trend della curva di resistenza in funzione del calibro viene riprodotta in tutte le curve relative ai parametri a valle della resistenza (tidal volume e driving pressure), confermando la diretta dipendenza tra resistenza delle vie aeree e ventilazione polmonare.

Nel caso di ostruzione più grave, la parte inferiore del sistema respiratorio può essere considerata disaccoppiata dalle vie aeree, infatti la HFJV non riesce a ventilare adequatamente nemmeno a 50 bpm, mentre durante la SHFJV anche una parte della componente a bassa frequenza è bloccata dall'ostruzione. Inoltre in questa condizione il grande valore di resistenza causa un aumento della costante di tempo espiratoria fisiologica del sistema respiratorio tale che anche solo la componente a 16 bpm possa causare iper-insufflazione e PEEP troppo elevate.

Aumentando il lume tracheale, la HFJV produce un V_T e una DP rilevanti solo fino a 150 bpm, mentre la SHFJV dà risultati molto migliori e che migliorano col diminuire del grado di ostruzione, grazie agli effetti della componente a bassa frequenza.

Il primo capitolo di questa tesi vuole essere un'introduzione che dia tutti gli elementi necessari per capire pienamente il lavoro svolto e i riusultati ottenuti. Verngono quindi illustrati i modelli meccanici del sistema respiratorio, gli effetti dell'interazione con un ventilatore meccanico e i diversi tipi di ventilatori meccanici, con un occhio particolare ovviamente alla jet ventilation e alle sue modalità. Alla fine si parla dei sistemi di misura dei volumi polmonari, della necessità di introdurre nuove tecnologie e quindi della Pletismografia Optoelettronica.

Il secondo capitolo descrive l'esperimento effettuato, la strumentazione utilizzata e

tutto il lavoro che è stato necessario per l'elaborazione dei dati e il calcolo dei risultati, spiegando nel dettaglio il funzionamento dei principali software sviluppati tramite la piattaforma Matlab. La prima parte si riferisce al calcolo dei parametri più *clinici*, ovvero le pressioni e volumi all'interno del sistema respiratorio, mentre la seconda parte spiega como sono stati calcolati i parametri meccanici del sistema respiratorio stesso, i quali descivono il comportamento del sistema da un punto di vista modellistico-ingegneristico.

Il terzo capitolo presenta tutti i risultati ottenuti, riassunti in grafici, con la relativa discussione dettagliata. Nelle prime pagine si tratteranno i risultati relativi ai parametri meccanici, da cui dipendono tutti i risultati presentati in seguito, in quanto caratterizzano la popolazione esaminata. Successivamente vengono illustrati i risultati relativi ai volumi (V_T e EEV) e alle pressioni (DP e PEP), durante HFJV e SHFJV e per ogni grado di ostruzione.

Chapter 1

Introduction

The purpose of this chapter is just to introduce to the main topic of this thesis, therefore the reader can refer to the bibliography in order to find a further description of the covered arguments.

1.1 Basics of the respiratory system

The respiratory system has three vital functions: activate the ventilation pump, transport gases in the airways and ensure the gas exchange. Its basic structures can be divided basing on their functions into two different parts: the airways, which transport gases from the openings to the lungs, and the lungs, in which the gas exchange takes place [1].

The airways are composed by the airways openings (nose and mouth), paranasal sinuses, pharynx, larynx, trachea and bronchi [2]; then the bronchial tree continues branching in the lungs until reaching the level of terminal bronchioles that lead to alveolar sacs, in which clusters of alveoli form the spongy structure of the lungs.

The air (or the gases) flows into these structures to get the lungs and the alveoli during the inspiration, and in the opposite direction during the expiration.

Alveoli are wrapped in blood vessels allowing gas exchange due to concentration gradients and diffusion phenomena. It is here that carbon dioxide is released by the bloodstream to the atmosphere and the oxygen in absorbed by the bloodstream. Since gas exchange takes place at the end of the brachial tree, the involved surface is very large (140 m^2 in adult) and the diffusion path is very short ($0.6 \cdot 10^{-3}$mm) [3].

It is now evident that is necessary a force to create the gas flow in the airways. This force, applied as a pressure difference, is provided by other structures: the respiratory muscles of the ribcage and the diaphragm, which is the main respiratory muscle and is situated in the abdomen. The coupling between lungs, diaphragm and rib cage is

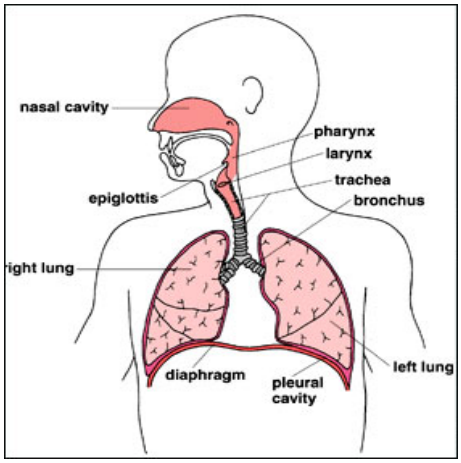

Figure 1.1: Representation of the respiratory system

ensured by the pleura, which is a membrane composed by two layers separated by a thin pleural cavity: the inner layer covers the lungs, the outer layer is attached on the chest wall. In this way, when respiratory muscles are activated for the inspiration, the chest wall gets bigger and lungs follow the chest wall movements due to the pleural coupling, leading to a negative lung pressure and to a consequent air flow towards the lungs. When inspiration and the action of respiratory muscles end, the rib cage collapses to reach the equilibrium position and the gases flow in the opposite direction. It is important to note that in normal conditions, the expiration is due to the elastic recoil of the respiratory system and not to the action of any muscle.

1.1.1 Definition of Lung Volumes

In order to describe the mechanical status of the respiratory system, the most commonly used indices are the absolute volumes and changes of volume of the gas space in the lungs achieved during various breathing manoeuvres, as showed in the Figure 1.2 [4].

Absolute Volumes:

TLC: Total lung capacity, it is the largest volume to which subject's lungs can be voluntarily expanded;

RV: Reserve Volume, is the smallest lung volume that the subject can reach by voluntary expiration;

FRC: Functional Residual Capacity, is the volume of the gas space after a normal expiration.

Volumes Changes:

VT: Tidal Volume, is the peak-to-peak volume change during a normal breath;

VC: Vital Capacity, is the change in the lung volume between the maximum voluntary inspiration and the maximum voluntary expiration. Also defined as VC=TLC-RV.

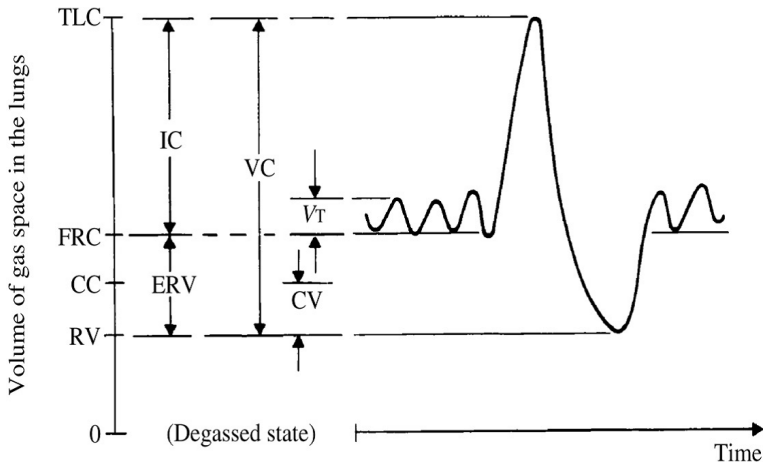

Figure 1.2: Representation of the volume of gas space in the lungs, with its indices. From Webster [4]

ERV: Expiration Reserve Volume, is the difference between the lung volume after a normal expiration and a forced expiration. *ERV=FRC-RV*.

IC: Inspiratory Capacity, is the difference between the lung volume after a normal expiration and after a forced inspiration. *IC=TLC-FRC*.

1.1.2 Mechanical Models of the Respiratory System

In addressing the question of how to model the lung mechanics in the simplest possible terms, the lung can be viewed as a balloon sealed over the end of a pipe. This model has both an anatomical analogy with the real lung, the pipe representing the airways and the balloon the parenchymal tissue, either a functional analogy, being the balloon inflated and deflated through the pipe in the same way that a lung inspires and expires.

As figure 1.3 shows, the alveolar compartment consists of a pair of telescoping canisters connected to each other by a spring which becomes stretched as the compartment volume (V) increases. The tension generated in the stretched spring produces an elastic pressure (P_{el}) inside the compartment that depends on the *elastance* of the spring itself. P_{el} is what makes the compartment return to its original volume when the inflating pressure is removed. This mimics the passive expiration that occurs in a lung when the respiratory muscles relax at the end of an inspiration. Some lungs are more easily inflated than others, so by choosing the appropriate stiffness for the spring, the model can be made to represent a particular lung.

A single conduit connects the compartment of the model to the outside world, taking a certain pressure (ΔP) to drive a given flow of gas through this conduit, in the same way that pressure is required to drive flow through the pulmonary airways. In other words, the conduit has a certain *resistance* to flow. This resistance is large

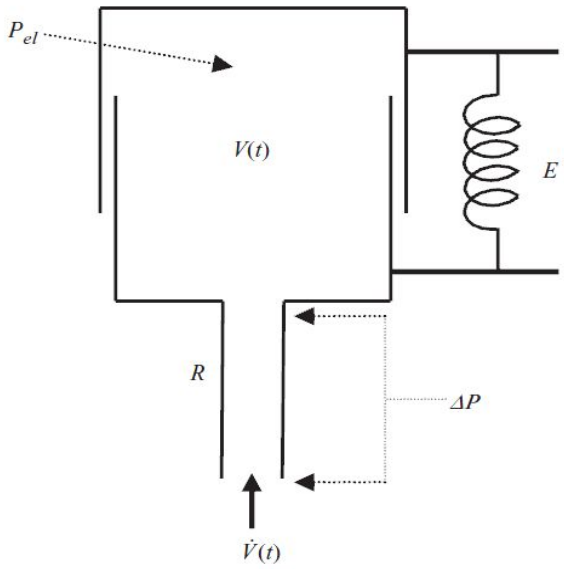

Figure 1.3: The single-compartment linear model of the lung.

(i.e. it takes a lot of pressure to produce a small flow) if the conduit is long and narrow, and small if the conduit is short and wide. By choosing the dimensions of the conduit appropriately, it can be given a resistance similar to that of any particular set of pulmonary airways.

This model is thus characterized by three variables (pressure P, volume V and flow $\dot{V}$) and two mechanical parameters (elastance E and resistance R), composing the *equation of motion*:

$$P = P_{el} + \Delta P = EV + R\dot{V} \tag{1.1}$$

The representation in Figure 1.3 has the advantage of being readily expandable to incorporate more detailed descriptions of lung tissue and its mechanical parameters: in fact the first description may suggest that the only resistive component of the lung comes from the airways (R_{aw}), but the real parenchyma dissipates energy when is stretched, thus also a lung tissue-related resistive term (R_t) should be taken in count in the model. To represent R_t we merely need to add a resistive element known as a *dashpot* between the two horizontal moving components of the alveolar compartment (figure 1.4), and to express the resistance R of the equation 1.1 as:

$$R = R_t + R_{aw} \tag{1.2}$$

One of the problems related to the simplicity of this model is that the rate of change of lung volume is equal at all times to the flow of gas entering the mouth, and this is not true because of the non-linearity of R and E. Moreover, a second order term

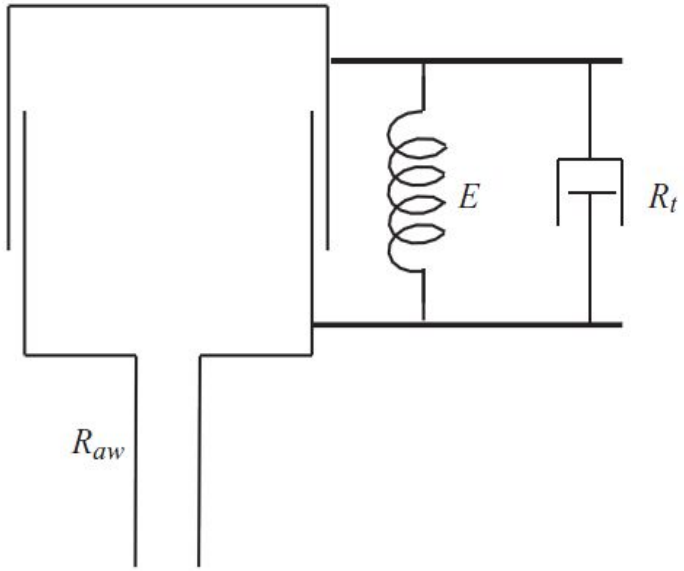

Figure 1.4: The single-compartment linear model of the lung, showing the subdivision of resistance into its two components, R_{aw} and R_t.

representing the inertance I should appear in the equation of motion, but it can be considered negligible:

$$P = P_{el} + \Delta P = EV + R\dot{V} + I\ddot{V} \simeq EV + R\dot{V} \tag{1.3}$$

Further models have been implemented in order to solve these and other problems, and their description can be found in Bates' work [5]. One of these models is important in order to introduce one of the main topics of this thesis, therefore it is described below.

In the *viscoelastic model* (figure 1.5), the relationship between P, V and $\dot{V}$ is not only dependent on time as in the non-linear models, but also on their history, modeling the viscoelasticity of the lung tissue.

The single conduit of the viscoelastic model represents the entire conducting airway tree and therefore has resistance R_{aw}. The mechanical properties of the tissues, however, are now represented by three elements: a resistor (known as a dashpot) and two springs. The three elements R_t, E_1 and E_2 together constitute what is known as a Kelvin body. The stiffness of the spring E_1 represents the static elastic behavior of the lung, while the series combination of R_t and E_2 (which together constitute a Maxwell body) account for its viscoelastic behavior.

This model explains easily two features of the real lung.

The first one in the *frequency dependence*: if lung volume is oscillated sinusoidally and the resulting P(t) and $\dot{V}(t)$ signals measured at the airway opening are fit to the single-compartment model, one obtains values of R and E that depend on the

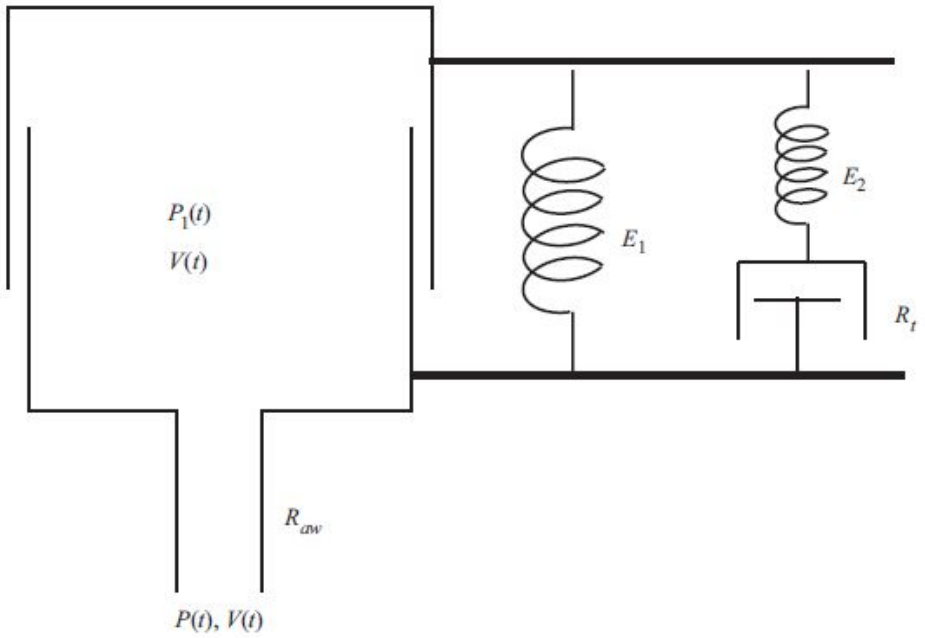

Figure 1.5: The viscoelastic model of the lung.

frequency of oscillation. In particular, R decreases monotonically with frequency while E increases. The mechanism by which frequency dependence occurs is most easily seen with respect to the viscoelastic model. When flow oscillates into the alveolar compartment of this model very slowly, the dashpot R_t is given sufficient time to move under the influence of E_2. That is, as soon as E_2 becomes stretched by even a little bit, it exerts a force on R_t, which then slides toward the force in order to eliminate it.

Consequently, the elastic behavior of the system is determined almost entirely by E_1, which always follows the alveolar volume changes precisely. By the same token, the system dissipates energy through R_t, so the tissues exhibit resistance. Conversely, when alveolar volume changes occur at a high frequency, the dashpot is given little time to slide in response to any tension in E_2 before the tension reverses direction. Consequently, the spring E_2 is forced to follow the alveolar volume changes, so the elastic properties of the system are given by the sum of both E_1 and E_2, with minimal dissipation occurring in R_t. As frequency increases, the apparent tissue resistance proceeds toward zero.

The second one is the *stress adaptation*, which is observed experimentally as a transient change in pressure at the airway opening following sudden interruption of flow leaving or entering the lungs: when the flow is interrupted, the initial pressure drop (ΔP_{init}) reflects the immediate obliteration of the resistive pressure drop along the airways, while ΔP_{dif} is due to the phenomenon known as *stress relaxation* related to gas redistribution (figure 1.6). Known the inspiratory flow, it is possible to compute

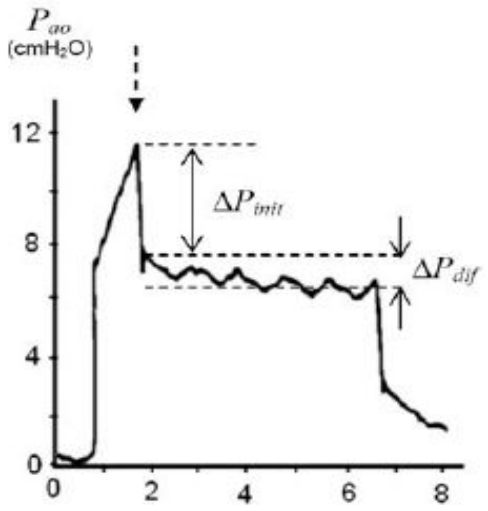

Figure 1.6: Example of stress relaxation in airway opening pressure measured in a human subject following a sudden interruption of inspiratory flow. The vertical dashed arrows indicate the instants of flow interruption.

R_{aw} and R_t (eq. 1.2) by measuring this pressure drop and applying the following equations:

$$R_{aw} = \frac{\Delta P_{init}}{\dot{V}_{insp}} \tag{1.4}$$

$$R_t = \frac{\Delta P_{dif}}{\dot{V}_{insp}} \tag{1.5}$$

The *compliance*, which is the inverse of the elastance and thus non-linear, is computed dividing the tidal volume by the pressure drop due to the expiration:

$$C = \frac{1}{E} = \frac{1}{E_1} + \frac{1}{E_2} = \frac{V_T}{\Delta P_{exp}} \tag{1.6}$$

These mechanical parameters determine the frequency response of the system, defining the physiological relaxation time constant τ as:

$$\tau = RC \tag{1.7}$$

Thus, the changes in lung volume at time t during an inspiration or an expiration can be expressed as:

$$V(t) = V_0(1 - e^{\frac{-t}{\tau}}) \tag{1.8a}$$

$$V(t) = V_0 e^{\frac{-t}{\tau}} \tag{1.8b}$$

Reaching the steady-state volume after $\simeq 3.5\ \tau$.

Finally, calculating C at different pressures and volumes, the P-V curve is obtained. This can be performed throughout several techniques, and the resulting curve shows the non-linearity of the compliance.

1.1.3 Pressure-Volume Curve

The relationship between pressure and volume, representing the compliance, is described by the pressure-volume (P-V) curve. This curve can be obtained during short periods of apnoea (static curve) or during very slow flow ventilation (dynamic curve), throughout three different techniques [6]:

In the *interrupted-flow technique*, the patient is inflated by regular intermittent steps, with short (2-3 seconds long) pauses. Usually, when airways pressure reaches 40 mmH_2O [7], the inflation is stopped and the deflation is performed in the same way. By plotting acquired pressure and volume for each step, the P-V curve is drawn. It is evident that in this case the equation of motion (equation (1.1)) changes, because the terms including flow and inertance are eliminated, therefore the relationship between pressure and volume depends only on the compliance.

In the *constant slow-flow method* the ventilation is performed using the flow as the control variable. This method is very simple and faster than the first method and allows to keep connected the patient to the ventilator, but the hysteresis increases because of the oxygen consumption, and the measurement during deflation is possible only in presence of a special system that limit the expiratory flow to a constant value. Moreover, since data are acquired in dynamic conditions, the equation of motion suffers of the presence of the flow-related term; therefore the compliance will be determined with an intrinsic error, which can be minimized by lowering the delivered flow.

The third option to get P-V data is the *multiple-occlusion method*, which consists in periodically interrupting the tidal breathing at different lung volumes to obtain each P-V point, but this technique imply the sedation or the paralysis to prevent any spontaneous breath during the measurement [8].

1.1.4 Positive End-Expiratory Pressure

As it is possible to notice from the Figure 1.7, the relationship between pressure and volume is not linear, but its slope changes within the entire range. The curve can be linearised in several tracts, and the central tract is the one with the highest slope; this means that in this region a small change in pressure causes a big change in volume, thus the value of compliance is maximum. In order to move the working point to a more compliant region, during mechanical ventilation the chosen baseline vari-

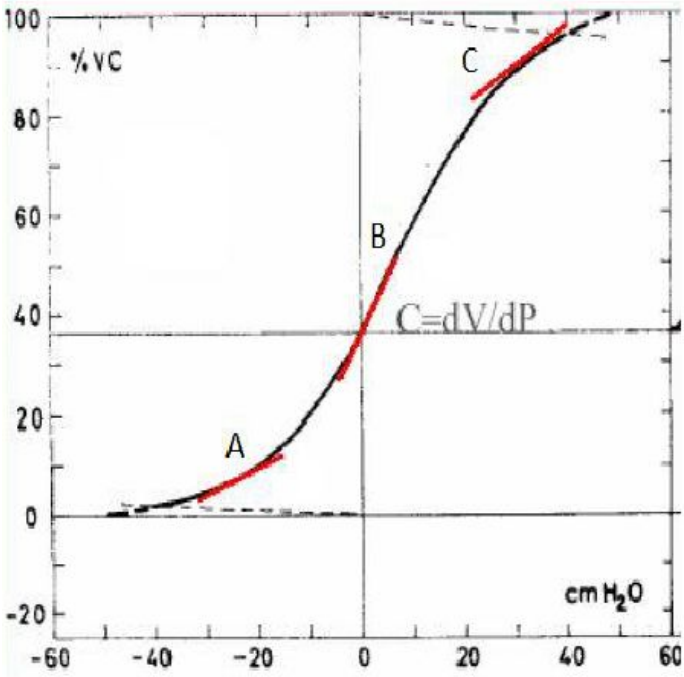

Figure 1.7: P-V curve. The three red segments represent the linearization in three different working points; the slope of the compliance is maximized in B.

able is a Positive End Expiratory Pressure (PEEP), that is the airways openings are maintained above atmospheric pressure. In this way the pressure needed to achieve a correct inflation is not so high and the risk of problems related to high pressures like barotrauma decreases [9]. In fact, it has been demonstrated that the application of PEEP in anaesthetized or paralysed patient produces an increase of End Expiratory Lung Volume (EELV) and upward displacement of respiratory system in the P-V relationship, preventing or reversing the closure of peripheral airways.

Furthermore, several studies demonstrated that application of PEEP in patient with acute reduction of lung volume due e.g. to oedema can improve arterial oxygenation by increasing functional residual capacity (FRC), stabilizing alveoli with low critical closing pressure and improving the matching of ventilation and perfusion.

A recent study [10] has demonstrated that in intensive care units (ICUs) the ventilation is performed with a mean PEEP of 5,6 cmH_2O in about 66% of the patients, and this value does not change significantly between different countries.

1.2 Introduction on Mechanical Ventilation

There are situations in which respiratory muscles are unable to do the work required for breathing, for example because of pathologies or unusual conditions like anaesthesia. In these cases mechanical ventilators can help the person to breath, allowing enough

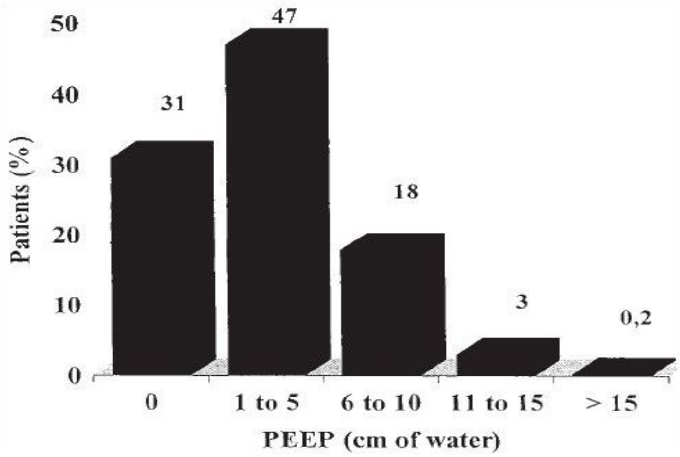

Figure 1.8: Percentage of ventilated patient with the respective used PEEP level. From [10]

minute ventilation, in order to clear the dead space and providing fresh air to the alveoli at the correct breathing rate, therefore maintaining an adequate gas exchange between alveoli and vessels. For this reason, mechanical ventilation was introduced more than three centuries ago, and it had an extraordinary development during the 1950's decade. Chatburn [11] defines the mechanical ventilator as "an automatic machine designed to provide all or part of the work required to move gas into and out of the lungs to satisfy the body's respiratory needs".

The necessary level of ventilation is monitored throughout the CO_2 concentration in the blood. For a given level of carbon dioxide produced by the body, the amount in the blood is inversely proportional to the level of ventilation [12].

By analysing the mechanics of breathing, it is possible to understand how mechanical ventilation affects the function of breathing and how ventilation can be controlled.

1.2.1 Basic Working Principle of Mechanical Ventilators

As already mentioned, the working principle of the respiratory system is based on variations of the internal lung pressure created by movements of the chest wall, which create an air flow through the airways.

It is easy to understand that, if the pressure at the airway openings (nose and mouth) is increased and the pressure on the body surface remains constant at the atmospheric, the chest wall would expand and the air is forced into the lungs [13].

On the other hand, if the pressure at the airway openings is kept constant at the atmospheric and the pressure on the body surface is decreased, there is a difference between the two pressures and the result is the same. These are the basic concepts of the Positive Pressure Ventilators and Negative Pressure Ventilators, respectively.

In both cases, the devices are designed in order to have a Positive End Expira-

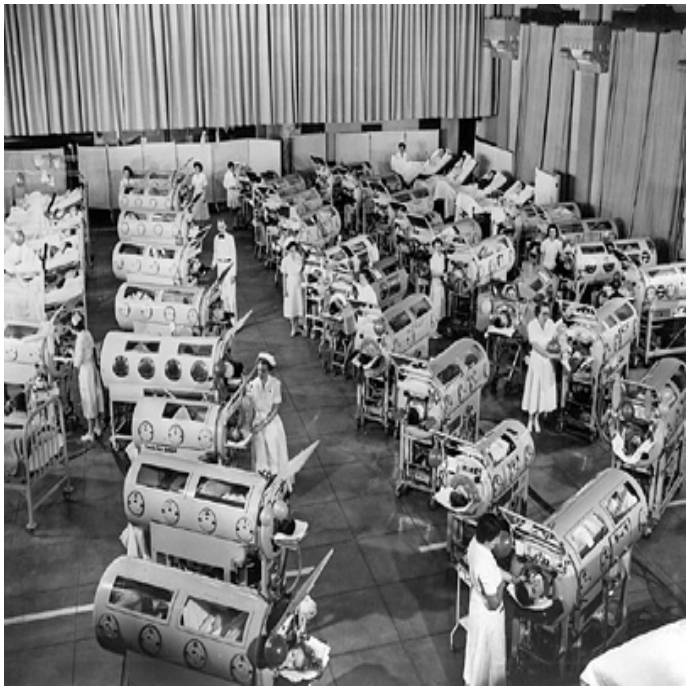

Figure 1.9: Hospital room with Negative Pressure Mechanical Ventilators. The dimension of these devices and the problems related to the limitation of mobility for the patient caused the success of the Positive Pressure Mechanical Ventilators.

tory Pressure (PEEP) in the lungs, which yields to reduce the work of breathing and improves the patient-ventilator interaction.

Considering what is written above, we can conclude that a simple pump activated by an operator and connected to the mouth of the patient can be classified as a mechanical ventilator. Chatburn [13] defines a mechanical ventilator as an automatic device that requires:

- a stable attachment of the device to the patient;
- a source of energy to drive the device;
- a control system to regulate the timing and size of breaths;
- a means of monitoring the performance of the device and the conditions if the patient.

1.2.2 Patient-Ventilator Interaction

It is now easy to understand that the use of a mechanical ventilator affects the equation of motion (1.1); the work originally required to the respiratory muscles in order to overcome resistance and elastic recoil allowing the inspiration (eq. 1.9) is partially or

totally performed by the ventilator:

$$P = P_{mus} = \Delta P + P_{el} \tag{1.9}$$

becomes:

$$P = P_{mus} + P_{vent} = \Delta P + P_{el} \tag{1.10}$$

by defining P_{vent} as the pressure applied by the ventilator.

1.2.3 Classification of Mechanical Ventilators

Having defined a mechanical ventilator, the new Chatburn's goal was to classify the different kinds of ventilators. For this reason he defined the requirements for a complete mode description, resumed in a three-level mode specification, ordered by increasing detail [11]. These three levels are:

1. Description of the breathing sequence and control variables within breaths;
2. The control type used within and between breaths;
3. The adjunctive control algorithms.

This 3-level classification is reported in the following list and explained in the next paragraphs.

1. Breathing Pattern
   (a) Primary Breath-Control Variable
      i. Volume;
      ii. Pressure;
      iii. Dual;
   (b) Breath Sequence:
      i. Continuous mandatory ventilation (CMV);
      ii. Intermittent mandatory ventilation (IMV);
      iii. Continuous spontaneous ventilation (CSV);
2. Control Type:
   (a) Tactical control (within breaths):
      i. Set point;
      ii. Auto-set-point

iii. Servo

(b) Strategic control (between breaths)

i. Adaptive

ii. Optimal

(c) Intelligent Control (Between patients)

i. Knowledge-based

ii. Artificial Neural Network

3. Operational Algorithm

(a) Phase Variables

i. Trigger

ii. Limit

iii. Cycle

iv. Baseline

(b) Conditional Variables

(c) Computational Logic

1.2.3.1 Breathing Pattern

(a) Control Variable

As we could see in the paragraph 1.1.1 the equation of motion (1.1) is expressed by three time-related variables, which are pressure, volume and flow. So, if one of these three variables is predetermined, it becomes an independent variable and can be used as control variable, since the other two will be dependent variables. The control variable, as specified in Chatburn's [11], is the variable used by the ventilator as a feedback signal to control inspiration. Depending on the chosen control variable, the ventilator can be pressure, volume or flow controlled. For example, in a pressure-controlled ventilator, pressure is the independent variable and volume and flow depend on the shape of the pressure waveform. In order to understand which one is the controlled variable, it is possible do connect the ventilator to different loads and look to the output waveforms. If the peak of the inspiratory pressure remains constant among the experiences, the control variable is pressure. If the peak pressure changes and the tidal volume remains constant, the control variable is volume. It is now easy to notice that volume control implies flow control and vice-versa, thus to distinguish which one is used as control variable, we have to look for the variable used as a feedback signal.

Traditionally, ventilators are controlled by a single control variable, but there are recent ventilators that use *dual control*, that is they can switch from volume to pressure or vice-versa during a single expiration.

Finally, it is possible to define a fourth control variable, the time, used in newer ventilation modes such as Jet Ventilation. In this case, it is possible to set only the inspiratory to expiratory ratio (I:E), and it is not possible to control any other variable.

(b) Breath Sequence

Defining a breath in which time and size are controlled by the ventilator (that is the breaths are cycled and triggered by the machine) as a mandatory breath and a breath in which time and size are controlled by the patient as a spontaneous breath, Chatburn stated that there are three possible breath sequences: Continuous Mandatory Ventilation (CMV) in which all breaths are mandatory and the spontaneous breaths are not permitted, Intermittent Mandatory Ventilation (IMV) in which spontaneous breaths are permitted between mandatory breaths, and Continuous Spontaneous Ventilation (CSV). The main difference between these two modes is that, in CMV, the clinical intent is to make every inspiration a mandatory breath, thus the assisted-inspiration is triggered even if the patient makes an inspiratory effort. Therefore, if the operator decreases the ventilation rate, the level of ventilation support is unaffected; in IMV the level of ventilation support depends directly on the rate settings, so a spontaneous breath is not assisted as a mandatory breath.

1.2.3.2 Control Type

Microprocessor-based control is under a continuous development, because of its countless fields of application and because the required level of control is growing as much as the technologies are. The bibliography about control engineering is very wide and detailed, but does not concern the aim of this study; therefore, in this section there is just a brief description of the listed control modes.

A control system is basically composed by three parts: the *process* represents the component whose output has to be controlled; the *actuator* is the device that influences the controlled variable; the *controller* is the component that controls the actuator, by computing the control signal [14].

The first basic distinction has to be done between open-loop and close-loop control system [15]:

In an *open-loop system* (Figure 1.10) the output signal is not fed back to the controller, so there is a lack of compensation for disturbances in the system and the performance of the system depends on the accuracy with which the mathematical model

Figure 1.10: Open-loop ventilatory system

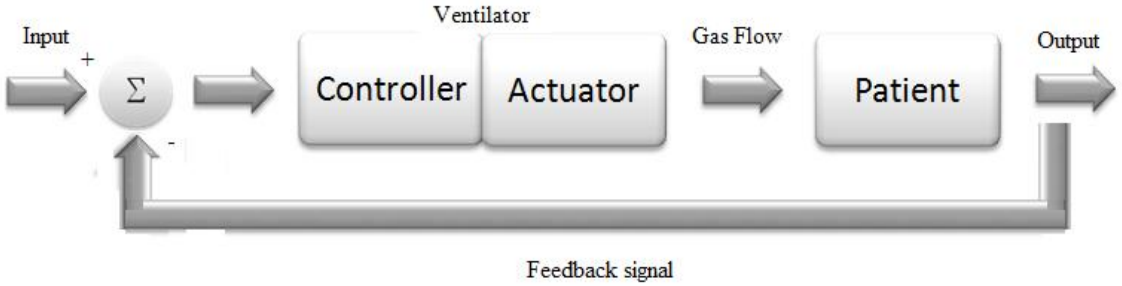

Figure 1.11: Close-loop ventilatory system

describes the process. An example of these systems is the jet ventilator, in which the operator can set just the driving pressure, the frequency and the inspiratory to expiratory ratio. The delivered pressure and volume depend on the breath by breath change in the mechanical load on the respiratory system.

In a *close-loop system* (Figure 1.11) the output signal is detected by a sensor and fed back to the controller; in this way it is possible to lower the sensitivity to disturbances and compute an output minimizes the difference between the new measured output signal and the input signal (which usually is the desired signal). The control types listed by Chatburn take in count this kind of systems.

(a) Tactical Control

At the most basic level there is the tactical control, which is focused on what happens within a breath, and the operator need to set static set-points (pressure limits, tidal volume).

In *Set-point control* the system's output follows a constant input, which can be a pressure or a flow limit and is set by the operator.

Auto-set-point control is the evolution of set-point control, the operator sets the control variable's priority, and the machine decides breath by breath which control variable will be used.

In *Servo control*, the ventilator follows a varying input, for example the patient's own flow pattern.

(b) Strategic Control

The next level is represented by the strategic control, in which the ventilator takes over some of the settings previously managed by the operator. Moreover, in strategic control set-points are dynamic and adjusted over the course of many breaths, thus taking effect on several breaths and not at the level of the single breath.

In *Adaptive control* one set-point (e.g. pressure limit) in automatically adjusted over several breaths by the ventilator to match another set-point (e.g. tidal volume) as the patient's conditions change.

In *Optimal control* the ventilator adjusts the value of set-points to optimize other variables as patient needs change. It is called 'optimal' because is based on mathematical models that maximize or minimize some system performance [16].

(c) Intelligent Control

Intelligent control is the highest level of control systems and they allow not only to have dynamic set-points, but also dynamic models (different for each patient) of desired performances, learning to their own experience to improve the performances.

Knowledge-based control uses the experience of human expert, whereas *Neural network control* is based on complex relations between input and output and on the ability of neural networks to learn basing on its own experience [17].

1.2.3.3 Operational Algorithms

Increasing more the level of detail, the mode description must describe the explicit instructions used by the control system to generate the breathing pattern, that is the phase variables, conditional variables and computational logic.

(a) Phase Variables

Phase variables are those variables important to define the four phases of the respiratory cycle, that is the change from expiration to inspiration, the inspiration, the change from inspiration to expiration and the expiration. These phase variables are used to synchronize the preset output values in the different phases of the respiratory cycle (previously defined) with the patient's real respiratory cycle, and are:

i. Trigger Variable: at the start of inspiration one of the variables associated with the equation of motion reaches a pre-set value and triggers inspiration. It can be pressure, volume or flow. If for example it is pressure, the patient's inspiratory effort causes a drop in the baseline pressure which is sensed by the ventilator.

ii. Limit Variable: during inspiration a upper bound level of a variable (e.g. pressure) is set in order to restrict its magnitude and avoid problems (e.g. barotrauma);

iii. Cycle Variable: it is the variable used to decide the end of the inspiration. It can be pressure, volume, flow or time. If, for example, the cycle variable is pressure, the inspiration ends when a preset value of pressure is reached.

iv. Baseline Variable: it is the parameter controlled during expiration. The most used baseline variable is PEEP.

(b) Conditional Variables

The conditional variables are those variables used by the controller to decide the output's characteristics that should be delivered. These variables are used in algorithms, whose basic structure is based on the *if-then-else* paradigm.

(c) Computational Logic

The computational logic represents the relationships between input, output and feedback signals. Chatburn suggests that, in order to avoid the generation of explicit decision rules, the use of artificial neural network or of the fuzzy logic may be a good solution [18].

1.3 Conventional Modes of Mechanical Ventilation

Since negative pressure mechanical ventilation requires big and uncomfortable machines, the majority of clinicians prefer positive-pressure based ventilators. Among all the possible ventilation modes, some techniques are commonly known as *conventional methods* of mechanical ventilation, which are briefly described in the following paragraphs.

1.3.1 Pressure- and Flow-Controlled Ventilation

The equation of motion shows a direct relationship between flow and pressure, defined by the mechanical properties of the respiratory system. Since modern ventilators can provide on-line feedback about output variables, either flow-controlled volume-cycled (VCV) or pressure-controlled time-cycled (PCV) ventilators can be used effectively and interchangeably during specific conditions, generating a similar pressure profile in the airways.

The major differences between pressure- versus flow-controlled ventilation appear after prolonged use: in PCV airway limit pressures are guaranteed but minute ventilation is a risk whenever lung impedance changes, in VCV the minute ventilation is guaranteed but there is no limits on the applied pressure.

For example, in PCV the clinician can set only three parameters: the applied inspiratory pressure, the mandatory frequency and the fractional inspiratory time. Tidal volume, flow, minute ventilation, intrinsic PEEP and alveolar ventilation depend on the mechanical properties of the patient's respiratory system [19].

In both PCV and VCV the inspiration is triggered by time or by a patient's inspiration effort.

1.3.2 Assist-Control Ventilation

Volume *Assist-Control Ventilation* (ACV) is one of the oldest ventilation modes and it is widely used in intensive-care units (ICUs). About 60% of ventilated patients receive this ACV, especially those with acute respiratory distress syndrome (ARDS) or chronic obstructive pulmonary disease (COPD) [20], [21].

In this mode the ventilator always deliver the same tidal volume, regardless on the mechanical load of the respiratory system and whether the breath is initiated by the patient or by the ventilator itself. In fact, in ACV the ventilator can be triggered by the patient, by sensing the pressure change due a inspiratory effort, or by the ventilator itself, if a pre-set time has elapsed from the previous inspiration and no inspiratory effort is sensed.

1.3.3 Intermittent Mandatory Ventilation

Intermittent Mandatory Ventilation (IMV) has been introduced in 1955 and mainly used with infants, but subsequently the breath-delivery design has been modified introducing the synchronization with the patient's inspiratory efforts [10]. During IMV a pre-set number of mandatory breaths are delivered while the patient breaths spontaneously. Mandatory breaths can be controlled in pressure, volume or both, setting the unused variables as limit or cycle variables, and the desired support level can be chosen by the clinician: with high IMV rates the patient's inspiratory effort is suppressed, with zero IMV rate, there is no support and the patient breaths spontaneously.

1.3.4 Pressure-Support Ventilation

Pressure Support Ventilation (PSV) is a mode of partial ventilation, that is the patients triggers the ventilator by a spontaneous inspiratory effort sensed by the ventilator itself. In this way there is not the problem of the synchronization between the patient's activity and the machine, and it is possible to control the disuse atrophy of the ventilatory muscles. The working cycle of the machine can be divided in three phases: the recognition of the inspiratory effort that triggers the ventilator, the pressurization in

which airways pressure raises a pre-set level allowing the inspiration, and the end of the inspiration that is flow-controlled, that is when the flow decreases under a threshold value, the inspiration is considered ended and the ventilator cycles the expiratory phase by opening the expiratory port until reaching the pre-set value of PEEP. In order to provide a safety feature, it is possible to set a minimal frequency or minute ventilation; in this way if the flow (or pressure) sensors do not sense any inspiration effort, the ventilator delivers the breath and avoids dangerous prolonged apnoea [22].

1.4 Alternative Methods of Mechanical Ventilation

The studies and the investigations about the control theory provided advanced technologies that can potentially substitute traditional pressure- and flow-controlled mechanical ventilators, introducing the possibility to set more parameters, reducing risks and increasing benefits of the mechanical ventilation. In the following paragraphs there is a brief description of the most diffuse modes, and the section 1.5 is completely dedicated to High Frequency Jet Ventilation (HFJV).

1.4.1 Adaptive Pressure Control

One of the problems related to the PCV is that there is not any control about the tidal volume, which depends on the mechanical properties of the respiratory system, thus minute ventilation is not guaranteed. The *adaptive pressure control* (APC) overcomes this problem by adjusting the pressure of the delivered breaths in order to maintain a pre-set minimal tidal volume: if the tidal volume decreases, the delivered pressure increases, if the tidal volume increases, the delivered pressure decreases. The adjustment of the inspiratory pressure occurs after the tidal volume is off-target in a number of breaths. It is important to highlight that in APC a minimal (but not a maximal) tidal volume is guaranteed. APC is not a volume-controlled mode because the tidal volume can vary, and in VCV it does not. Moreover, since delivered breaths are pressure-controlled, the pressure in the airways is maintained constant, therefore if the patient generates an inspiratory effort, he receive flow as demanded. This means that this mode can automatically reduce the ventilator support as the patient's inspiratory efforts become stronger [23].

1.4.2 Adaptive Support Control

Adaptive Support Ventilation (ASV) is an evolution of mandatory minute ventilation implemented on APC. Minute ventilation mode guarantees target minute ventilation

set by the operator, by delivering mandatory breaths if the patient's spontaneous activity is not enough. In ASV delivered pressure-controlled breaths are optimal, that is the machine automatically calculates the parameters of the breaths (tidal volume, frequency, normal minute ventilation) in order to minimize the work of breathing, basing on subject's characteristics (weight, dead space), which are set or estimated by means of some 'test breaths'. Then, during the ventilation, target tidal volume is achieved by APC, and the ventilator automatically adjusts the other parameters according to the mechanics of the respiratory system. It has been demonstrated that this ventilation mode can accelerate tracheal extubation after cardiac surgery [24].

1.4.3 Proportional Assist Ventilation

The *proportional assist ventilation* (PAV) was introduced by Younes in 1992, and it provides pressure-controlled breaths proportional to the patient's inspiratory effort. Greater is the effort, greater is the delivered pressure. The operator sets the percentage of necessary support, and the ventilator measures compliance and resistance of the respiratory system, and patient-generated flow and volume and on the basis of those it delivers the proportional amount of inspiratory pressure. Therefore, in PAV all breaths are spontaneous and size and timing are controlled exclusively by the patient, even if some safety parameters can be set. A recent study has demonstrated that PAV improves the patient-ventilator interaction [25], but there are some groups of patient in who this mode should be used with caution, like those with high ventilator rates, severe hyperinflation or respiratory depression [10].

1.4.4 Airway Pressure Release Ventilation

Airway Pressure Release Ventilation (APRV) delivers pressure-controlled, time-triggered and time-cycled breaths by intermittently switching between two levels of positive pressure, P_{high} and P_{low}, but allows spontaneous breaths at any point of the cycle. Generally, the inspiration time T_{high} is much longer than the expiration time T_{low}, therefore APRV is an extreme form of Inverse Ratio Ventilation (IRV) with an I:E ratio of 4:1. Biphasic Positive Airways Pressure Ventilation is based on the same working principle but it is characterized by more conventional I:E ratios [23].

1.4.5 High Frequency Ventilation

High Frequency Ventilation (HFV) is a non-conventional ventilation method introduced in the end of 1960s, in which small tidal volumes (less than dead space) are delivered at high rates (more than 1 Hz). This ventilation mode allowed to identify some of the

factor causing ventilator-interaction lung injury (VILI), and it has been demonstrated that HFV permits a more homogeneous aeration of the lungs, protecting them against injuries caused by over-distension and by repetitive openings and closings in regions of ongoing atelectasis [26].

Initially, HFV was used in different kinds of studies: Sjöstrand tried to eliminate breathing-caused changes in arterial pressures by ventilating at high rates, Emerson tried to move secretions, Bryan stated that gas mixing increases with the increasing of frequency. By the way, HFV did not become popular in ICUs, because a physiopathological rationale was necessary to use high rates and small tidal volumes instead of conventional modes.

In the 1970s it was evident that many patients in ICUs had problems related with low lung volumes, with consequent lower pulmonary compliance, higher resistance and increased work of breathing. Since the benefits of the application of Continuous Positive Airways Pressure (CPAP) were well-known, alveolar aeration had to be optimized by the application of higher mean pressure, but lower peak pressures, than those provided during CMV, thus the small-volume cycles of HFV seemed a good solution. In fact, it is now well-known that HFV enables gas exchange to be achieved with low tidal volumes and peak airway pressures, thus offering the possibility of reducing barotrauma in patients with severe, acute lung disease [27].

Now there are several HFV modes, differentiated by sources, frequencies and volumes used, but the most used are:

- High Frequency Positive Pressure Ventilation (HFPPV)
- High Frequency Oscillatory Ventilation (HFOV)
- High Frequency Jet Ventilation (HFJV)

In HFPPV a pneumatic valve generates an intermittent flow characterized by a frequency from 1 up to 5 Hz, delivered by a catheter placed within the endotracheal tube, thus forming an open system where gas entrainment does not occur [28]; this configuration reduces the anatomical dead space and the peak pressure, lowering the effects on the changes of pressure of heart and veins. A study [27] demonstrated that dead space decreases when frequency increases up to 0,75 Hz, and after this value it remains constant even if frequency continues to increase; at higher ventilatory rates than 2 Hz, gas exchange becomes similar to the conventional respiratory physiology.

Smith et al. [28] reported results of the application of HFPPV on dogs, using double-lumen tracheal tubes with several diameter ratios between the inspiratory and the expiratory port. With this instrumentation, and changing parameters like frequency and driving pressure, it was possible to collect data about different conditions

and conclude that with frequencies higher than 100 bpm gas trapping may occur (with 1:1 and 1:4 tracheal tubes) and $P_{a_{CO_2}}$ increases, while $P_{a_{O_2}}$ decreases; opposite variations can be obtained by increasing driving pressure and thus tidal volume. The best configuration is represented by the 1:10 tracheal tube with the frequency of 100 bpm.

In clinical practice HFPPV has been employed for rigid bronchoscopy and laryngoscopy.

In HFOV an electromagnetic device (oscillator) creates flow oscillation at frequencies from 5 to 40 Hz that are superimposed to a constant distending airway pressure. These oscillations cause small tidal volume and a rapid gas mixing in the lungs due to the oscillatory behaviour of the intrapulmonary pressure, which oscillates around a mean value, higher than the CMV mean value but without high pressure peaks that can damage both airways and the lungs [26].

In 1980 it has been experienced that HFOV with a frequency of 15 Hz produces an adequate gas exchange, thanks to at least five modes of gas transport [27]:

1. convective mixing of gases in airways;
2. direct alveolar ventilation of the regions of the lungs close to the upper airways;
3. convective transport of gases due to the asymmetry between inspiratory and expiratory flow profiles;
4. diffusion in the alveolar capillary membrane region;
5. longitudinal and radial dispersion due to turbulences;

In contrast with CMV, a decrease in frequency from 15 Hz to 12 Hz causes a decrease in $P_{a_{CO_2}}$ and an increased tidal volume, but a further frequency decrease is responsible also for a decrease in $P_{a_{O_2}}$ [29]. By handling airways pressure it is possible to modify the alveolar recruitment and the CO_2 elimination, since an higher mean airway pressure causes an increase of lung volume and, thus, a better oxygenation, and an increase of the amplitude of pressure changes is related with an increase in tidal volume and in CO_2 elimination.

Finally it is possible to state that HFOV reduces the risk of ventilator-induced lung injury due to over-distension or to high peak pressure, reduces the conversion of surfactant into small aggregate forms, stabilizing alveoli and thus expands the lungs to a greater extent than CMV does.

1.5 High Frequency Jet Ventilation

High Frequency Jet Ventilation (HFJV) was introduced in 1970s by Smith and Klain, when they demonstrated that normocapnia and good oxygenation could be maintained by delivering jets of oxygen through a very small catheter (14-gauge), using high frequencies (up to 20 bpm) and high pressures (3.5 - 5 bar) controlled by a fluidic-logic controller.

These experiments revealed good arterial oxygenation, no hemodynamic impairment and normal gas exchange up to 400 bpm, whereas at higher frequencies a fall in cardiac output and heart rate was detected. They speculated that turbulent gas flow produced by the high frequency jets creates adequate movement of gases towards and outwards the lungs, with no clearly differentiated expiratory or inspiratory phase [30].

HFJV is classified as a non-conventional ventilation method because it cannot be controlled neither in pressure nor in volume, since it is an open system and air entrainment occurs, thus the control variable is the time, by means of I:E ratio; the other settings are frequency and driving pressure. Moreover it is classified as a HFV technique, since the delivered tidal volume is smaller than dead space and the respiratory rate is greater than 1 Hz.

1.5.1 Mechanisms in HFJV

The catheter used in HFJV is placed within the endothracheal tube (Figure 1.12), forming an open system that allows the essential phenomena of the air entrainment and jet mixing. In fact, as cited earlier, gases are delivered through a narrow cannula under high pressures and velocity, which increase proportionally with the source pressure and in inverse proportion with the diameter of the catheter. Gases exit from the nozzle with an high kinetic energy that is dependent on the speed of the jet flow and impact into a larger volume of relatively immobile gases represented by the content of the endotracheal tube. At this point an energy transfer occurs and the airway gases acquire a forward momentum in the same direction as the jet flow.

Since it is an open system, a port opened to a gas reservoir under the same pressure conditions as the airway gases provides gas which will be entrained to replace those which have moved forward, therefore a volume much larger than that delivered by the jet moves to the lower airway, decreasing pressure and speed.

This gas entrainment is the operating principle which distinguishes HFJV from any other high rates ventilation method, and it has many important physiological consequences, allowing to deliver larger tidal volumes with lower airway peak pressures (but higher mean pressure) and to choose the delivered tidal volume by setting the

(a) Jet cannula for transtracheal jet ventilation and jet catheter for jet ventilation

(b) Jet laryngoscope for SHFJV

Figure 1.12: Jet ventilator equipment. (a) The catheter is made of polytetrafluoroethylene, the typical length is 330 mm. It is composed of parallel tubes: the central one is the jet ventilation nozzle (inner diameter 2.7 mm, total length 285 mm) and opens 45 mm from the tip of the catheter. The second lumen (inner diameter of 1 mm) is designed for monitoring airway pressure and opens 75 mm from the tip of the catheter. At the tip of the catheter, a basket (length 45 mm) helps to align the catheter to the trachea and prevent direct contact of the jet ventilation noozle with the tracheal wall. From G. Friedrich, G. Mausser, M. Gugatschka. Die Jet-Ventilation in der operativen Laryngologie, HNO 2008, 56:1197–1206.

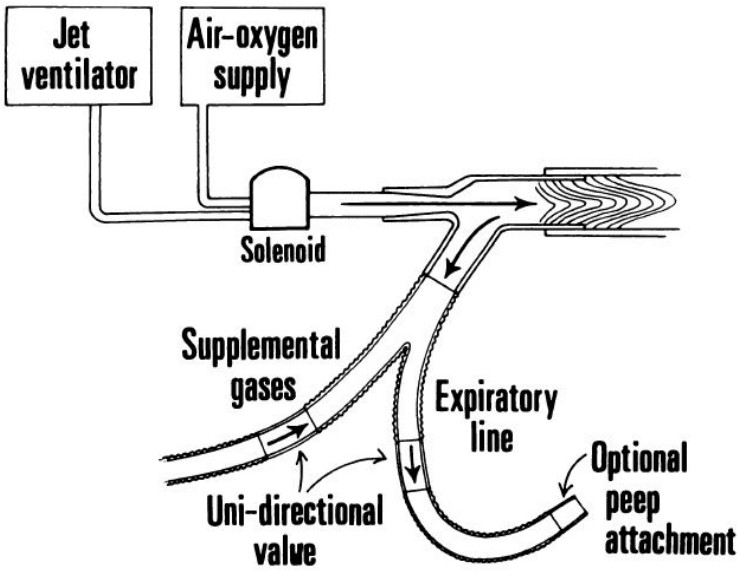

Figure 1.13: Schematic representation of a jet ventilator and its components, highlighting inspiratory line with the unidirectional solenoid valve and the expiratory line with the PEEP valve. From [39]

driving pressure and thus the kinetic energy of the jet flow.

In fact, Carlon et al. [31] found a significant linear correlation between tidal volume and driving pressure, concluding that tidal volume increases approximately 10 ml for every pound per square inch (70.3 cmH_20) of driving pressure.

However, there is a weak relationship between tidal volume and alveolar ventilation, since greater jet pressure causes greater turbulences which decrease the average linear distance travelled by gas molecules and thus the fraction of tidal volume which gets the lungs. This does not imply a decrease in gas exchange, since increased turbulences may improve gas exchange by diffusion, but these processes are not completely clear and researchers have different opinions about this topic.

1.5.2 Humidification system in HFJV

During HFJV, the high velocity of the jet stream, the Venturi's effect and the Joule-Thompsen effect could cause problems to the the airway's surface, which can be damaged if the injected gases are not adequately humidified and warmed.

Adverse effects have been observed in several studies, and depend on the interaction between the gas flow and the tracheal mucosa: initially there is an increase in blood supply to the irritated region, as a result of local vasodilation. Then, there is an increase of the osmolality of the mucous secretion, and the latter becomes increasingly hyperosmolar and dry, being trapped and encapsulated beneath the surface, under which is finally forced by the jet-stream.

Other studies report damages to the epithelial cells of the trachea, destruction of cilia, tissue inflammation and necrosis due to prolonged use of mechanical ventilation [32].

Humidification is provided by a parallel cannula (Figure 1.14) which deliver a warmed saline infusion that is propelled and nebulized by the high pressure jet stream. In Kraincuk et al [32], the 0.9% saline infusion was warmed to $39°C$ and delivered at 20 ml/h, but they had to increase the humidification even to the 200% to avoid tissue damages. Moreover, they stated that adequate humidification does not prevent damages if the gas is not sufficiently warmed as well.

1.5.3 HFJV-induced PEEP effect

As already mentioned, HFJV delivers small breaths at high rates, therefore researchers had to take in count the phenomenon of gas trapping that occurs because the spontaneous relaxation time of the respiratory system, which defines the expiratory time, is longer than the expiratory time set in the ventilator, driving to a breath-by-breath

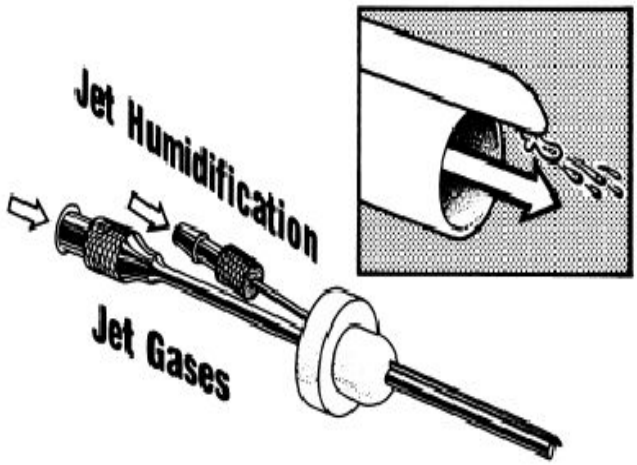

Figure 1.14: Representation of jet injector cannulas, one for the jet-stream, the other provides fluids for humidification. From [39]

increase of lung volume due to the amount of gas that did not have time do be exhaled.

This phenomenon varies its magnitude breath-by-breath: the spontaneous relaxation time constant depends on the mechanical characteristics of the respiratory system, that is resistance and compliance, and since the latter is not linear, the relaxation time of the respiratory system depends on its working point.

From this statement it is easy to notice that increasing the amount of trapped air, and therefore increasing the lung volume, compliance decreases and consequently the relaxation time constant shortens, being defined as the product of the resistance (R) by compliance (C). Thus, spontaneous expiratory time shortens breath-by-breath and when spontaneous relaxation time equals the expiratory time set in the ventilator, gas trapping ceases. The overall effect can be seen in Figure 1.15.

Finally, it is possible to conclude that in patients with "stiff" lungs the HFJV-induced PEEP effect will be moderate, and in patients with normal or compliant lungs, thus characterized by higher time constant, the HFJV-induced PEEP effect will be greater.

From the point of view of the ventilator-related settings, Rouby et al. [34] demonstrated that HFJV-induced PEEP effect depends not only on I:E ratio and driving pressure (thus tidal volume), but also on frequency. If fact, there are two distinct responses to the increase in frequency, depending on the underlying pulmonary mechanics. In patients characterized by decreased lung volume, lung stiffness or chest wall rigidity, increase in frequency do not change pulmonary volume above FRC (Figure 1.16), but in those patient in whom compliance and resistance are increased, they observed an increase in pulmonary volume above FRC (Figure 1.17). For this rea-

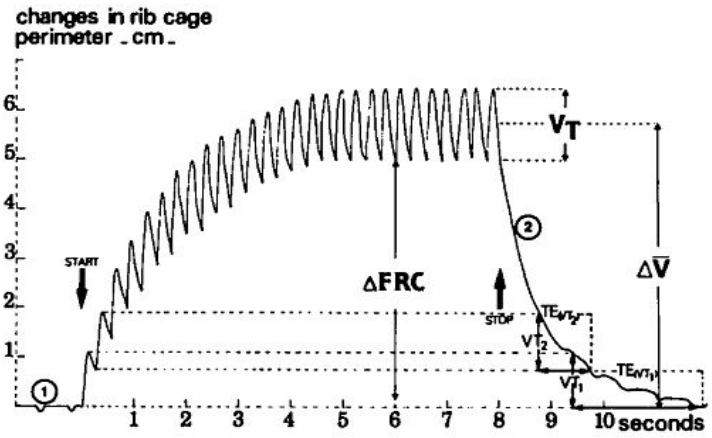

Figure 1.15: Recording of changes in rib cage perimeter induced during a short period of HFJV.$\triangle$ FRC=increase in FRC. $\triangle$ V=mean pulmonary volume above apneic FRC. V_T=Tidal Volume. V_{T1}= First V_T. V_{T2}= Second V_T. TE_{VT1}=spontaneous relaxation time of V_{T1}. TE_{VT2}=spontaneous relaxation time of V_{T2}. From [34]

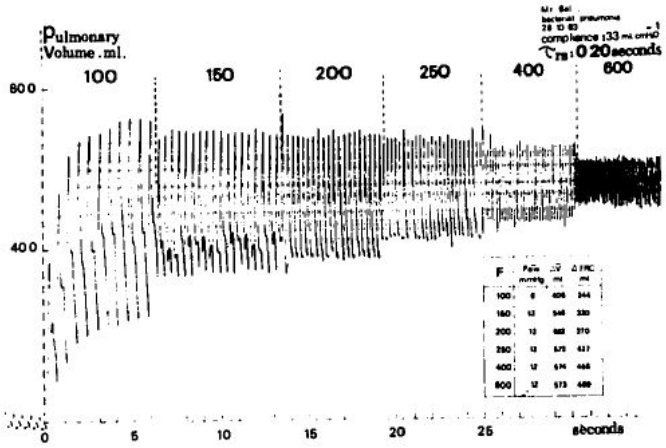

Figure 1.16: Respiratory effects of increasing frequency in a patient with low CRS. From [34]

son, they suspected that the use of HFJV in obstructed or distended patient could be deleterious.

1.5.4 Gas Exchange during HFJV

Since its beginning, HFJV has been object of several studies in order to understand the mechanisms that allow the gas transport through the airways and the gas exchange between alveoli and blood. Such studies were difficult because, being an open system, it was difficult to measure correctly data about delivered tidal volume, airway pressure and so on, but the researchers were able to reach conclusions which are very useful in order to understand the potentialities of this ventilation method.

One of the main parameters to evaluate the performances of a mechanical ventilator

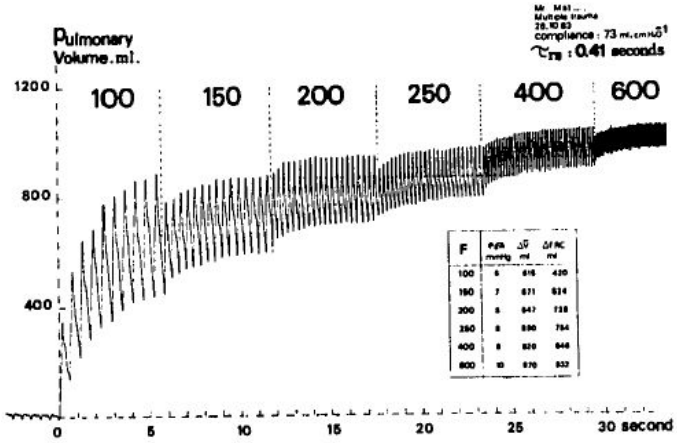

Figure 1.17: Respiratory effects of increasing frequency in a patient with higher CRS. From [34]

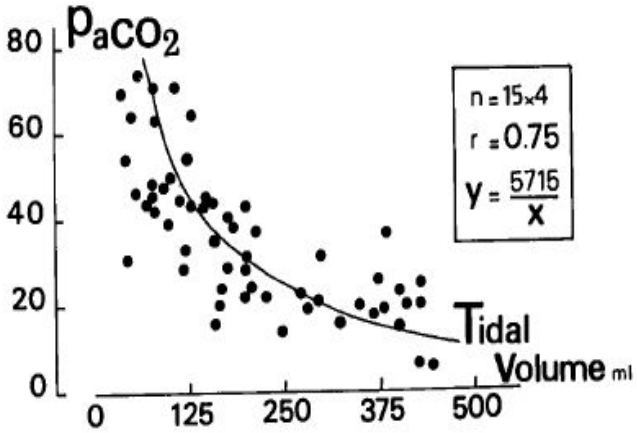

Figure 1.18: Relationship between arterial P_{CO_2} and tidal volume. Four different frequencies (100, 200, 400 and 600 min^{-1} are used. Constant DP = 2.6 atm and I:E ratio = 0.43 From [34]

is the arterial P_{CO_2}, which is inversely related to tidal volume because higher is the latter, higher is the amount of carbon dioxide that is washed out (Figure 1.18).

Sykes [35] suggested that that at respiratory rates above 1 Hz, and adequate alveolar ventilation can be achieved only by using very high minute ventilation, nevertheless his experiment demonstrated that using frequencies higher than 1 Hz and tidal volume smaller than deadspace, CO_2 elimination is very much reduced, the volume eliminated being less than normal CO_2 production (4.3 l/min in a resting adult), leading to the conclusion that CO_2 clearance depends on tidal volume and not on minute ventilation.

Rouby et al. [34], [36] reported similar results, that is increasing frequency from 100 to 600 bpm lead to:

- an increase of arterial P_{CO_2} leading to hypercapnia above 400 bpm, meaning a

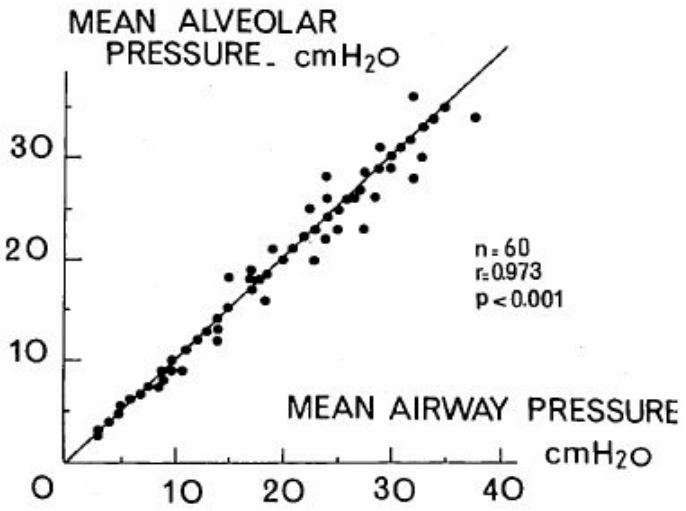

Figure 1.19: Relationship between mean alveolar pressure and mean airway pressure. From [36]

weaker and weaker CO_2 washout

- an increase of mean airway pressure and apnoeic volume over FRC
- an increased pH
- a decrease of jet volume and tidal volume.

Arterial P_{O_2} does not change its value.

Furthermore, these authors verified that by increasing either I:E ratio from (0.25 to 0.67) or driving pressure (from 1.8 to 2.6 atm), tidal volume, jet volume, mean airway pressure, FRC and arterial P_{O_2} increased (Figures 1.19 and 1.20), whilst arterial P_{CO_2} decreased.

All these data confirm what is written above about the relationship between driving pressure, tidal volume and arterial P_{CO_2} and about the benefits on oxygenation provided by the application of PEEP, which is set through parameters such as I:E ratio or frequency. The fact that P_{aCO_2} is closely related to tidal volume suggests that bulk convection by direct alveolar ventilation rather than augmented dispersion plays a major role in gas transport during HFJV.

Finally, also Smith and Klain [30] concluded that in HFJV the CO_2 washout and arterial oxygenation depend both on the setting parameters of the ventilator and on the mechanical parameters of the respiratory system, but they found a further dependence: the design of the jet cannula.

In fact, by varying the number of holes and their position, they noticed a change in both CO_2 washout and oxygenation; the best configuration was the cannula with

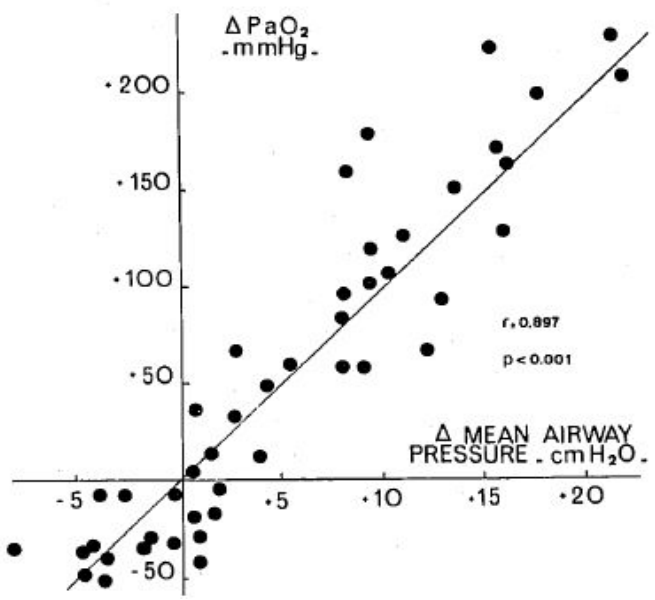

Figure 1.20: Relationship between arterial oxygenation and mean airway pressure. From [36]

one opening at the tip and two side holes 0.5 cm below the tip. Either increasing or decreasing the number of holes CO_2 washout deteriorated, and the nearer was the orifice to the carina, the more pronounced was the effect of unequal ventilation if the jet stream was not pointing directly to the center of the carina.

1.5.5 Comparison with CMV

In order to understand if HFJV is at least as reliable and effective as CMV, several comparisons have been made by many researchers, leading to similar results.

Carlon et al. [39], [31] compared HFJV to volume cycled ventilation (VCV) obtaining identical rate of survival and small differences in other indices, even if VCV can provide better oxygenation than HFJV at equivalent PEEP, but with higher peak inspiratory pressures. This can increase risks of barotrauma, but could help opening those alveoli which have a critical opening pressure; carbon dioxide clearance was slightly better on HFJV. VCV is therefore a representative model of the ventilatory strategy based on shunt reduction and compliance improvement, whilst HFJV is a model for controlled ventilation at low pulmonary volumes and with oxygen transport as the primary end point of the therapy.

An important effect was analysed by Johnston [37]: with CMV large tidal volumes are delivered, therefore mean intra-thoracic pressure is raised and thoracic venous flow impeded, central venous pressure elevated and ventricular filling pressure decreases, driving to a decreased cardiac output. With HFJV the use of small tidal volumes

in combination with an airway open to the atmosphere results in low intra-thoracic pressure and negligible effect on the cardiac output.

Finally, Carlon et al. concluded that, even if the mode of action of the two system is completely different, from a strictly clinical point of view there is not difference between HFJV and VCV, nevertheless the operator should take in count the mechanical characteristics and the pathology of the patient to choose the correct ventilation mode, as it is described in the next paragraph.

1.5.6 Clinical considerations on HFJV

The final goal of the studies about HFJV is to understand its clinical utility, its possible applications and the problems related to its use, in order to know the advantages and the disadvantages of using HFJV in presence of the different kinds of pathologies of the respiratory system.

Carlon et al. [31] suggested that the use of CMV in presence of bronchopleural or tracheoesophageal fistula is not effective, since a part of it is lost through the fistula and an increase of delivered tidal volume will cause higher peak airway pressure that could lead to barotrauma. The same effects could be created by using CMV in presence of lung fibrosis, since a decreased lung compliance implies the use of PEEP and higher pressures in order to re-expand alveoli and achieve a correct ventilation.

The characteristics of jet ventilator, which can deliver variable tidal volumes without increasing airway peak pressure, closely matches the specifications of the device that might be useful in some forms of respiratory failure as those previously described, in fact many other studies as Smith and Babinski's [38] reported numerous cases of successful treatments of bronchopleural fistula using HFJV and an evident decrease of barotrauma [39]. Moreover, in this study, HFJV was successfully used during laryngoschopy, thoracic surgery and for other intraoperative uses.

Similar results have been reported in [34] and [36], and these authors suggested to avoid the use of HFJV in patients who have pulmonary distension or obstructive diseases because the occurrence of inadvertent PEEP and consequent lung over-distension. As a matter of fact, they concluded that HFJV should be to considered to be contraindicated in all types of respiratory failure characterized by increased compliance and elevated resistance, such as acute respiratory failures complicating chronic obstructive pulmonary disease or asthma.

Finally, HFJV's instrumentation design offers practical advantages during either tracheal, laryngeal, vocal cords surgery or laser surgery:

- the small catheter placed within the endotracheal tube allows to have laryngeal structures freely accessible with surgical instruments;

- the catheter does not hide the view of the operating field and did not interfere with laser surgery;
- the catheter allows to ventilate those patients who cannot be intubated because of severe stenosis or other laryngeal pathologies that inhibit gas exchange and the insertion of ventilation tubes;
- HFJV can be used as an emergency tool to manage difficult airways that cannot be quickly intubated or ventilated;
- the ventilators have a long life because there is only one moving part (the solenoid) which is tested to have a life expectancy of 100 million cycles;
- it has been demonstrated that HFJV prevents aspiration event without a cuffed tube.

1.5.7 Low Frequency Jet Ventilation and Superimposed High Frequency Jet Ventilation

1.5.7.1 Low Frequency Jet Ventilation

Jet Ventilation is classified as Low Frequency Jet Ventilation (LFJV) when jet pulses are delivered at frequencies not greater than 1 Hz, that is between 8 and 20 bpm. The driving pressure is set around $1 \div 1.5$ bar [40] and the jet stream is delivered through the same cannula as that used to deliver HFJV, which has been described in figure 1.12.

Low frequency jet acts in the inspiration phase and overcomes the resistance to respiratory movements by the thorax and the lungs, assuring a basic gas supply and an adequate inspiratory pressure plateau; in the expiration phase LFJV allows to have a better CO_2 washout, but a major gas loss can occur because of the elasticity of the thorax and the lungs.

Aloy et al. [40] used a lung simulator in order to study separately the effects of high frequency and low frequency jet ventilation and they concluded that neither high nor low frequency alone had a noteworthy effect in increasing tidal volume, therefore they tried to superpose the two jets (Figure 1.21). They obtained a jet ventilation characterized by adequate pressure plateau, good carbon dioxide washout and pulmonary ventilation provided by the low frequency jet (12 bpm, 1.5 bar), and by a positive end expiratory pressure that avoid alveolar collapse provided by the high frequency jet (400 bpm, 0.9 bar).

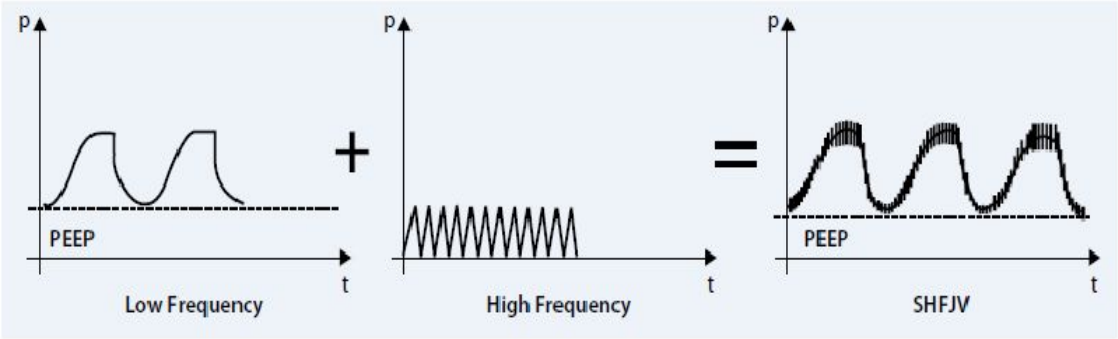

Figure 1.21: Low Frequency, High Frequency and Superimposed High Frequency Jet Ventilation

1.5.7.2 Superimposed High Frequency Jet Ventilation

The advantages of using small catheters to ventilate patients coupled with the advantages of superposing low and high frequency jets drove researchers to experiment SHFJV in different conditions and different modalities, in order to demonstrate its benefits and to compare this technique with monofrequent jet ventilation.

First of all, Aloy et al. [40] found the best position of the two jets in order to optimize the effect of gas superposition, by placing them offset distally with respect to the outflow opening. The jet stream had to be caudally oriented so it could be continued into the trachea along a median line, thus the angle of incidence of both jets has been placed at 18°. It has been observed that this configuration guarantees an optimal use of Venturi's effect while keeping negative pressures distant from the site of surgery, avoiding a suction effect which could possibly lead to aspiration of blood or tissue part.

To implement this results, special laryngoscopes were obtained by modifying the existing ones; an example is that developed by Bacher et al. [41]: the larygoscope is made of steel and is equipped with two nozzles (inner diameter 1.5 mm) for the simultaneous administration of high- and low-frequency jet ventilation, which are integrated in the main lumen and open into the main lumen at distances that depend on the size of the laryngoscope (Figure 1.22).

In his study, Bacher has compared supraglottic SHFJV with subglottic monofrequent jet ventilation, demonstrating that with first technique it is possible to maintain better arterial oxygenation and carbon dioxide elimination, since administered tidal volume were greater superposing high and low frequency (600 and 15 bpm) due to a greater air entrainment. Moreover he noticed that using a single frequency the measurement of the airway pressure can be corrupted by the Venturi's effect, therefore the risks due to an hyperinflation are higher because the system is not able to measure the

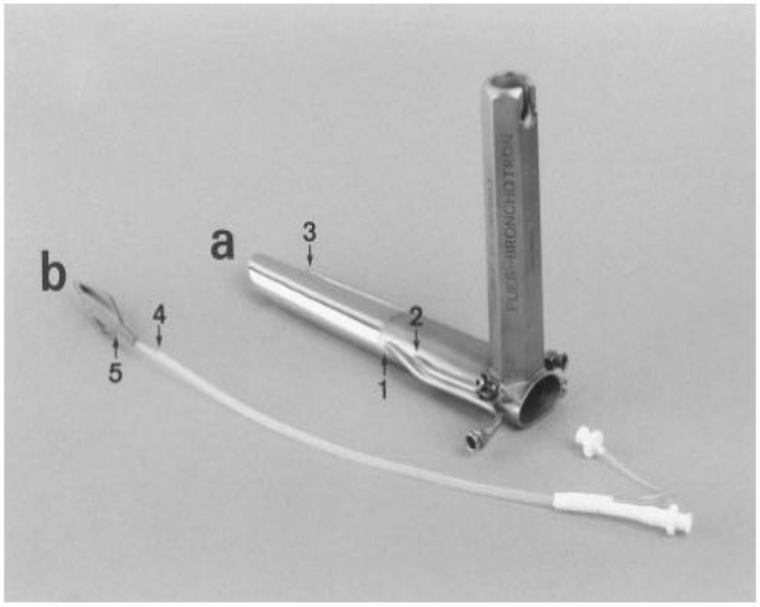

Figure 1.22: Laryngoscope for SHFJV and catheter for delivering jet stream. 1 and 2 are, respectively, the high and the low frequency nozzle, 3 is the airway pressure monitoring port. From [41]

real value of the airway pressure. Using SHFJV and the laryngoscope in figure 1.22, this measurement is easier and more accurate.

These result have been confirmed also by other researchers, who have concluded that the greater air entrainment causes a bigger drop in the air flow pressure; in fact, passing through the jet nozzles, the gas stream changes from an high pressure source (1-2 bar) and a low flow (20 l/min) to a low pressure (6-10 mbar) and high flow (up to 200 l/min, depending on the driving pressure). This involves less damages to the airways and no adverse hemodynamic effects [42].

Bacher has then compared subglottic SHFJV with supraglottic SHFJV, concluding that the first produces better results than the subglottic monofrequent JV, decreasing $P_{a_{CO_2}}$ by 9% and increasing $P_{a_{O_2}}/F_{IO_2}$ by 18%, but supraglottic SHFJV is still the most efficient [43].

Moreover, with a supraglottic ventilation and using long inspiratory time and high driving pressure, it is possible to overcome high inspiratory resistance and to ventilate adequately even those patients who have a severe tracheal or laryngeal stenosis. On the contrary, with translaryngeal or transtracheal catheters the gas insufflation is distal from the stenosis and therefore there is an high risk of barotrauma, which is even higher if the catheter is placed within the residual lumen of the stenosis.

For the same reason, SHFJV is superior also in cases of chronic obstructive pulmonary disease, restrictive pulmonary disease, coronary artery disease and extreme obese patients [44].

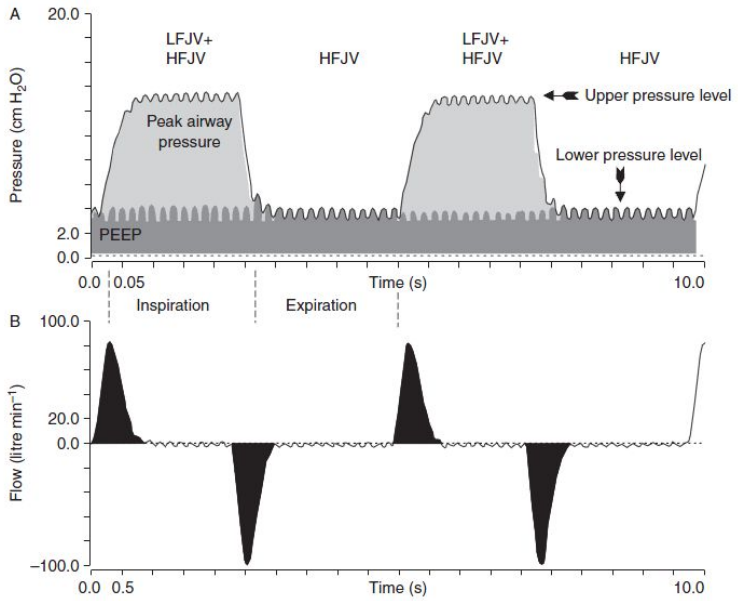

Figure 1.23: Typical pressure and flow curves during SHFJV. From [44]

1.6 Measurement of Lung Volumes

Measuring lung volumes by integrating signals coming from spyrometers or pneumotacographs could seem simple, but in practice there are a lot of factors affecting the records. These techniques need the patient breathing through masks or mouthpieces and they may require the use of nose-clips, which limit patient's mobility and may introduce leaks, thus it is not practicable for long time and it is extremely difficult to get accurate data from children, uncooperative adults, during sleep or during phonation [45].

The use of spyrometer can be done just for short periods because it introduces additional dead space and the integration of flow to determine volumes suffers from integrations drift, which may affect the record of tidal volumes or absolute volumes. Furthermore, new ventilation techniques, such as High Frequency Jet Ventilation, require new measurement instrumentation which can measure breath-by-breath changes in volume even if the ventilator-patient system is an open system and suffers of gas entrainment.

1.6.1 Volumes measurement during jet ventilation

The characteristics of jet ventilation enhance the problems related to the measurement of volumes, and in particular of tidal volume, which are listed in the previous paragraph. As already extensively explained, in fact, during Jet ventilation, the patient-ventilator is an open system, therefore the volume delivered by the ventilator is enhanced by air

entraining which depends on driving pressure, I:E ratio and frequency [46] and causes several problem to the conventional measurement system:

- tidal volume results from the addition of the entrained volume and the gas volume delivered by the ventilator;
- any interposition of measurement apparatus may modify gas entrainment and consequently the tidal volume;
- the frequency response of the flow meter is not as high as the frequency employed in HFJV;
- the measurement is affected by the gas composition which is made unknown by gas entrainment, but calibration should be made with the same gas used for ventilation;
- humidity of the air may cause condensation on the resistance of pneumotacograph, altering the measurement;
- the integration of the flow over time may be affected by a drift due to the baseline value of flow.

1.6.2 Other measurement techniques

These problems induced researchers to find other techniques to measure lung volumes; since lungs are directly coupled with the rib cage and the diaphragm, ventilation can be measured by detecting the external chest wall surface motion. Chest wall is defined as all the anatomical structures that surround the lungs: rib cage, abdomen and diaphragm.

This kind of measurement have been originally made by rubber strain gages, differential linear transducers (DLT) - used in Rouby's study [34], magnetometers and respiratory inductive plethysmography (RIP), even if only the last two have been widely used in clinical practice.

Since involved forces, interactions and movements vary within the chest wall, it was early evident that the chest wall must be divided in two different regions, the rib cage and the abdomen, the measurement has to be made in more than one site. This necessity implies to use more than one device together, increasing those problems relative to calibration that were already highlighted by the fact that the estimated volumes were accurate only under the conditions matched during the calibration.

1.7 Opto-Electronic Plethysmography

Researchers were always looking for new methods to improve the accuracy and the reliability of the volume measurements and in 1994 [47] a study reported the application of an opto-electronic three-dimensional motion analysis system to analyse respiratory kinematics. This system was based on a television-image processor (ELITE - ELaboratore di Immagini TElevisive – Politecnico di Milano) that assesses volumes changes by computing the coordinates of passive markers placed on relevant landmarks of the thorax and the abdomen and allows to divide the chest wall in three regions: upper thorax, lower thorax and abdomen. Since the chest wall is directly coupled to the lungs through the pleura, the chest-wall volume changes reflect the changes in lungs' volume.

This technique has many strengths, because it is non-invasive, non-ionizing, leaves maximum freedom of movement, can be used in presence of other instrumentations like mechanical ventilators, does not required any calibration in presence of the subject, and with the following developments of instrumentation and of the computational algorithms the system became very accurate and reliable.

1.7.1 Principle of Measurement

Opto-Electronic Plethysmography (OEP) measures the changes of the shape of the chest wall by using a number of strategic points of the rib cage and the abdomen as reference. The three-dimensional position and displacements of these points are measured by CCDs camera that acquire the signal generated by the reflective properties of the passive spherical markers (whose dimension is 8-10 mm of diameter) placed on the skin, lighted by infra-red fleshing LEDs synchronized with the cameras themselves. Since the light is reflected by the markers with a maximum angle of 10°, these LEDs are organized in three coaxial rows in order to optimize the working volume and the power of the detected signal; in fact, if the lighted marker is close to the flash, it is lighted by the most internal row, and as the marker moves far away, as the effect of the external rows increases.

This acquisition system works at up to 100 frames per second, providing an high time resolution, and it is also characterized by an high special resolution ensured by the dimension of the voxels composing the working volume. A shutter system helps to improve the signal to noise ratio by avoiding the comet-tail effect.

Eventual noise, represented by signal coming from other objects placed in the working volume or from the external illumination, is then removed either in the following hard-ware or in the soft-ware levels based on shape and dimension recognition [48].

Output data bring now information only about the position of the markers, therefore

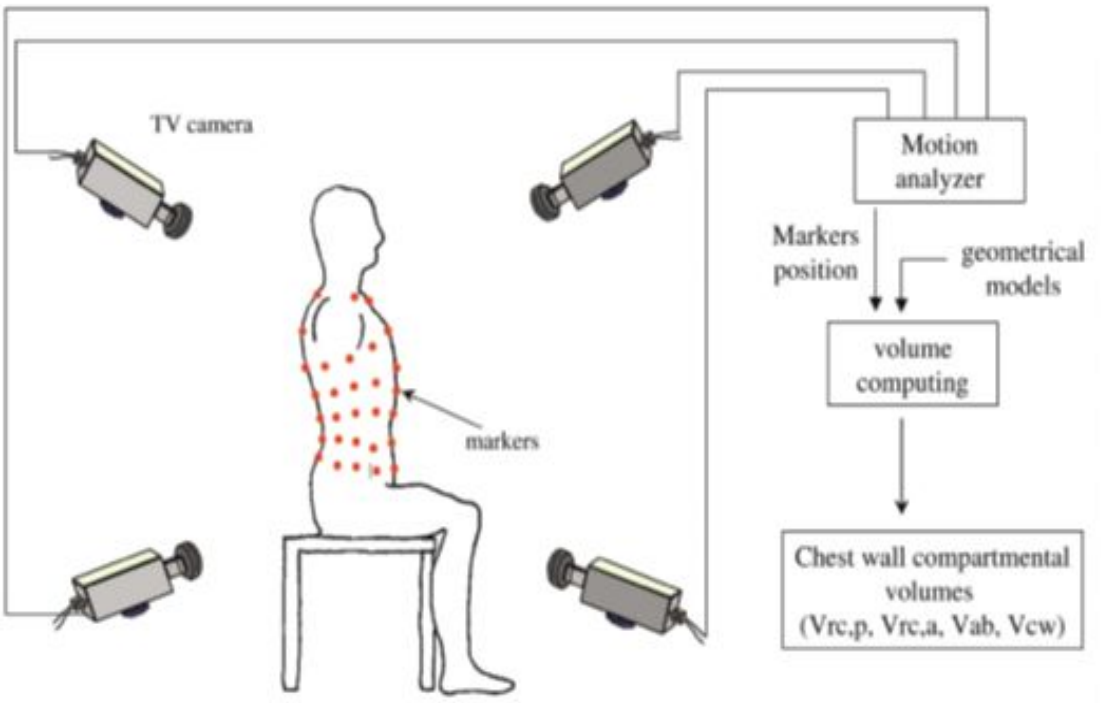

Figure 1.24: Opto-Electronic Plethysmography. From [45]

it is possible to determine the three coordinates of each marker combining data of at least two cameras by applying stereo-photogrammetry.

The close surface is determined by interpolating the acquired points according to a geometric model that forms triangles (mesh of triangles – Figure 1.26) whose vertexes are the point themselves. For each triangle area and direction of the normal are determined, therefore it is possible to compute the internal volume by applying Gauss' Theorem (or divergence theorem):

$$\int_{S_{CW}} \overrightarrow{F}\,\overrightarrow{n}\,dS_{CW} = \int_{S_{CW}} \overrightarrow{\nabla F}\,dV_{CW} \tag{1.11}$$

Where V_{CW} is the volume enclosed by the surface S_{CW} and $\overrightarrow{F}$ is a vector field defined at every point of S_{CW}, $\overrightarrow{n}$ is the outward pointing normal vector at every point of S_{CW}.

By choosing $\nabla F = 1$, we get:

$$\int_{S_{CW}} \overrightarrow{F}\,\overrightarrow{n}\,dS_{CW} = \int_{V_{CW}} dV_{CW} = V_{CW} \tag{1.12}$$

which in discrete form becomes:

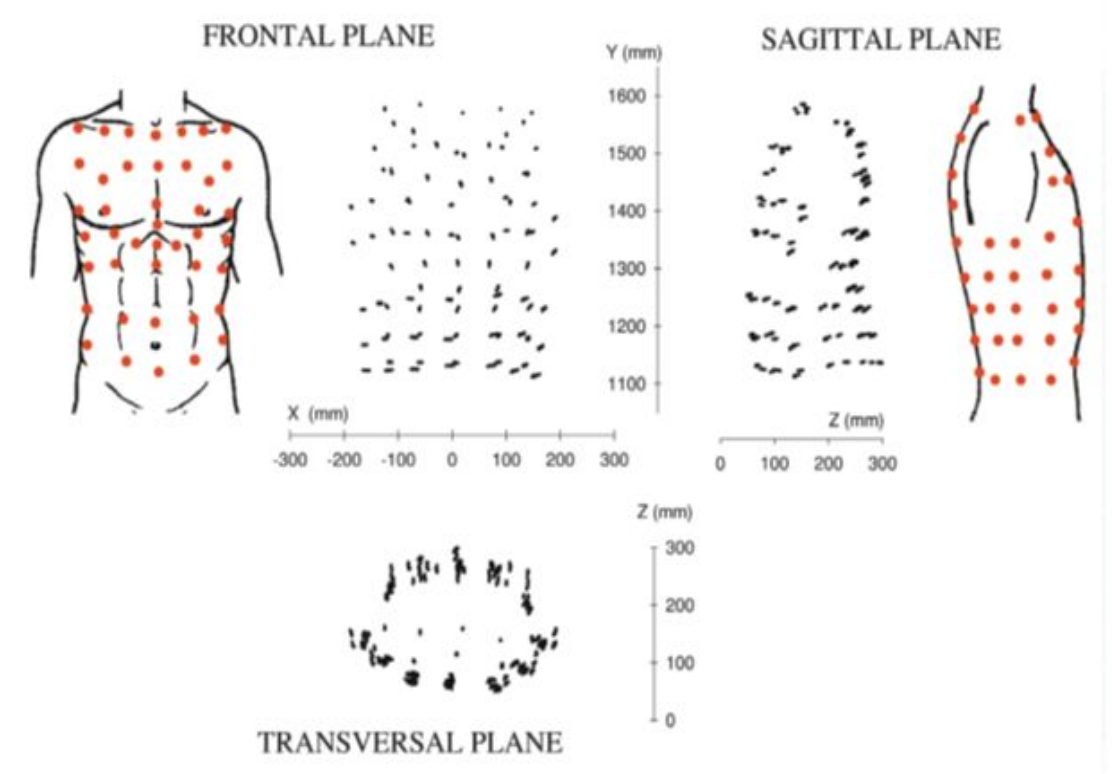

Figure 1.25: Displacements in the frontal, sagittal and transversal planes of the marker during normal breathing. From [45]

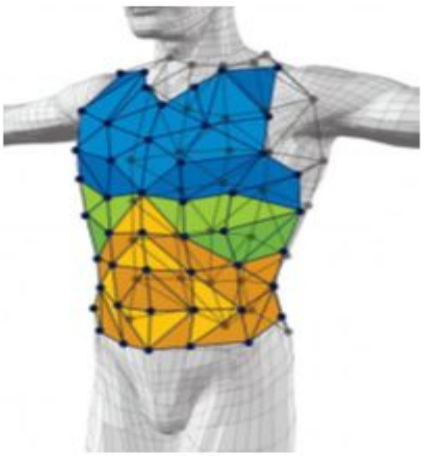

Figure 1.26: Mash of triangles built on the chest-wall surface.

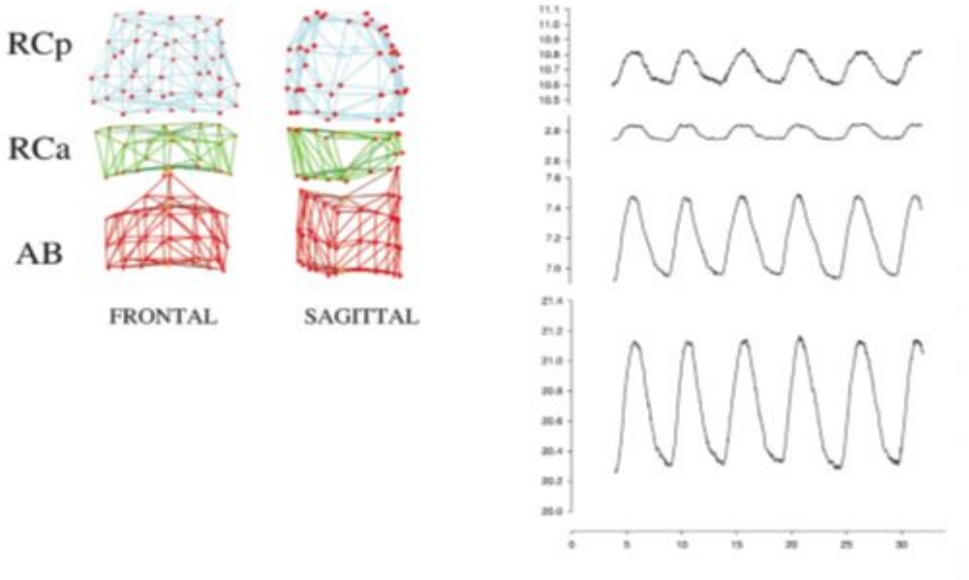

Figure 1.27: Volume changes for each compartment. Total Chest Wall volume is the sum of RCp, RCa and AB. From [45]

$$\sum_{i=1}^{K} \overrightarrow{F}\overrightarrow{n} A_i = V_{CW} \tag{1.13}$$

Where K is the number of triangles, A_i is the area of the *i-th* triangle and $\overrightarrow{n_i}$ is its outward normal vector.

From (1.26) it is possible to notice that the human geometric model divides the chest wall into three different regions, highlighted by different colors. In fact OEP allows to compute also the volumes of each region, that are, the rib cage (RCp), abdominal rib cage (RCa) and abdomen (AB). This is very useful if the goal of the analysis is for example the asymmetry of the respiratory muscles action or the behaviour of different structures under abnormal conditions (e.g. anaesthesia or mechanical ventilation).

Chapter 2

Materials and Methods

In this section will be described everything concerns the development of our study. Therefore the first part discusses about the entire experimental setup, that is the characteristics of the pigs and their preparation, the instrumentation used to acquire data, and the protocol followed for each pig. In the second part the reader can find a step-by-step description of the data processing, which has been performed from original data till the results shown and described in the next section.

2.1 Experimental Setup

The experiments took place at the Uppsala University Hospital, at Uppsala, Sweden. An overview of the experimental setup is reported in Figure 2.1, and it is basically composed by:

- Opto-Electronic Plethysmography (OEP) system;
- Analog Sensors (two for Pressure and one for Flow)
- Jet Ventilator
- Conventional Ventilator
- Arterial line for blood gas sampling

All these components are described in the following paragraphs.

2.1.1 OEP system

The OEP system used in this experiment was the BTS® OEP system, which is composed by six infra-red cameras, the flashing LEDs, the reflective markers placed on the

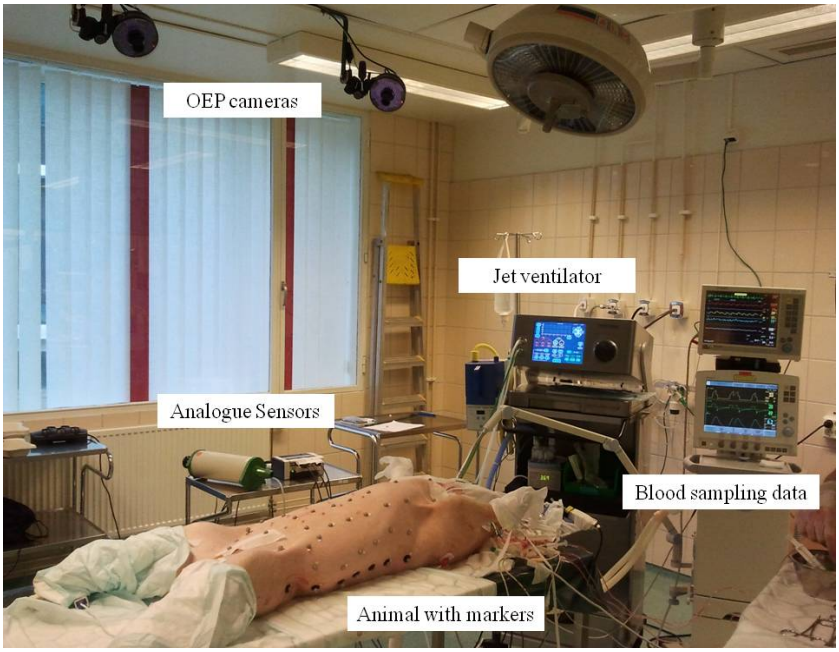

Figure 2.1: Overview of the experimental setup.

pigs and the process unit. The video cameras operate at a sampling frequency of 60 Hz, warranting high spacial resolution and time resolutions.

Before the acquisition, the system must be calibrated in order to ensure the reliability of detected data and defining the working volume, that is the volume containing the subject and its related markers where spacial resolution is warranted (figure (2.2)).

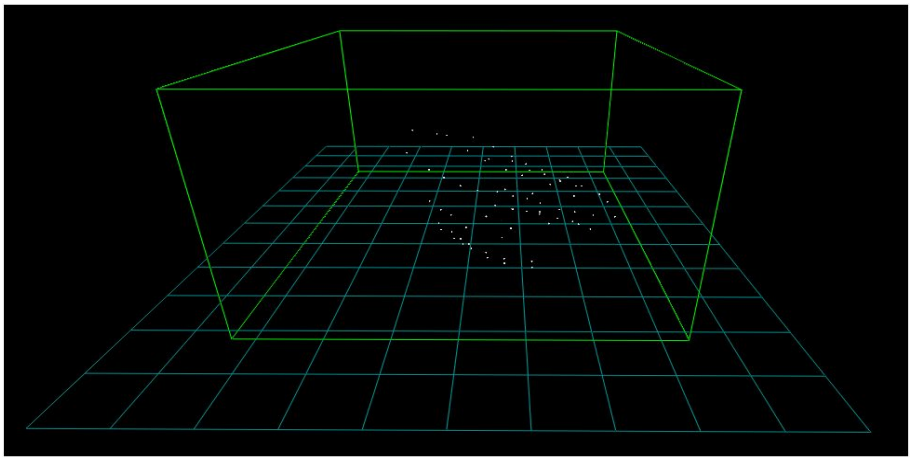

Figure 2.2: The green polyhedron is the calibrated volume, the checked plane is the reference plane (the bed) defined by the OEP's three-coordinate reference system, the white points are the detected tracks, which are supposedly related to the markers.

The calibration is performed in two different steps. First of all the OEP's three-coordinates reference system is positioned on the bed where the acquisition will take place, defining the three reference axes. A 600 frame axis acquisition is started, and

Figure 2.3: The pressure sensor used during the experiments

since each axes is characterized by a specific number of markers, the position and orientation of the reference system are recognized by the OEP system and set up.

Finally, during a 5000 frames acquisition, a small three-markers pole must be moved within the desired working volume, trying to cover each one of its voxel, "brushing" more where an higher resolution is desired. At the end of the calibration, a convergence message ensures that the OEP system has been successfully calibrated.

2.1.2 Analog sensors

2.1.2.1 Pressure Sensors

Pressures were measured by two Sensortechnics RCEM250DU (figure 2.3), whose characteristics are:

- linearity;
- differential;
- small size.

The technical characteristics are listed in table 2.1.

2.1.2.2 Flow sensor

Flow measurement is performed by a pneumotachograph, which is a resistance made up of a grid or capillary tubes that cause a pressure drop between the input and the output. Referring to the equation of motion (1.1) and knowing the resistance's value, the flow is calculated measuring the pressure drop.

Table 2.1: Technical characteristics of the pressure sensors

Characteristic	
Range of Pressure	$0 \div \pm 250$ cmH_2O
Dynamic Range	$0 \div 100$ Hz
Total Accuracy	$\pm$ 1.0%
Response Delay	0.5 ms

This kind of measurement is affected by the problem listed in paragraph 1.6.1, therefore this method is not suitable at all during jet ventilation, providing reliable data only during CVM.

2.1.2.3 Calibration

As the OEP system, also the analog sensors had to be calibrated before the acquisition.

Pressures sensors were calibrated by a simple u-tube manometer: they were connected to the column of water and steps of 5 cmH_2O were progressively imposed, starting from 0 to 40 cmH_2O upward and downward, and the output voltage signal (figure 2.4(a)) was recorded by the OEP system.

Flow sensor is calibrated in a similar way: a syringe containing a known volume (2 liters) is repeatedly emptied and overfilled through the sensor, and its output (figure 2.4(b)) is recorded by the OEP system as well.

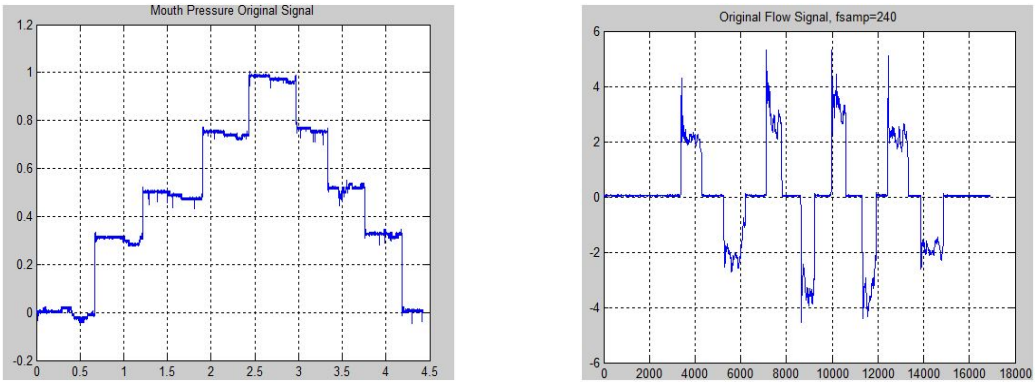

(a) Pressure (b) Flow

Figure 2.4: Signal acquired during pressure (a) and flow (b) calibration.

Then, taking advantage of the sensors' linearity, the Matlab® function *AnalogCal.m* estimates the parameters of the linear regression curve that allow to transform voltage values into pressure or flow values.

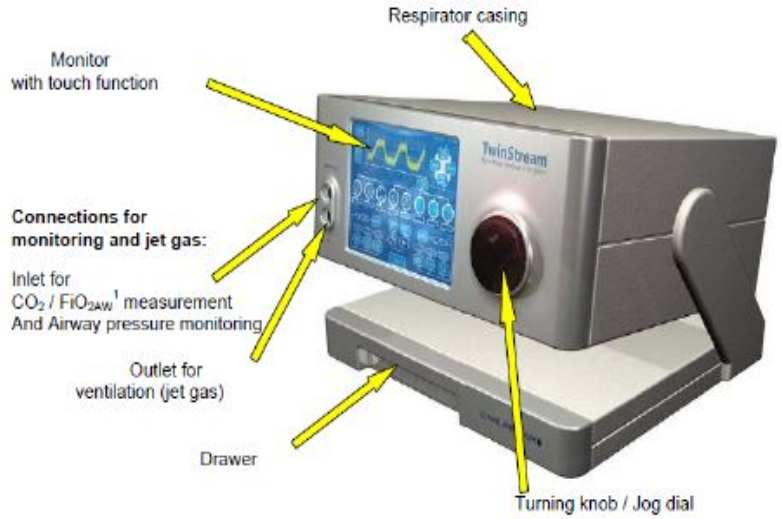

Figure 2.5: The Twin Stream front panel.

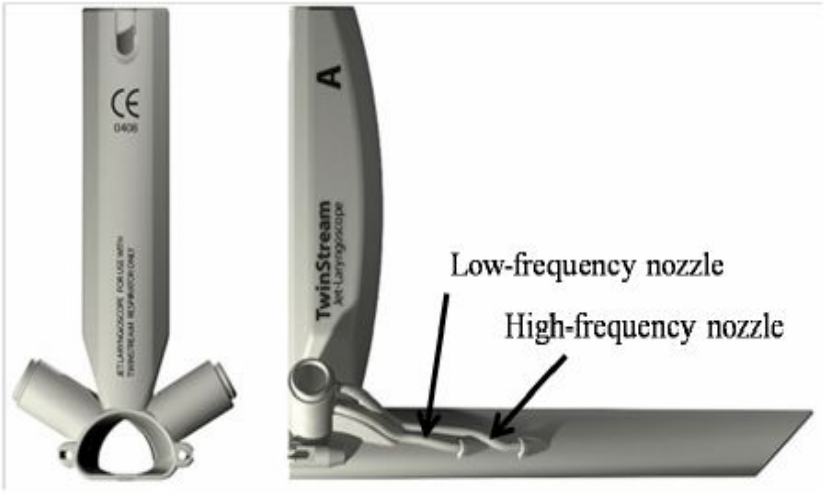

Figure 2.6: Twins Stream's laryngoscope

2.1.3 Jet Ventilator

The jet ventilator used in this study was the Carl Reiner GmbH Twin Stream®, which can be employed for seven different ventilation modes for all forms of jet ventilation. The clinician sets the ventilation mode from the touchscreen menu (figure 2.5) and the ventilator calculates automatically the initial ventilator settings according to the patient's weight.

The gas is delivered through two nozzles (one for HF and the other for LF jet) integrated in a special laryngoscope (figure 2.6), which has a central opening on the top that 'opens' the system allowing gas entrainment and permits the access to the airways to either surgery instruments or humidifier.

Easyconnectors® ensure the optimal connection between the tubes and the ventilators, being equipped by three O-rings which avoid performance impairments that may lead to incorrect pressure values or incorrect gas analysis.

Finally, Twin Stream® is equipped with two independent oxygen sensors for accurate gas management: one sensor measures the FiO_2 delivered by the ventilator, the second measures the FiO_2 in the airway.

2.2 Population and its preparation

This study has been made over a population of 10 pigs, characterized by an average weight of 28.99 ± 1.93 kg and an average age of 3 months.

The pigs were premedicated by intramuscular injection of Xylazine 2.2 mg kg^{-1}, Tiletamine 3 mg kg^{-1} and Zolazepam 3 mg kg^{-1}. After approximately 10 minutes, the pigs were placed supine and vascular access was established by cannulation of an ear vein.

A bolus of 100-500 μg Fentanyl was injected intra-venous and the animals' tracheas were orally intubated (Hi-Contour ™ Tracheal Tube, inner diameter (ID) 8.0 mm, length cut to 210 mm, Mallinckrodt Medical, Athlone, Ireland) and volume control ventilation was started (Servo-I, Maquet, Sweden) with tidal volumes of 10 ml kg^{-1} and respiratory rate was adjusted to achieve normocarbia (5-6 kPa).

Then, a high open tracheotomy was performed and the endotracheal tube was advanced until the cuff balloon reached the stoma. Inflation of the balloon sealed the stoma in an airtight manner. The stoma was later used to insert the obstructive stents, consisting on 2 cm long cylinders characterized by inner diameter (ID) of 2, 4, 6 and 8 mm and outer diameter of 9.7 cm. The stent was held in place and air leakage at the side of the stent was avoided by external compression of the trachea using a cotton band.

Intravenous anaesthesia was started and maintained intravenously using Pentobarbital (7-9 mg (kg h)$^{-1}$) and morphine (420-540 μg (kg h)$^{-1}$). After ascertaining that anaesthesia was adequate, Pancuronium (280-360 μg (kg h)$^{-1}$) maintained neuromuscular block. Subsequently, the neck vessels were dissected and an arterial line for invasive blood pressure measurement and blood gas sampling was placed in the left carotid artery. A pulmonary artery catheter was inserted into the left internal jugular vein and advanced into wedge position verified by pressure monitoring. Suprapubic urinary bladder catheterization was performed by a minilaparotomy and incision of the urinary bladder. ECG monitoring was started and SpO_2 was measured by photoplethysmography on the tail base.

Figure 2.7: The chest-wall of the pig with the 57 passive markers for the OEP acquisition.

2.2.1 Preparation of the animals for OEP acquisition

The pigs were positioned on a rigid bed in the supine position. The legs of the pig were tied to the bed in order to maximize the visibility of every markers for the cameras. 57 reflective markers were positioned on the anterior chest wall of the pig (figure 2.7), according to the geometrical model described paragraph 2.5.3, in order to allow the circumferential measurement of the chest wall displacements. The chest wall has been divided in two compartments, the rib-cage and the abdomen, following the anatomy of the pig and choosing the lower costal margin as a reference.

2.3 Protocol

The aim of this study was to analyse the effects of the application of High Frequency Jet Ventilation (HFJV) and Superimposed High Frequency Jet Ventilation (SHFJV) at several ventilation rates on animals whose tracheal caliber is reduced to 2, 4, 6 and 8 mm by means of a stent. The protocol has been chosen in order to perform each ventilation mode in all the pigs and for every obstruction grade, always ensuring the same initial condition to nullify the effects of the previous modes.

HFJV has been delivered at 50, 100, 150, 200, 400 and 600 bpm, and SHFJV was obtained by superposing to these high frequencies a LFJV set at 16 bpm. It is evident that that application of all these ventilation modes for each stent made the protocol

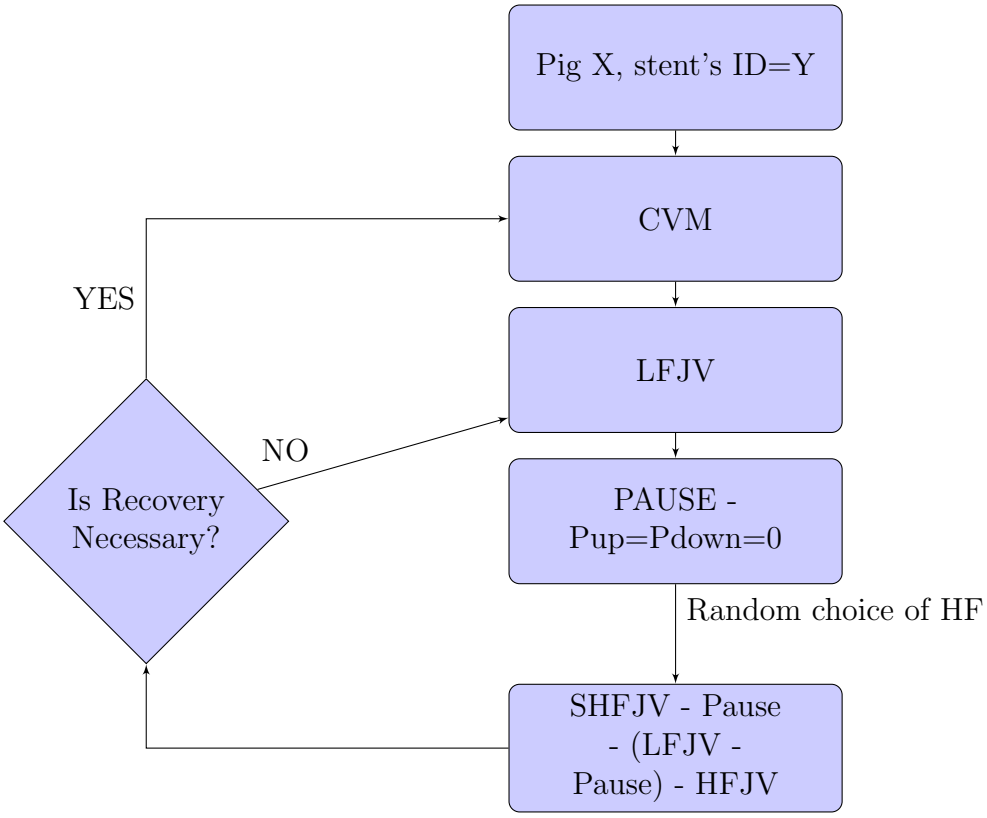

Figure 2.8: Description of the protocol employed for each pig and for each obstruction grade. Stent's ID=stent's Inner Diameter, CVM=Conventional Ventilation Mode, LFJV=Low Frequency Jet Ventilation (16 bpm), HFJV=High Frequency Jet Ventilation, SHFJV=Superimposed High Frequency Jet Ventilation. Each ventilation mode was performed for about 5 minutes.

very long, near to 12 hours long for each pig.

As Figure 2.8 shows, mechanical ventilation started with the application of CVM that ensured good oxygenation and good carbon dioxide washout. After 4-5 minutes the steady state was reached so it was possible to switch to LFJV only (at 16 bpm) that has been used in order to facilitate the return to optimal initial conditions.

At the end of LFJV a pause has been performed. The pause is very important because it persists until both upstream and downstream pressures return at the atmospheric value, therefore the end of this pause can be considered as a reference point, being the common initial condition for every ventilation mode, and allowing the comparison of the effects of each ventilation mode.

Finally, the high frequency to apply is randomly selected and the related HFJV and SHFJV are performed (settings are reported in Table 2.2), intermediated by a Pause or sometimes by the sequence *Pause - LFJV - Pause* that ensures the common initial conditions.

Table 2.2: Ventilator settings during the experiment

Parameter	Settings
LF	16 bpm
LF Driving Pressure	1.6 bar
HF Driving Pressure	0.8 bar
LF I:E ratio	1:1.5
HF I:E ratio	1:1.5
FiO_2	50%

At this point the health condition of the pig is evaluated through the arterial blood gas analysis. If a recovery is necessary, for example because of hypercapnic condition, the protocol proceeds restarting from the application of CVM (FiO_2 100%) that allows the recovery of the pig, otherwise it continues directly from the application of LFJV only and follows with the application of the other high frequencies.

This protocol has been repeated for each obstruction and for each pig.

2.4 Data acquisition

2.4.1 3D data

During the entire protocol, chest-wall volumes was measured by the OEP system because, as already explained, tidal volume measurements during jet ventilation are complex because the patient-ventilator is an open system and delivered volume depends also on the amount of entrained air. For these reasons, conventional techniques such as spyrometers or integration of flow are not suitable for this application, and total body plethysmography could not be realized in the operating room. Moreover, OEP works at the sampling frequency of 60 Hz that allows to acquire reliable data without loss of information, whereas conventional techniques cannot work as such high frequencies.

The first of the two problems related to the acquisition by means of the OEP system is that all the markers must be constantly seen by the cameras, and this is not always possible because during the acquisition the surgeon entered in the field of view of the cameras (e.g to perform blood gas analysis or to fix some problem with the obstruction or with the markers) causing loss of information about one or more markers for few frames. This problem can be solved during data processing only if no more that two or three markers disappear for few frames.

Second, the system acquires anything has characteristics (shape and dimension) similar to the markers, therefore it is possible that reflexes coming from the environment or from the instrumentation could be recorded as marker. These tracks, called *outliers*

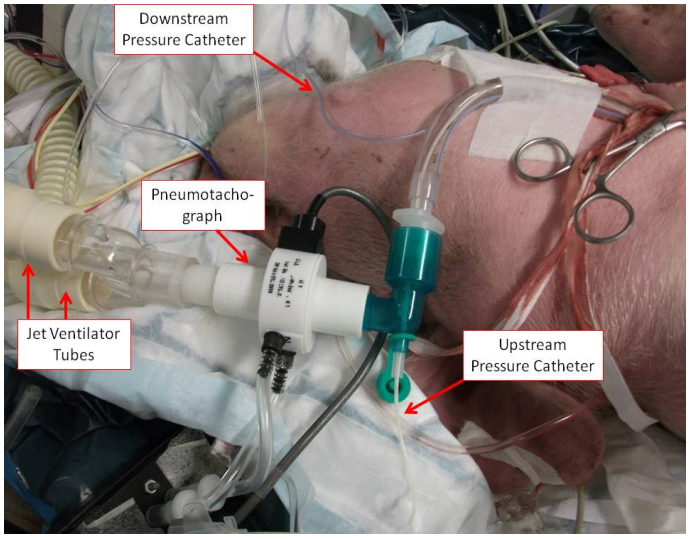

Figure 2.9: Connection of jet ventilator, pneumotachograph, endotracheal tube and pressure sensors.

can be easily removed during data processing either automatically or manually in dependence of their position; in fact if an outlier is within the other tracks, it is hardly erasable by an algorithm and the manual-way is preferred.

Data acquired by the OEP system is synchronized and completed by pressure and flow data coming from analog sensors, and stored in a *.tdf* file. Since each acquisition cannot be longer than ten minutes and the protocol was about twelve hours long, several recordings were stored and subsequently merged by an algorithm, as explained ahead.

2.4.2 Analog Data

Analog sensors acquired pressure and flow data during all the protocol. The experimental layout is represented in figure 2.9: flow is detected by a pneumotachograph positioned at the beginning of the endotracheal tube, thus the breaths delivered by the either the conventional ventilator or the jet ventilator pass trough the pneumotachograph to reach the endotracheal tube. For this reason during CVM the system is closed by *cuffing* the end of the endotracheal tube and the flow is correctly measured, while during JV no cuff is used, thus the open system does not permit a correct flow measurement.

Pressures are measured by means of two catheters connected to the analog pressure sensors: one catheter passes through the endotracheal tube and measures the pressure above the obstruction (Upstream pressure), while the second catheter enters in the trachea below the obstruction, measuring the Downstream Pressure. The outputs of the three analog sensors are then acquired by the OEP system and synchronized with

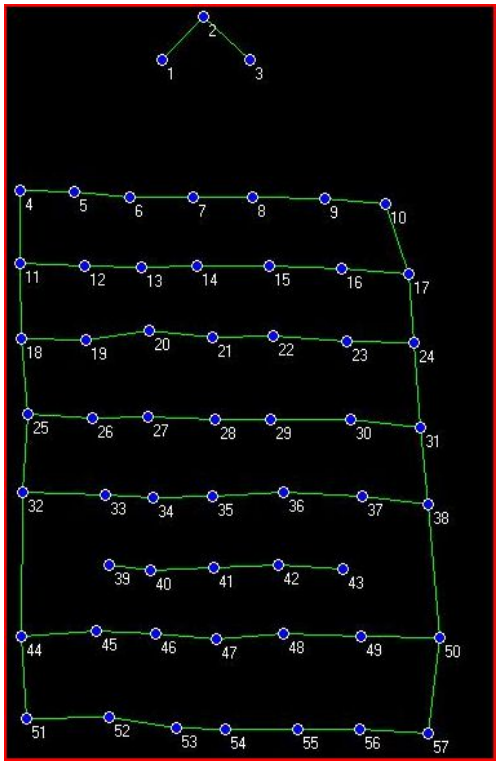

Figure 2.10: The markers classification model. The detected tracks must be ordered accordingly to this model.

three-dimensional data.

2.5 3D data processing

The OEP system provides 3D data in form of a matrix containing the three coordinates (X-Y-Z) of any detected track in function of time, synchronized with analog data, which are tension values related to measured pressures or flow. As described in the paragraph 1.7.1, the goal is to compute the volume enclosed by the surface described by the markers, in order to obtain time-varying signals that represent the volume variations of rib-cage, abdomen and chest wall.

When markers are detected by OEP, their respective tracks are randomly classified, and this condition does not permit a correct computation of the volume. In fact, tracks must be classified according to a pre-designed model (figure 2.10) in order to correctly perform the interpolation of the tracks themselves, which corresponds to the application of a geometric model that consists in the mash of triangles discussed in paragraph 1.7.1.

2.5.1 Labeling

The first step of the 3D data processing is the classification of the tracks for each stored file. This process is called *labeling*. In this study, since the protocol was very long and has been repeated for 10 pigs, it was necessary to label about 1200 files, therefore, an automatic labeling software has been developed.

Since this software operates by applying geometric consideration, it was necessary to orient the pig according to a known frame of reference, represented by the Cartesian Coordinate System of the OEP system calibration (figure 2.11). This has been implemented by the Matlab® function *GiraPig.m*, which requires a manually-labeled file to generate the roto-translation matrix that must be applied to each file related to that OEP calibration.

At this point the coordinates of the tracks are referred to a known reference system and are contained in a $M\ X\ 3N$ matrix (Figure 2.12), in which columns are the X-Y-Z coordinates of the N tracks (randomly sorted) and rows represent the M frames composing the acquired file.

Subsequently the labeling software, which is the Matlab® function *TrackingPig.m*, implements both labeling and tracking for each file as described below:

- the coordinates' matrix is copied and the software works on the copy in order to avoid eventual corruption of original data.

- the first row of the matrix(corresponding to the first frame of the file) is closed off. Since the OEP sensor detects markers and anything that can be mistaken for a marker, it may be possible that the number of the N tracks is bigger than the numbers of markers, and therefore it may be dangerous to consider a random frame that may contain tracks related to a noisy environment. For this reason, all the geometric considerations are applied only on the first frame, where is easy to check the eventual presence of any outlier that can be identified and removed by means of additional geometric considerations.

- the software identifies one-by-one each track following the flow-chart reported in figure 2.13, classifying it according to the order stated in the model (figure 2.10). After the classification of each track, its original coordinates values are set up in order to not interfere with following classifications (the software is not working on the original matrix, thus original coordinates are not lost).

- at the end of the classification, the software moves the original matrix's columns related to each classified track in the right position according to the classification

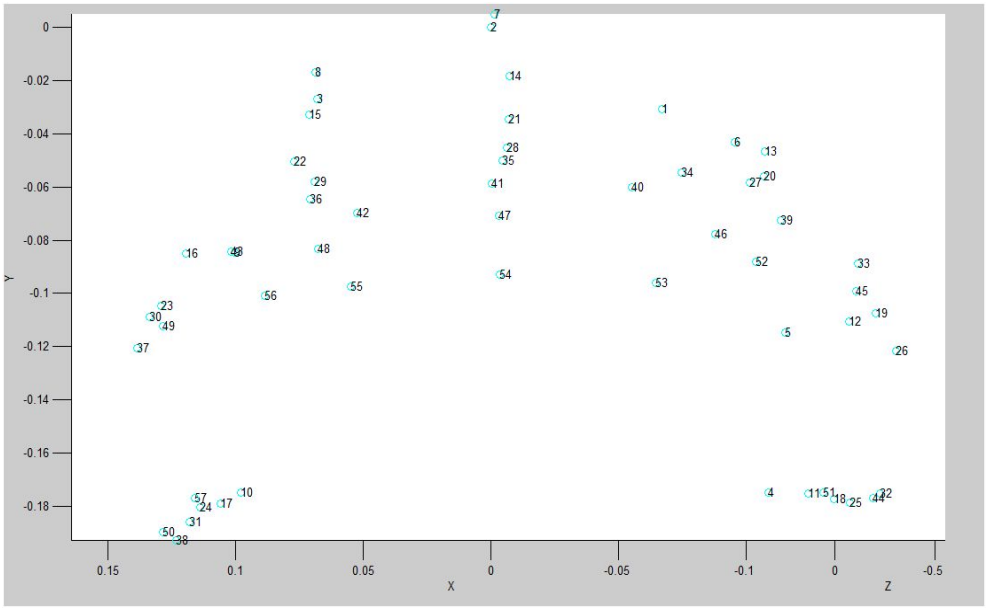

(a) Y-X

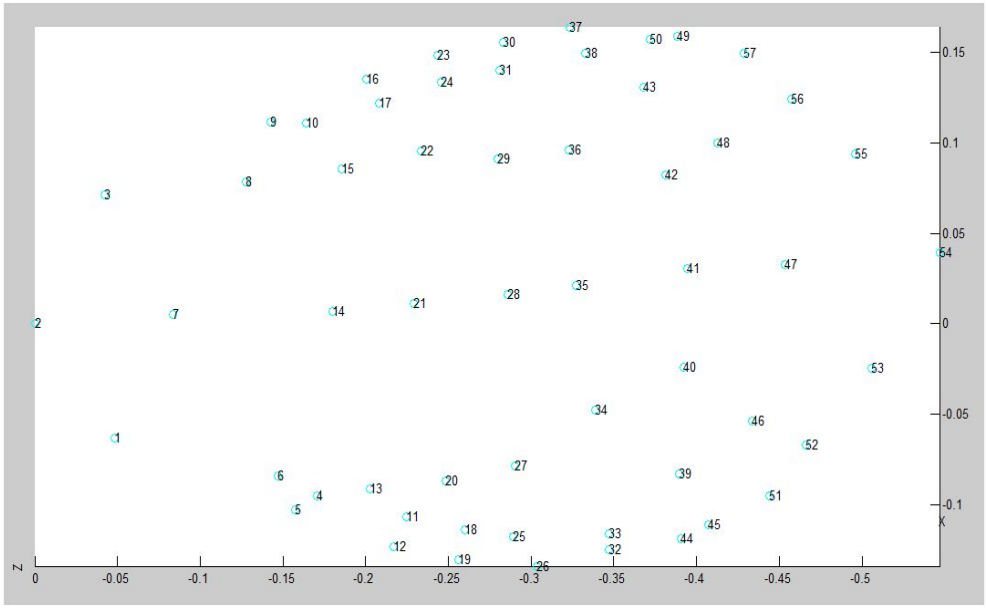

(b) Z-X

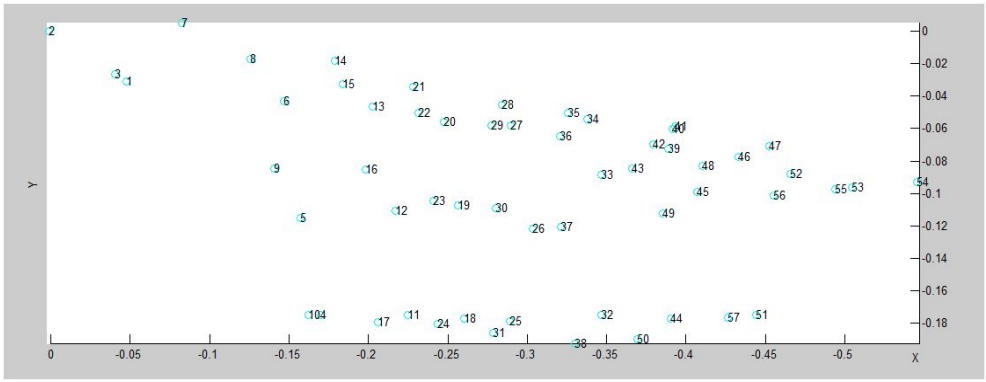

(c) Z-Y

Figure 2.11: Tracks related to the markers on the chest-wall of the pig. View of the Y-X (a), X-Z (b) and Z-Y (c) plane, where X corresponds to the medio-lateral, Y to the antero-posterior and Z to the cranio-caudal axes of the pig.

	X track 1	Y track 1	Z track 1	X track 2	Y track 2	Z track 2	...
Frame1							
Frame2							
...							

Figure 2.12: Representation of the matrix containing the X-Y-Z coordinates of the tracks.

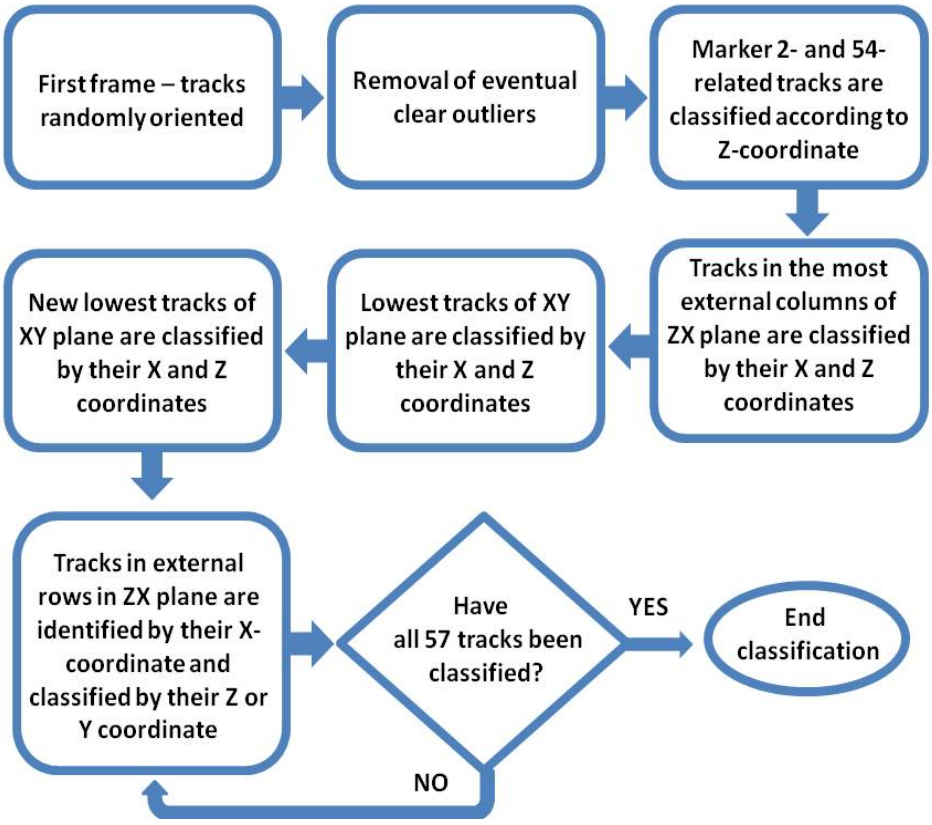

Figure 2.13: Flow-chart of the labeling software. After the classification of each track, its coordinates are set up at 100 in order to not interfere with following classifications.

order(figures 2.14 and 2.15 report an example) and applies the new labels, numbering progressively the ordered tracks from 1 to 57 in order to make possible the following label-based interpolation.

- *Tracking* is then performed extending the new order of the first row to all the rows, that is the ordered tracks are 'chased' frame-by-frame for the entire acquisition.

It is important to highlight that the columns related to tracks that pop up during the acquisition (thus are not classified in the first frame) are not deleted but are kept in the matrix, because they may be related to either outliers (therefore they can be easily manually removed) or marker whose signal has been lost for some instants, representing information that cannot be eliminated.

2.5.2 References Generation

At this point we have chosen that marker arrangement that allows to build the anterior chest-wall surface of the pig, but, being the pig in a supine position, the posterior part of the chest wall is not accessible to the cameras, therefore it is not possible to apply the divergence theorem (equation 1.11) necessary to compute the volume. This problem has been solved by Aliverti et al. [49] considering that the hidden part of the trunk is fixed on a rigid bed and it remains still over the whole acquisition, therefore virtual markers placed on the horizontal plane of the bed define the posterior surface that allows to get the chest-wall close surface, from which volume is then calculated.

The virtual markers are created by the Matlab® function *UppsalaPigBedGeneration.m*, which reconstructs the reference plane by using the lower lateral real markers, that are the closest to the real bed. One file at the beginning of the acquisition was chosen, and, considering the first 60 seconds of acquisition, the lowest lateral real marker was identified and used to define the reference plane by lowering its y-coordinate of 2 cm. Then, the x- and z- coordinates of the all lateral markers were projected in this plane, forming the virtual markers that define the plane where the pig's chest-wall posterior surface lies.

These virtual markers are then applied to all *.tdf* files (referring at the same OEP calibration) and labeled as if they were real markers by the Matlab® function *UppsalaNewPigModel.m*.

It is evident that the choice of the virtual markers' position affects the computation of absolute volumes, but since the aim of the investigation is to quantify only volume variations, this error will not influence the final results.

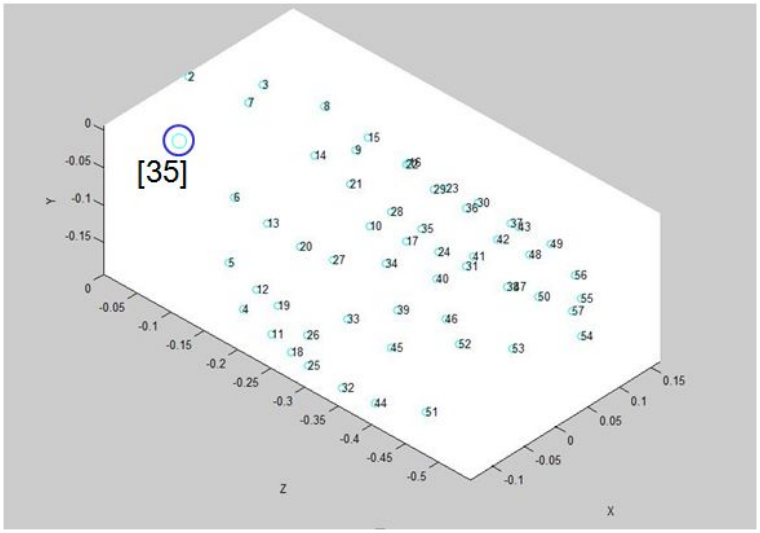

Figure 2.14: Roto-traslated tracks related to the markers on the pig. Tracks 35 is highlighted, and corresponds to the marker 1.

(a)

	X track 1	Y track 1	Z track 1	X track 2	Y track 2	Z track 2	...
Frame1							
Frame2							
...							

(b)

	X track 35	Y track 35	Z track 35	X track X	Y track X	Z track X	...
Frame1							
Frame2							
...							

Figure 2.15: Representation of the column shift used for labeling. (a) represents the randomly ordered matrix of tracks, then, since track 35 refers to marker 1, its related columns are moved in the first position (b).

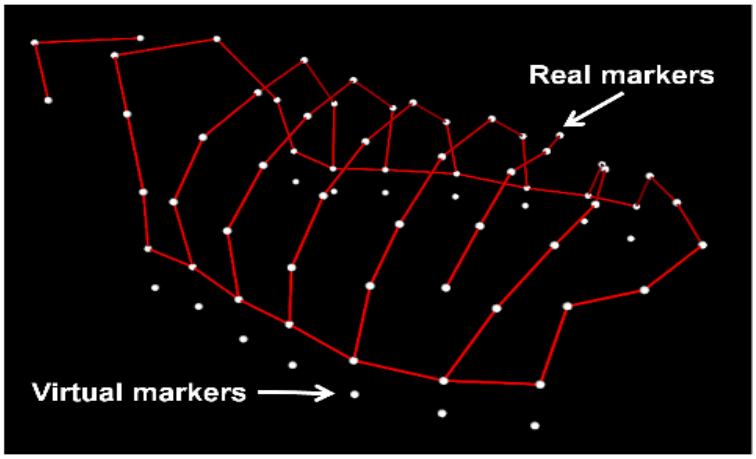

Figure 2.16: Representation of the 57 real markers detected by OEP and linked following the right order, with the virtual markers used to identify the reference plane.

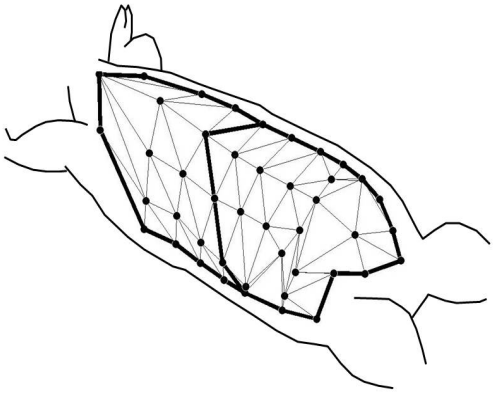

Figure 2.17: The geometrical model used to interpolate the key-points. It is possible to notice the upper region, that is the rib-cage, and the lower region, that is the abdomen.

2.5.3 Surface reconstruction and Volume Computation

The next step is the interpolations of the tracks, also called key-points, throughout a geometrical model that defines a mesh of triangles whose vertexes are the points themselves and divides the entire chest-wall in two compartments, as described in the description of OEP (paragraph 1.7.1):

a previously implemented program called *vemgbis*, applies the geometrical model to the cloud of 71 markers (57 real + 14 virtual) and applies the divergence theorem, computing the rib-cage, abdomen and chest-wall volumes for each frame that compose each *.tdf* file, obtaining a time-varying signal for the volumes. Moreover, this program applies the calibration parameters to the analog pressure and flow signals estimated as described in paragraph 2.1.2, providing as output a *.dat* file (figure 2.18) containing:

- time;
- rib-cage volume vs time;
- abdomen volume vs time;
- chest-wall volume vs time;
- flow vs time;
- upstream pressure vs time;
- downstream pressure vs time.

Then, then Matlab® function *FirstLastMin.m* links together all the *.dat* file related to the same pig with the same obstruction, obtaining the global pressure, volume and flow time-related signals over the entire protocol.

2.5.4 Extraction of Parameters

The study of the ventilatory pattern implies the measurement of volume and pressure variations due to the application of each ventilation mode, therefore the following parameters have been evaluated (figure 2.19):

- tidal volume (V_T)
- end expiratory volume variation (ΔEEV)
- end inspiratory volume variation (ΔEIV)

for both rib-cage, abdomen and chest-wall, and, in terms of both upstream and downstream pressure:

- driving pressure (DP)
- peak expiratory pressure (ΔPEP)
- peak inspiratory pressure (ΔPIP)

Looking to the graphs it is evident that it is not possible to evaluate these parameters at any breath, because in the first seconds of any ventilation mode there is a transient period that drives the system to the equilibrium condition (figure 2.20), in which parameters variations cannot be taken in count. As explained in paragraph 1.5.3, the transient is due to the fact that the physiological relaxation time is longer

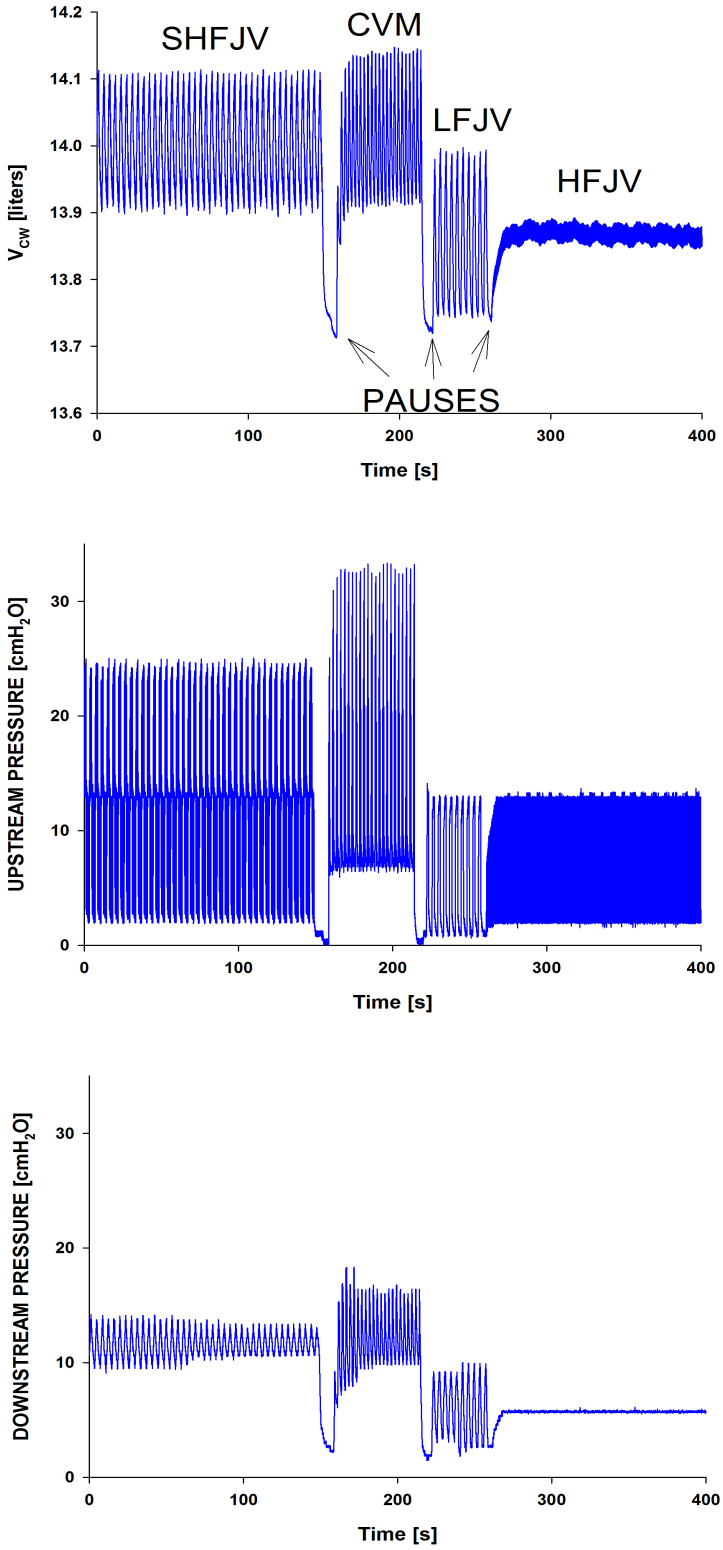

Figure 2.18: Example of chest-wall volume, upstream and downstream pressures tracks contained in a *.dat* file. Ventilation modes and pauses are highlighted. Please note the magnitude difference between the upstream and the downstream pressure, which is due to the obstruction (in this case 4 mm).

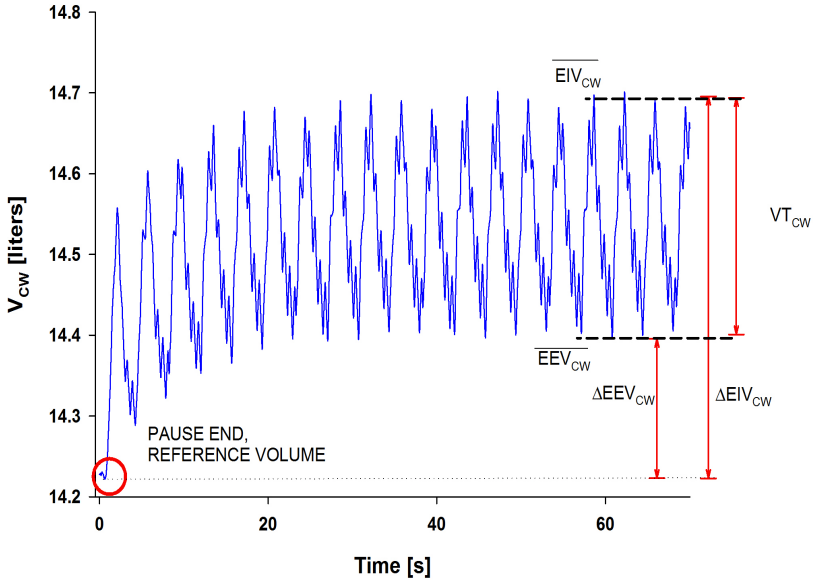

(a) V_{CW} during SHFJV

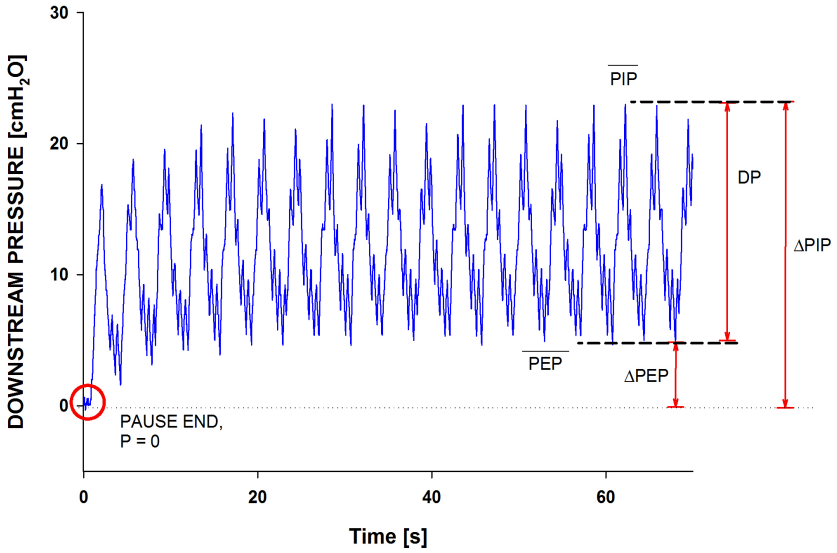

(b) $P_{downstream}$ during SHFJV

Figure 2.19: Representation of parameters: (a) VT_{CW}=tidal volume, ΔEEV_{CW}=end-expiratory chest wall volume variation, ΔEIV_{CW}=end-inspiratory chest wall volume variation, $\overline{EIV_{CW}}$=end inspiratory average volume, $\overline{EEV_{CW}}$=end expiratory average volume. (b) ΔPEP=peak expiratory pressure, DP=driving pressure, ΔPIP=peak inspiratory pressure. $\overline{PEP}$=average peak expiratory pressure, $\overline{PIP}$=average peak inspiratory pressure. Note that ΔPEP should be equal to $\overline{PEP}$ and ΔPIP should be equal to $\overline{PIP}$, since the reference pressure should be zero.

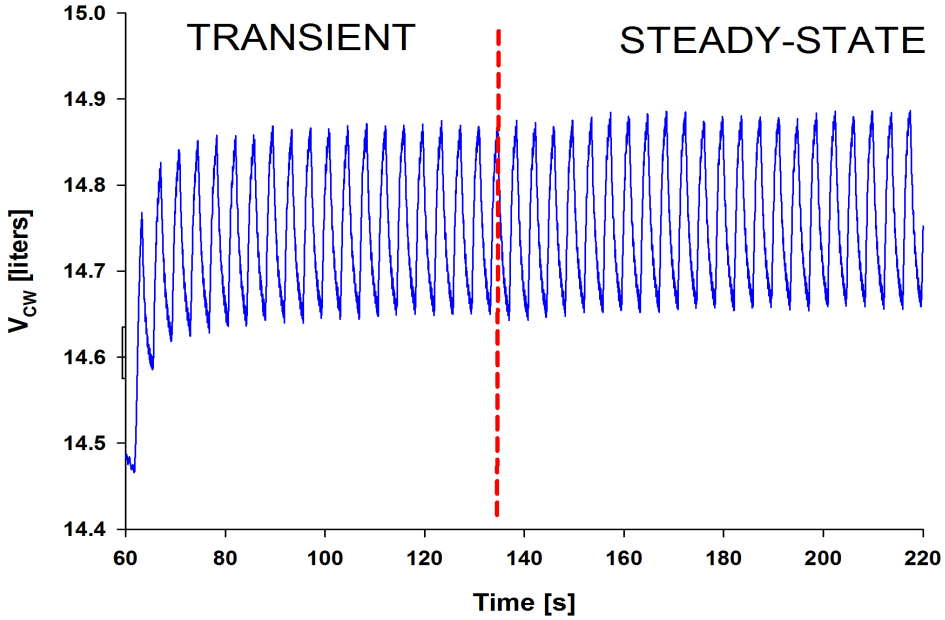

Figure 2.20: Transient and steady state periods during SHFJV.

than the ventilator's expiratory time, causing air trapping until when the equilibrium condition has been reached.

In this study the last 30 seconds of each ventilation mode have been considered to represent the steady-state condition where the parameters have been computed, even though in some cases the steady-state condition was not perfectly defined at any time. In fact, with the 2 mm ID stent, the chest-wall volume increased for the entire application of the ventilation modes since the highly increased resistance made τ much longer than normal.

The software Diamov® has been employed to select those points that permit the computation of the parameters (figure 2.21):

- the end of the pause, corresponding to the reference point;
- each maximum and each minimum within the last 30 seconds of the following ventilation mode, which correspond respectively to the end-inspiratory and end-expiratory points of each breath.

At this point any single breath within the steady-state is defined by three points (figure 2.21(b)); the Matlab® function *UppsalaPigRestricted.m* computes the parameters for any single selected breath and calculates the mean values (indicated as e.g. $\overline{EEV_{CW}}$) and the related standard deviations. Finally, it writes the results in a Microsoft® Excel® worksheet that will contain all the parameters characterizing the application of any ventilation mode on each pig.

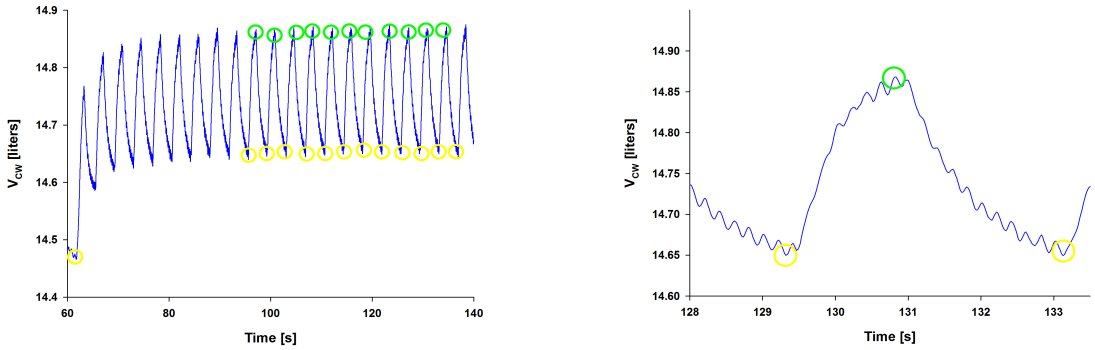

(a) (b)

Figure 2.21: (a)Maxima and Minima selected in a SHFJV's volume track.(b)Zoom of a single breath defined within two end-expiration points (yellow circles), with its end-inspiration point(green circle).

For each ventilation mode the parameters are computed as:

- variations of end-expiratory (EEV) and end-inspiratory (EIV) volumes are calculated evaluating both rib-cage, abdomen and chest-wall volumes in correspondence of the selected points, referring to the volume at the end of the pause;

$$\Delta EEV_{MODE} = \overline{EEV_{MODE}} - V_{PAUSE} \tag{2.1a}$$

$$\Delta EIV_{MODE} = \overline{EIV_{MODE}} - V_{PAUSE} \tag{2.1b}$$

- tidal volume is computed as the difference between $\overline{EIV}$ and $\overline{EEV}$:

$$VT_{MODE} = \overline{EIV_{MODE}} - \overline{EEV_{MODE}} \tag{2.2}$$

- variations of PEP and PIP are evaluated looking for the maximum (PIP) and the minimum (PEP) value within the breath and referring them to reference pressure (P_{PAUSE}, which should be zero), for both upstream and downstream pressures. Instead of PIP and PEP, it was possible to evaluate end-inspiratory and end-expiratory pressures by considering pressure data in correspondence of the points defining the breath (end-inspiration and end-expiration), but in this way results would be characterized by higher standard deviation due to the subjective phase shift between volume and pressure in presence of high ventilation frequencies.

$$\Delta PEP_{MODE} = \overline{PEP_{MODE}} - P_{PAUSE} \tag{2.3a}$$

$$\Delta PIP_{MODE} = \overline{PIP_{MODE}} - P_{PAUSE} \tag{2.3b}$$

- the difference between PIP and PEP is the driving pressure:

$$DP_{MODE} = \overline{PIP_{MODE}} - \overline{PEP_{MODE}} \tag{2.4}$$

- the difference between upstream and downstream pressure is the pressure drop across the obstruction:

$$\Delta P_{R_{ins}} = \overline{PIP_{MODE_{upstream}}} - \overline{PIP_{MODE_{downstream}}} \tag{2.5a}$$

$$\Delta P_{R_{exp}} = \overline{PEP_{MODE_{upstream}}} - \overline{PEP_{MODE_{downstream}}} \tag{2.5b}$$

Subsequently all these parameters have been grouped by obstruction and ventilation mode, in order to compute average values and standard deviations over the entire population for each group, and these value are represented in the graphs reported in the next chapter.

Two pigs died during the experiment (pig 8 and pig 10) and in some cases the computation of the parameters presented some technical problems, due for example to problems with sensors or to missing markers, which led to wrong and unreliable results that have not been taken in count for the computation of the mean values over the population. However, no parameter has been computed over less than 6 pigs, ensuring the validity of the obtained results.

2.5.5 Statistical Validation

Results have been plotted in the graphs reported in the next chapter, and although some considerations could seem evident, a statistical validation was necessary to ensure the validity of the reflections.

For this purpose all processed data were grouped in two main groups, one concerning HFJV and the other concerning SHFJV, and a *Two-Ways ANOVA* test has been performed for each group, choosing as factors the jet ventilator's high frequency and the obstruction grade in order to evaluate the influence of these factors on the parameters listed below:

- Tidal Volume for Chest-Wall, Abdomen and Rib-Cage;
- End-Expiratory Volume of Chest-Wall, Abdomen and Rib-Cage;
- Upstream Driving Pressure;
- Downstream Driving Pressure;

- Downstream Peak Expiratory Pressure.

The results of the test are resumed in the graphs indicating their respective *p-value*, that is defined as *the probability of obtaining a test statistic at least as extreme as the one that was actually observed, assuming that the null hypothesis is true.* In other words, when p-value is less than the significance level (which is 0.05) the null hypothesis is rejected and the results are statistically significant, meaning that the evaluated parameter depends on the factors.

2.6 Computation of Mechanical Parameters

The second aim of this study was the estimation the mechanical parameters of the pigs' respiratory system, that is Resistance and Compliance, in presence of the different obstruction grades. As already discussed, these parameters determine the relaxation time constant of the respiratory system, and therefore they are related with the increase in the end-expiratory volume and with the chest-wall mechanics in general.

Referring to the viscoelastic model of the respiratory system reported in the beginning of this thesis, total Resistance and Compliance can be easily determined during flow- or volume- controlled ventilation considering the pressure drop correspondent to the pause between inspiration and expiration. In this study, a short pause (about 0.2 s) was evident on both flow and pressure signals related to CVM (figure 2.22), therefore it was possible to compute both R and C as follows:

$$C_{RS} = \frac{V_T}{P_2 - P_{ee}} \tag{2.6a}$$

$$R_{RS} = \frac{P_{max} - P_2}{\dot{V}_{insp}} \tag{2.6b}$$

According to the viscoelastic model, it would be possible to compute the airways resistance and the lung tissue resistance separately, considering also P_1. However, since P_1 is difficultly identifiable, only total resistance has been calculated.

As figure 2.22(a) shows, during HFJV, SHFJV and LFJV the patient-ventilator is an open system and the flow sensor connected to the endotracheal tube did not recorded any considerable flow; thus, only CVM could be considered to compute the mechanical parameters.

The software Diamov® has been employed to select all maxima and minima of the CVM volume signal, identifying each breath by three points that are used by the Matlab® function *NormalizzaBreath.m* to compute the "model" breath, which is the

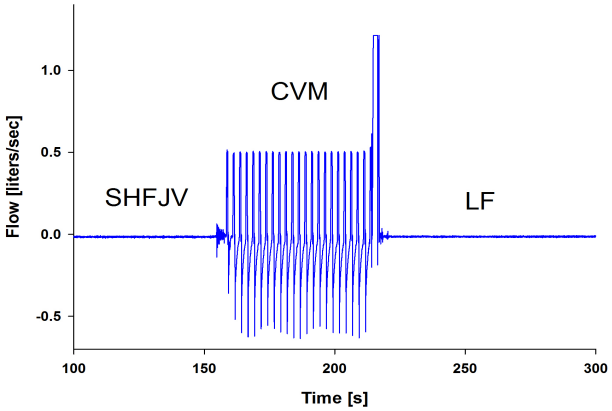

(a)

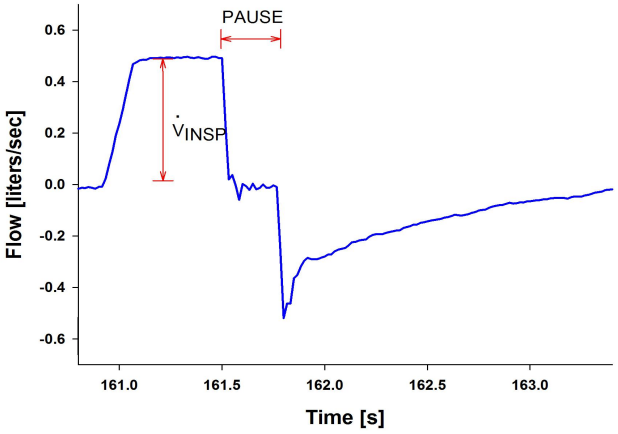

(b)

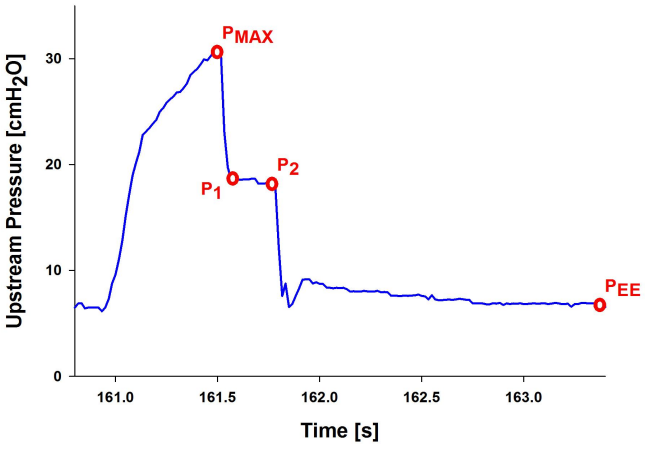

(c)

Figure 2.22: (a)Recorded flow during SHFJV, LFJV and CVM. It is evident that during jet ventilation the output signal is similar to a white noise, whereas during CVM the signal corresponds to the flow delivered by the ventilator. Zoom of flow (b) and pressure (c) signal during a single CVM breath.

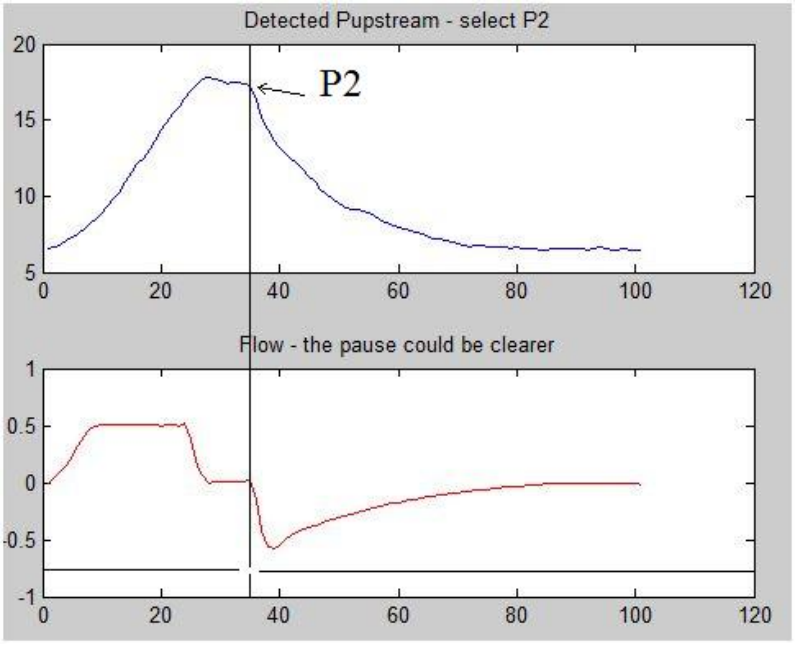

Figure 2.23: GUI showing upstream pressure and flow curves in order to easily identify P_2.

average of all the selected breaths in terms of pressure (upstream and downstream), volume and flow.

On the "model" breath the software *NormalizzaBreath.m* automatically calculates tidal volume and identifies the points P_{max} and P_{ee} looking for, respectively, the maximum and the minimum value of the upstream pressure. Then, its GUI asks the user to choose throughout the mouse the point P_2 in the upstream pressure curve, and two points on the flow curve whose average is considered as the inspiratory flow value.

At low obstruction grade (especially with 8 mm ID stent), the point P_2 is not so evident on the pressure curve, therefore also the flow curve is plotted on the same GUI. Here, in fact, the pause set in the ventilator between inspiration and expiration is clearer, and the user can identify much more easily P_2 (figure 2.23).

In this way the algorithm gets all those information it needs to apply equations 2.6 and computes R_{RS} and C_{RS}: in the next chapter the results are plotted in function of the obstruction grade.

Furthermore, this software computes also the resistance provided by the only obstruction. This is implemented by considering the curve of the pressure drop ΔP across the obstruction (ΔP=$P_{upstream} - P_{downstream}$) during the inspiration:

$$R_{OS} = \frac{\Delta P_{insp}}{\dot{V}_{insp}} \tag{2.7}$$

R_{RS} and R_{OS} are calculated also considering as flow the derivative of V_{CW}, expecting similar results. The software *NormalizzaBreath.m* computes the derivative term, which

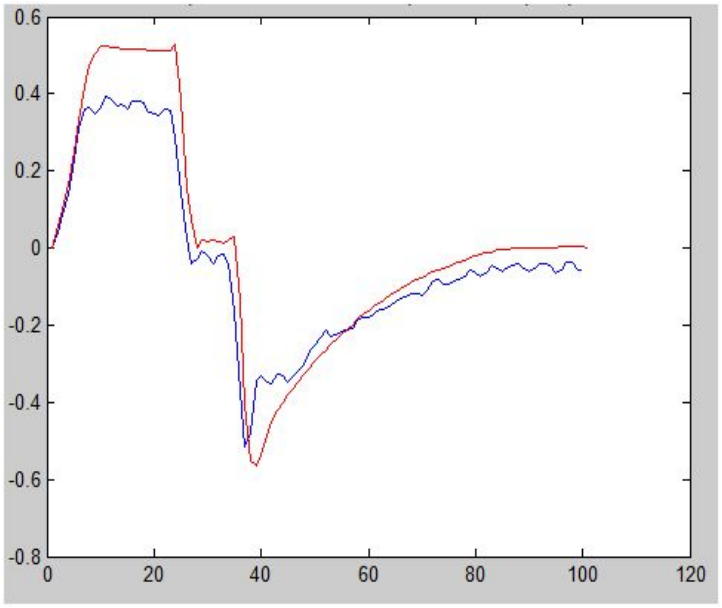

Figure 2.24: Plot of measured flow (red curve) and flow computed as the derivative of V_{CW}(blue line). During the inspiration, the computed flow reaches lower values because of the gas compression.

is affected by high frequency noise and is characterized by lower magnitude because of gas compression (figure 2.24), and subsequently the GUI asks the user to select two points in order to define the inspiration plateau of the computed flow, used to calculate the resistance values as follows:

$$R_{RS}\_d = \frac{P_{max} - P_2}{\frac{dV_{T_{CW}}}{dt}} \tag{2.8a}$$

$$R_{OS}\_d = \frac{\Delta P_{max} - \Delta P_2}{\frac{dV_{T_{CW}}}{dt}} \tag{2.8b}$$

Finally, the function *NormalizzaBreath.m* calculates C_{RS} also taking the integrative of the inspired flow as tidal volume:

$$C_{RS_I} = \frac{1}{P_2 - P_{ee}} \int_{t_0}^{t_{insp}} \dot{V}\, dt \tag{2.9}$$

All the results, referring to each obstruction grade, are reported in the next chapter.

Chapter 3

Results and Discussion

In this chapter are presented the results in form of graphs, obtained from data processing over the entire population except for the pig 8, who is died at the beginning of the protocol. The tables with all numeric results are reported in Appendix B grouped by obstruction grade and ventilation mode.

The first part reports the mechanical parameters (resistance and compliance) computed as described in the previous chapter, which characterize the respiratory system of the population. As it will be shown, the resistance variations due to the different obstruction grades will characterize the variations in all downstream parameters, such as tidal volume and downstream pressure, according to the mechanical model described in the introduction.

The second part concerns pressure and volume parameters (figure 2.19) for both HFJV and SHFJV, whose data processing is described in the first part of the previous chapter, including the statistical validation that is resumed in the graphs. These results lead to interesting conclusions about the behaviour of jet ventilation in presence of tracheal stenosis, and confirm not only the direct dependence between delivered pressures and volume and mechanical parameters, but also some of the consideration about jet ventilator's settings reported in table 2.2.

The graphs represent the mean values and the standard deviations of the computed parameters, calculated by grouping the entire population by the obstruction grade and by the ventilation mode, obtaining results characterizing homogeneous groups representing each *ventilation mode-obstruction grade* combination. The obstruction grade is reported as *caliber*, which is the inner diameter (ID) of the tracheal lumen in correspondence of the obstruction, thus as lower is the caliber, as more severe is the obstruction.

The results of the statistical validation have been reported in the graphs as follows:

- Red characters concern Tidal Volume;

- Green characters concern End-Expiratory Volume;
- Blue characters concern Driving Pressure;
- Purple characters concern End-Expiratory Pressure.

Asterisks ($*$) refer the significant interaction between the parameter and the high frequency, whereas crosses ($+$) refer the significant interaction between the parameter and the obstruction grade, with a p-value of:

- $***$ or $+++$ mean $p < 0.001$;
- $**$ or $++$ mean $p < 0.01$;
- $*$ or $+$ mean $p < 0.05$.

As already cited, some data of few pigs could not be taken in count because of technical problems during the acquisition, anyway each parameter has been computed over at least 6 pigs, ensuring the reliability of the results.

3.1 Mechanical Parameters

3.1.1 Resistance

The following graphs report the resistance characterizing the respiratory system of the pigs, that is R_{RS}, and the resistance of the only obstruction, that is R_{OS}, calculated taking in count the measured flow.

R_{RS_D} and R_{OS_D} are computed using the derivative of V_{CW} as flow, thus their values are always higher than those calculated with measured flow because the gas compression dampens the chest wall variation's due to the inspired flow.

Obviously, the respiratory system's and the obstruction's resistances strongly depend on the obstruction inserted in the trachea, and R_{RS} is not significantly different than R_{OS}, being R_{OS} much higher than the resistance of the rest of the respiratory system. The values of resistances are reported in table 3.2.

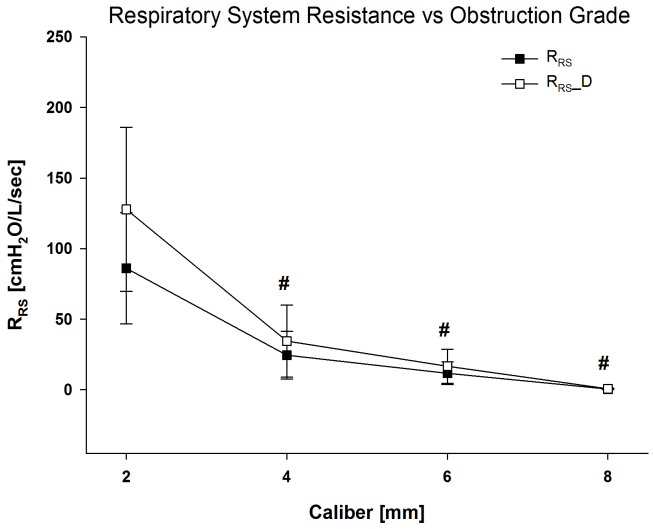

(a)

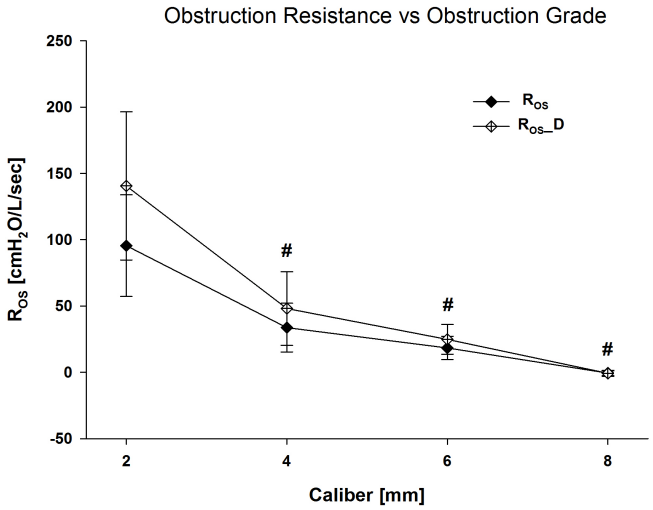

(b)

Figure 3.1: Resistance of the whole respiratory system (a) and across the obstruction (b). Hash indicates significant difference with the value at 2 mm ID ($p<0.01$), while the difference between R_{RS} (R_{OS}) and R_{RS_D} (R_{OS_D}) is not significant.

Table 3.1: Results of the resistances' computation. Being R=$(P_{max} - P_2)/\dot{V}$, R_{RS_D} and R_{OS_D} are always lower than R_{RS_D} and R_{OS_D}, and the negative values are because, with the largest ID stent, the difference between upstream and downstream flow was very small, thus oscillations in the detected signal could influence significantly the results. The values are expressed in $cmH_2O{\cdot}s/L$

Caliber	R_{RS}		R_{RS_D}		R_{OS}		R_{OS_D}	
	Mean	St. Dev.	Mean	St. Dev.	Mean	St. Dev.	Mean	St. Dev.
2 mm	86.06	39.48	127.81	58.15	95.50	38.34	140.53	55.89
4 mm	24.46	16.86	34.45	25.53	33.73	18.37	48.06	27.77
6 mm	11.68	7.99	16.63	12.00	18.40	8.75	24.81	11.22
8 mm	0.48	0.36	0.66	0.51	-0.59	1.73	-0.79	2.35

The difference between the resistance at 8 mm (which is similar to normal conditions) and the resistance at 2 mm is huge, near to two orders of magnitude, even if the first is not reliable because it has been computed over only two pigs. This is confirmed by the comparison of the results with those reported in [51]: the resistance's value at 6 mm is similar to that reported by Guerin et al., while the value at 8 mm is significantly lower.

Figure 3.1 shows that the resistance with the 2 mm tracheal lumen is significantly different from the resistance at the other obstruction grades: in fact the slope of the first tract of the curve is higher then the rest and from 4 to 8 mm the resistance's decrease is linear, forming a 'knee' in correspondence of the 4 mm caliber. In the next pages it will be evident that the trend of this curve will characterize also the curves about the pressure and volumes parameters, meaning a direct dependence between the mechanical parameters and the system's responses. In fact, the obstruction placed in trachea increases the airways resistance, affecting the flow passing though it and therefore influencing tidal volume and downstream driving pressure.

3.1.2 Compliance

C_{RS} is computed using measured tidal volume (VT_{CW}), and C_{RS_I} using the integrative of measured flow over the inspiration as tidal volume. The compliance does not vary significantly among the different obstructions, depending only on lung's and chest-wall's elastance, and the values are congruent with those reported in [51]. Theoretically C_{RS_I} must be greater than C_{RS} because of the compression of the inspired gas, but the results show the contrary; this may be related to the extremely short pause (about 0.2 s) between inspiration and expiration, while to get reliable results the pause should be 3-4 seconds long.

Table 3.2: Results of the compliance's computation in ml/cmH_2O.

Caliber	C_{RS}		C_{RS_I}	
	Mean	St. De.	Mean	St. Dev.
2 mm	17.02	7.05	7.55	2.02
4 mm	22.01	6.06	14.16	4.35
6 mm	20.75	6.00	12.17	2.20
8 mm	21.43	4.14	19.75	4.84

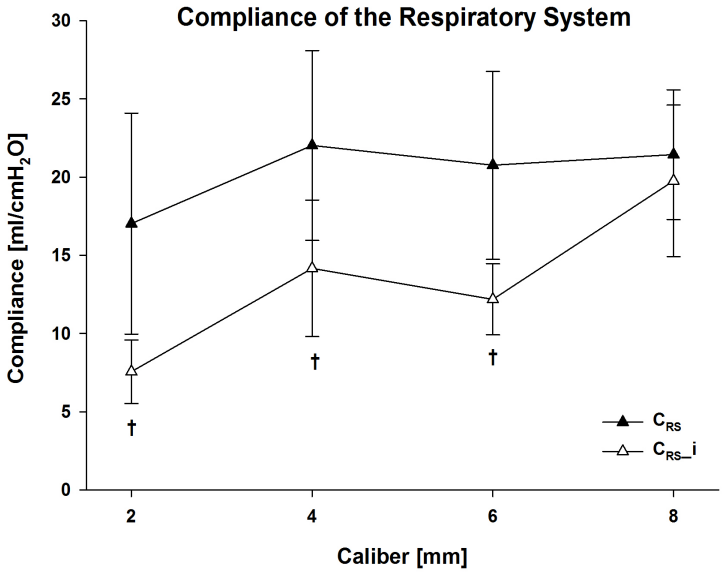

Figure 3.2: Compliance of the respiratory system. The statistical analysis has not revealed any significant difference among the value at different calibers, while the cross indicates significant difference ($p<0.05$) between C_{RS} and C_{RS_I}.

3.2 HFJV - Volumes

The following graphs report the variation of End-Expiration and End-Inspiration chest-wall volume in dependence on the high frequency set in the jet ventilator, for each obstruction grade. The graphs related to rib-cage and abdomen are reported in the Appendix I. The difference between the inspiration and the expiration curve represent the tidal volume, whose variation is explicited forward.

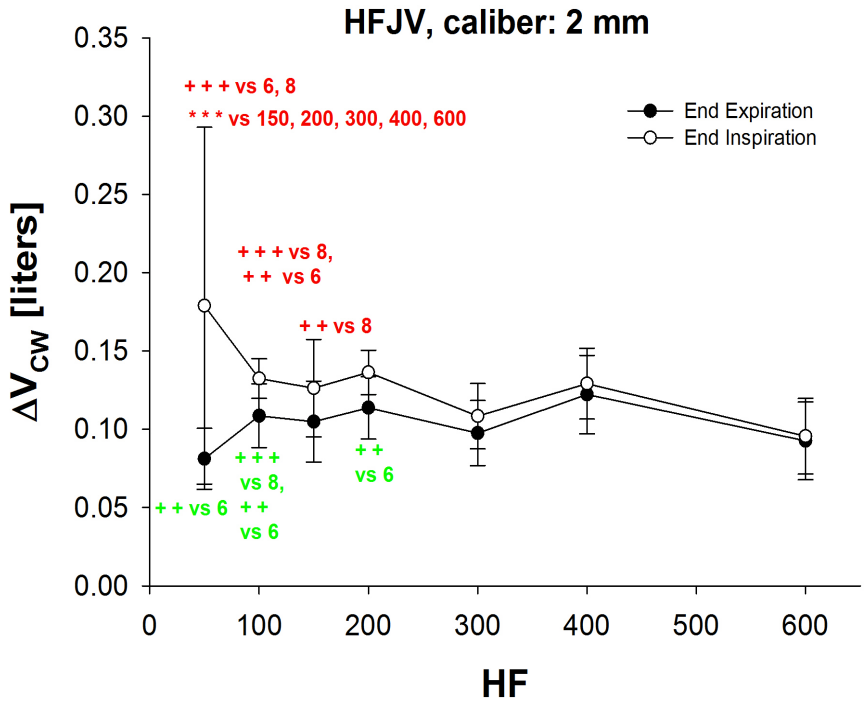

(a)

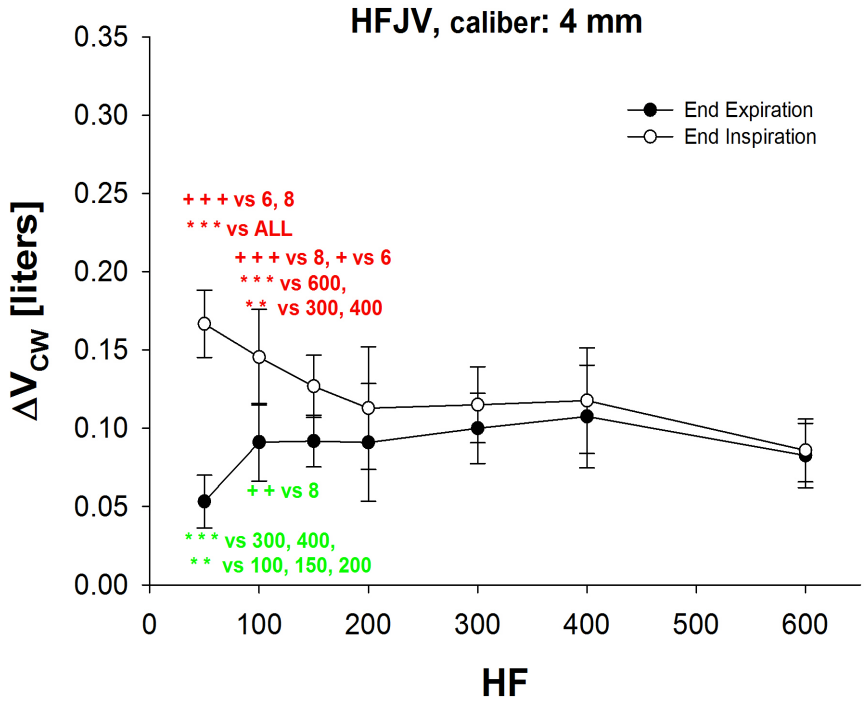

(b)

Figure 3.3: Chest-Wall volume with 2 mm (a) and 4 mm (b) tracheal caliber.

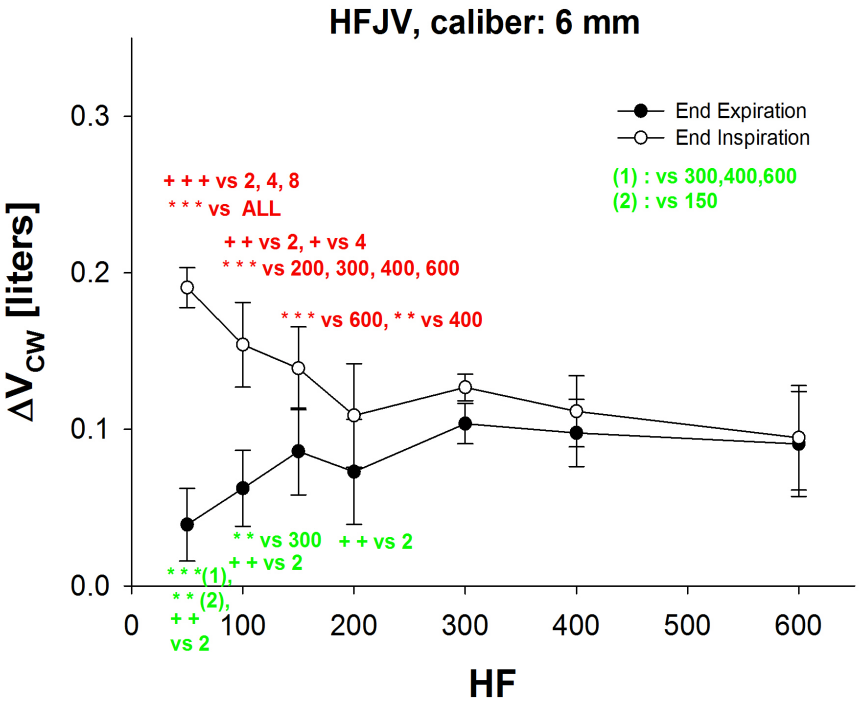

(a)

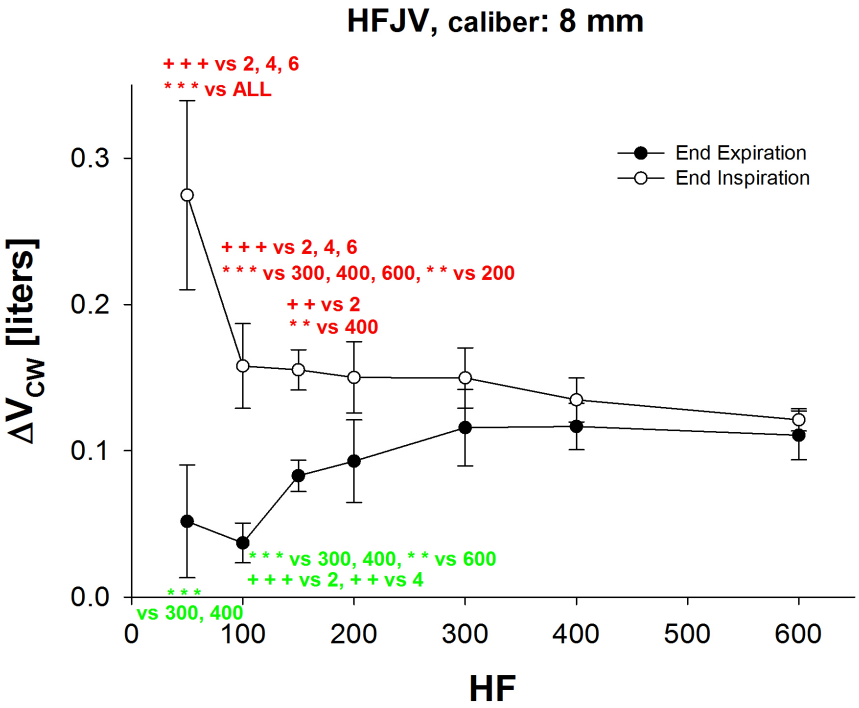

(b)

Figure 3.4: Chest-Wall volume with 6 mm (a) and 8 mm (b) tracheal caliber.

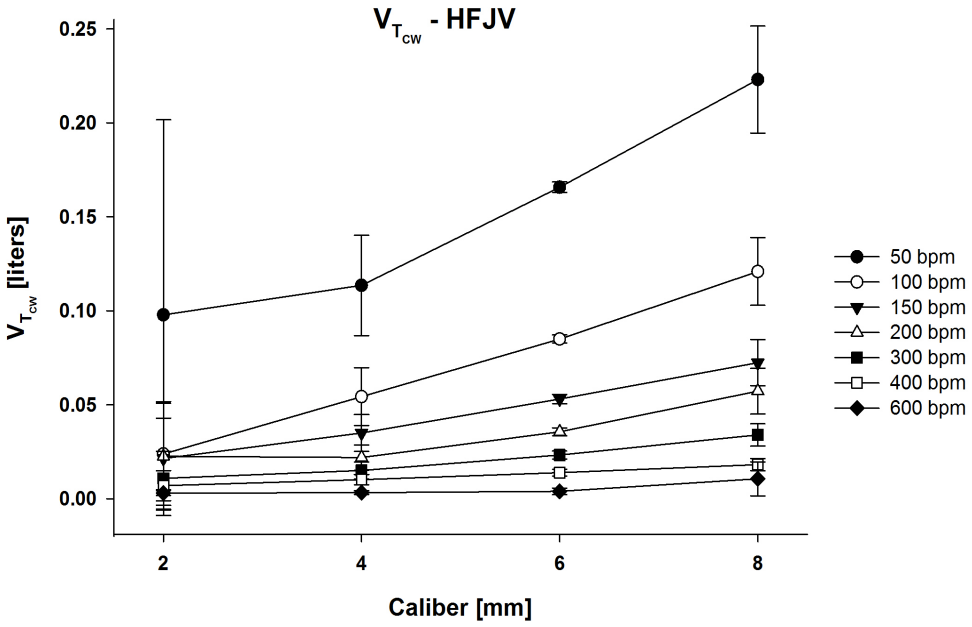

Figure 3.5: Comparison of the chest-wall tidal volume at the different obstruction grades, for all ventilation rates.

3.2.1 Discussion

3.2.1.1 Tidal Volume

The graphs and the statistical analysis revealed that during HFJV, tidal volume, end expiratory volume and frequency response are similar within two main groups: one formed by highly obstructed pigs (2 and 4 mm caliber) and the other formed by less obstructed pigs (6 and 8 mm caliber).

At the lowest ventilation rates (from 50 to 150 bpm), in fact, the chest-wall tidal volume was higher and similar in presence of the lowest obstructions, being about 150 and 220 ml at 50 bpm (figure 3.3). This value was considerably lower when the tracheal caliber was reduced to 2 or 4 mm, being respectively 98 and 114 $\pm$ 27 ml at 50 bpm (figure 3.4).

Then, when the ventilation rate is higher than 100 bpm, tidal volume becomes very low in the highly obstructed pigs, being less than 50 ml; with lower obstruction, this "high-frequency limit" moves to 200 bpm, but at higher frequencies (above 300 bpm - according to [50]) there are no significant differences between tidal volumes independently on the obstruction, as shown in figures 3.5 and 3.6 that report, respectively, the changes in tidal volume at the different obstruction grades and at the different high frequencies set in the ventilator.

Finally, tidal volume variations at lowest frequencies and obstructions are mostly due to the abdomen, being the less stiff and the most compliant compartment (fig-

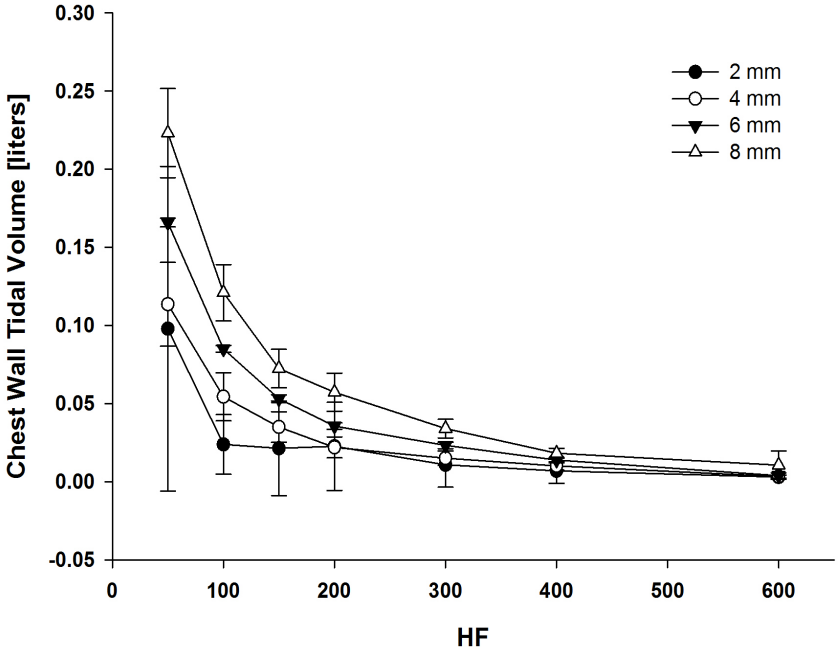

Figure 3.6: Comparison of the chest-wall tidal volume at the different frequencies, for all obstruction grade.

ure 3.7). This difference between abdomen and rib-cage decreases by increasing the obstruction grade, and with the 2 mm ID stent there are no differences. In this condition, in fact, trachea is almost completely occluded and the lower part of the respiratory system is uncoupled from the upper airways.

3.2.1.2 End-Expiratory Volume

At high frequencies (from 150 up to 600 bpm) there are no significant differences between the end-expiratory volume independently on the obstruction, having reached an inflation of about 100 ml.

Significant differences in the end-expiratory volumes are evident only during HFJV at 50 and 100 bpm and in presence of severe obstruction. In these cases, in fact, the graphs shows End-Expiratory volumes significantly higher than with lower obstruction, being 89 ml at 50 bpm. This means that a tracheal caliber of 2 mm leads to an increase of the resistance of the respiratory system, getting longer its physiological relaxation constant and causing air trapping even if the ventilation rate is not such high. This is an important result for two reasons:

- it becomes clear that gas trapping may easily lead to hyperinflation in case of severe obstruction;

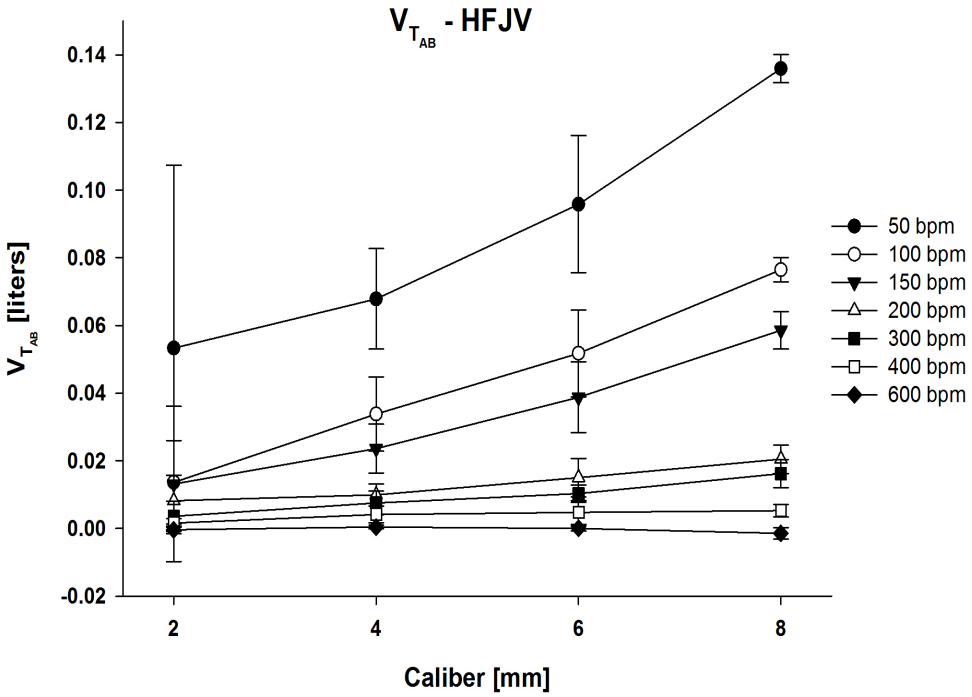

(a)

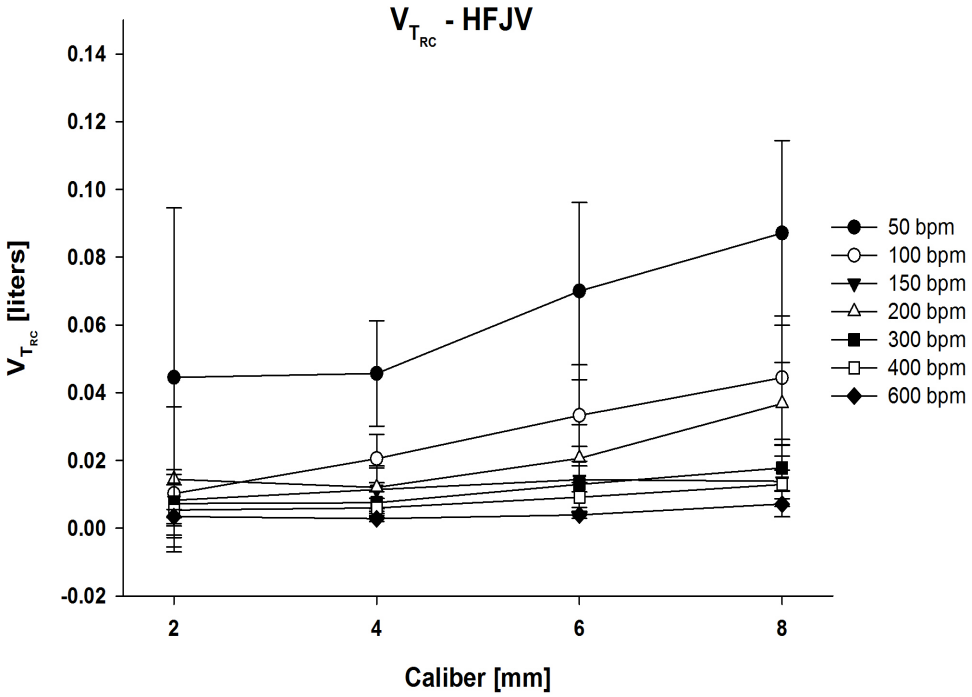

(b)

Figure 3.7: Tidal volume in the abdomen (a) and in the rib-cage (b).

- it explain why tidal volume is lower in these conditions.

3.3 HFJV - Pressures

In this section are reported the graphs concerning the peak inspiratory- and peak expiratory- upstream pressures, measured above the obstruction, and downstream pressures, measured below the obstruction. The difference between the two curves in each graphs represent the driving pressure, whose statistical analysis is reported in blue, and the expiratory curve in the downstream pressure's graphs represents the peak expiratory pressure that can be considered to observe the PEEP effect.

3.3.1 Upstream Pressure

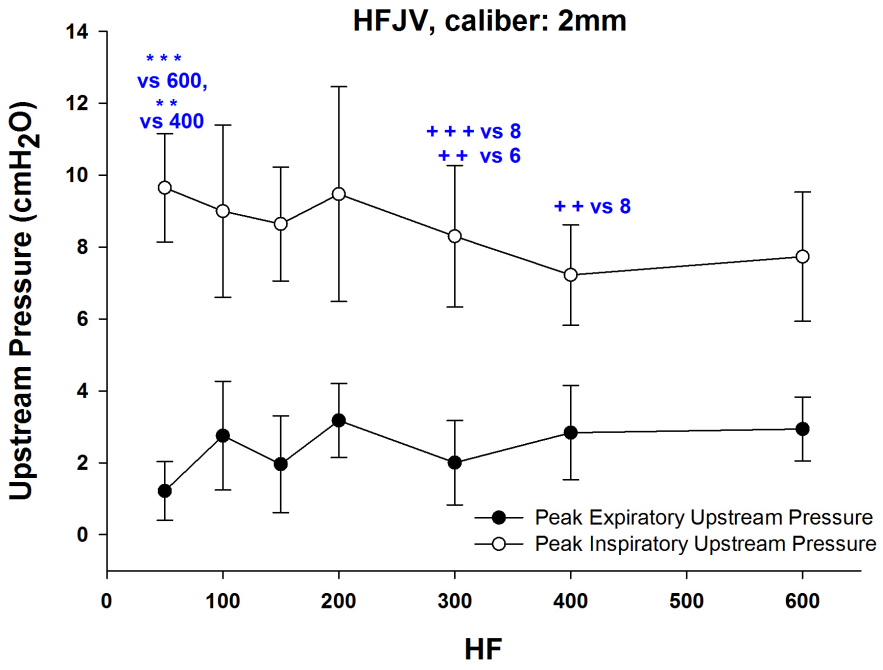

Figure 3.8: Upstream pressure with 2 mm tracheal caliber.

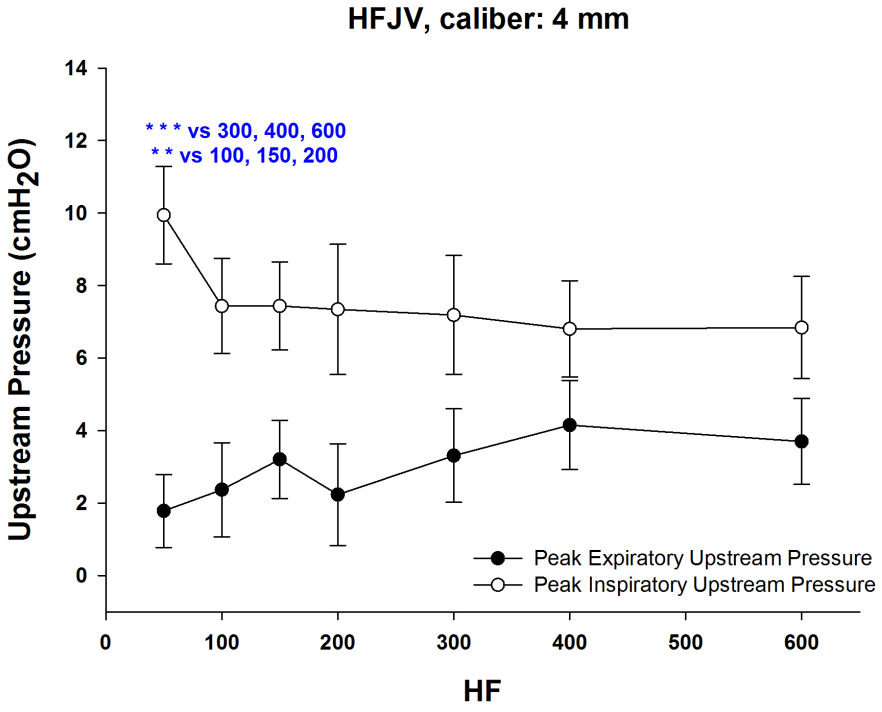

(a)

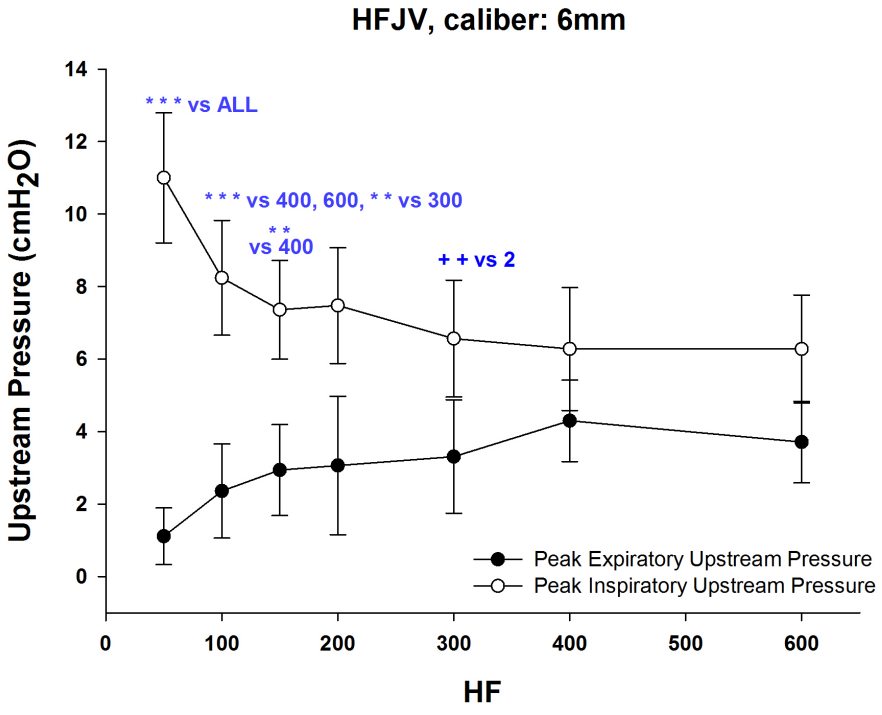

(b)

Figure 3.9: Upstream pressure with 4 mm (a) and 6 mm (b) tracheal caliber.

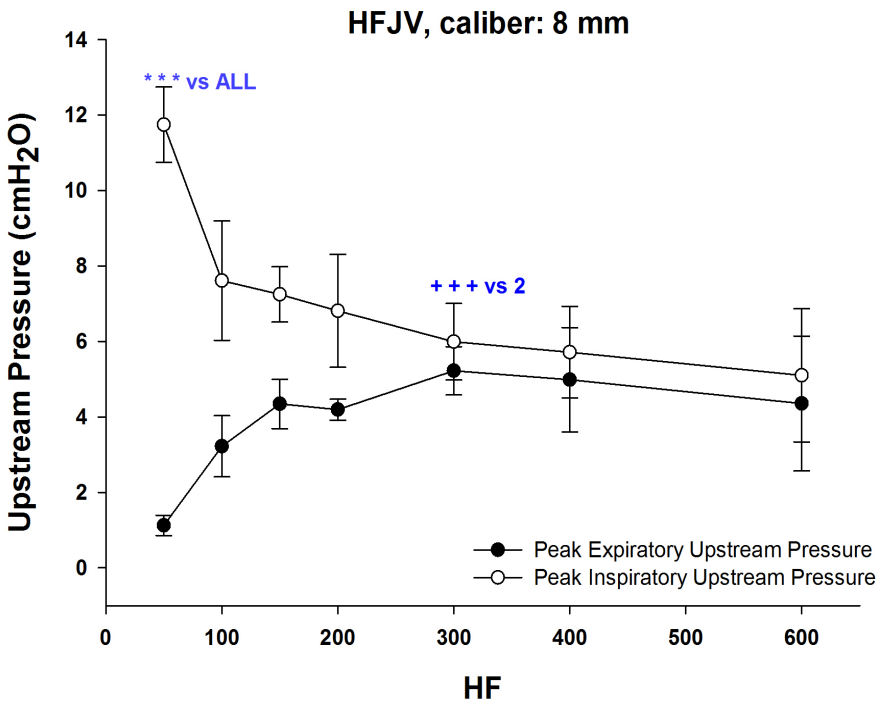

Figure 3.10: Upstream pressure with 8 mm tracheal caliber.

3.3.2 Downstream Pressure

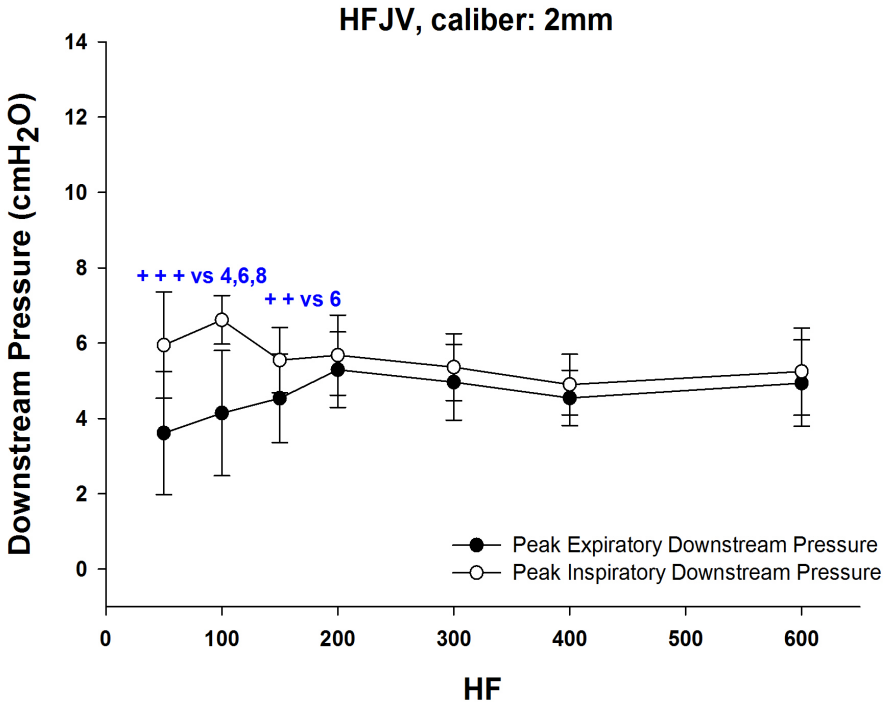

(a)

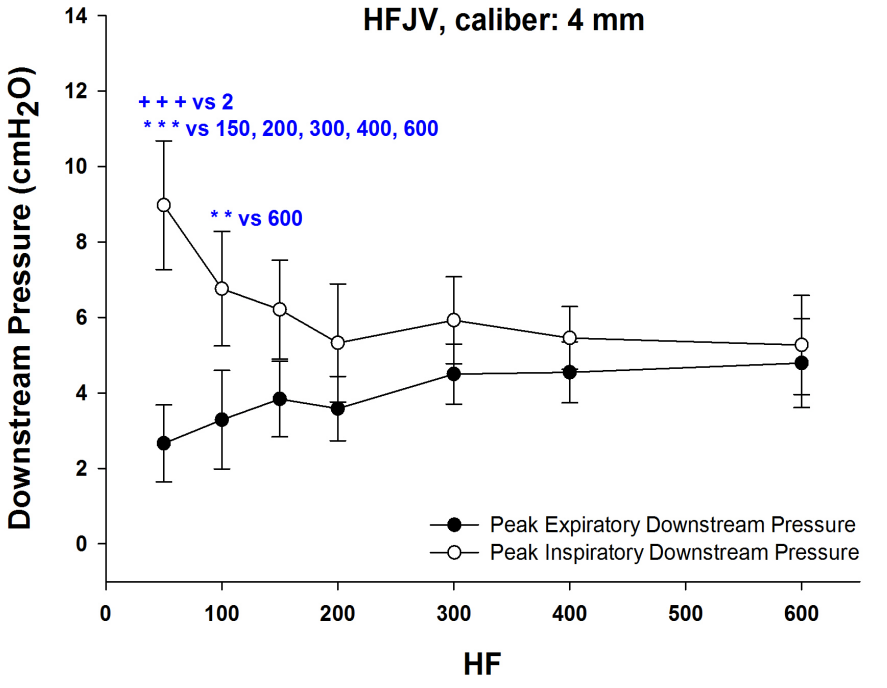

(b)

Figure 3.11: Downstream pressure with 2 mm (a) and 4 mm (b)tracheal caliber.

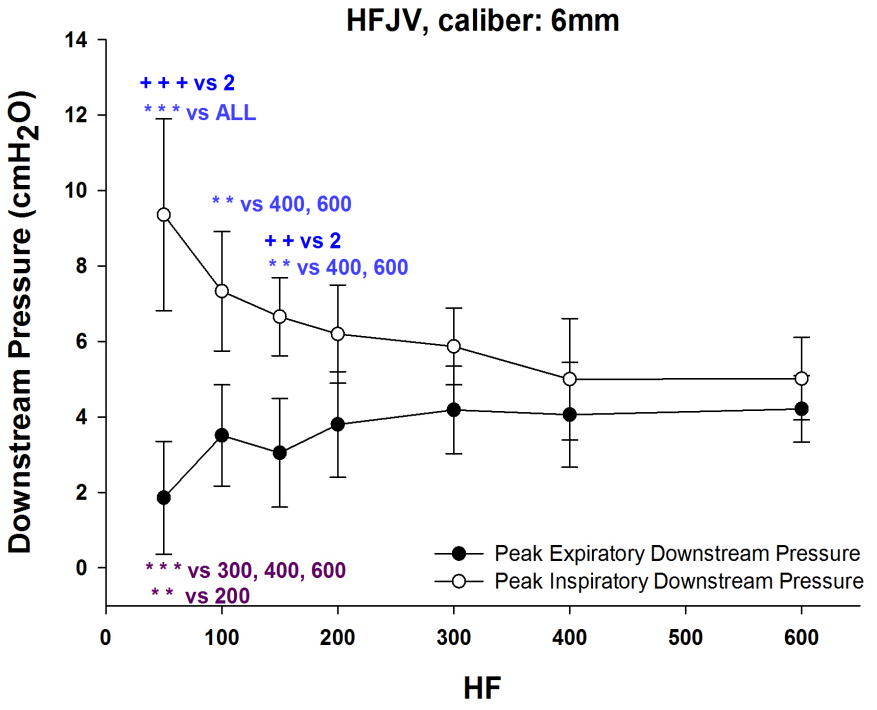

(a)

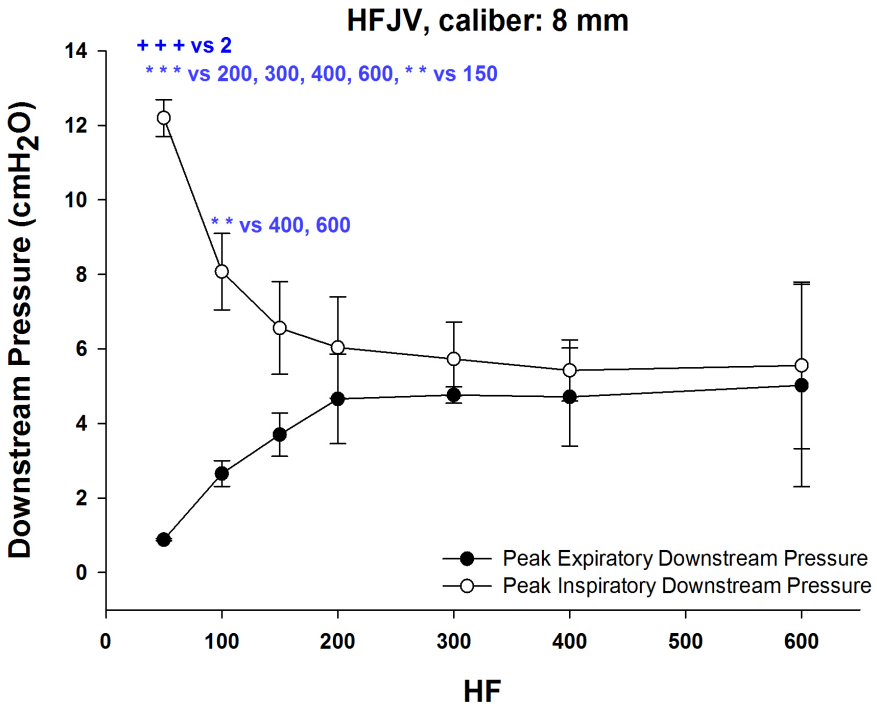

(b)

Figure 3.12: Downstream pressure with 6 mm (a) and 8 mm (b)tracheal caliber.

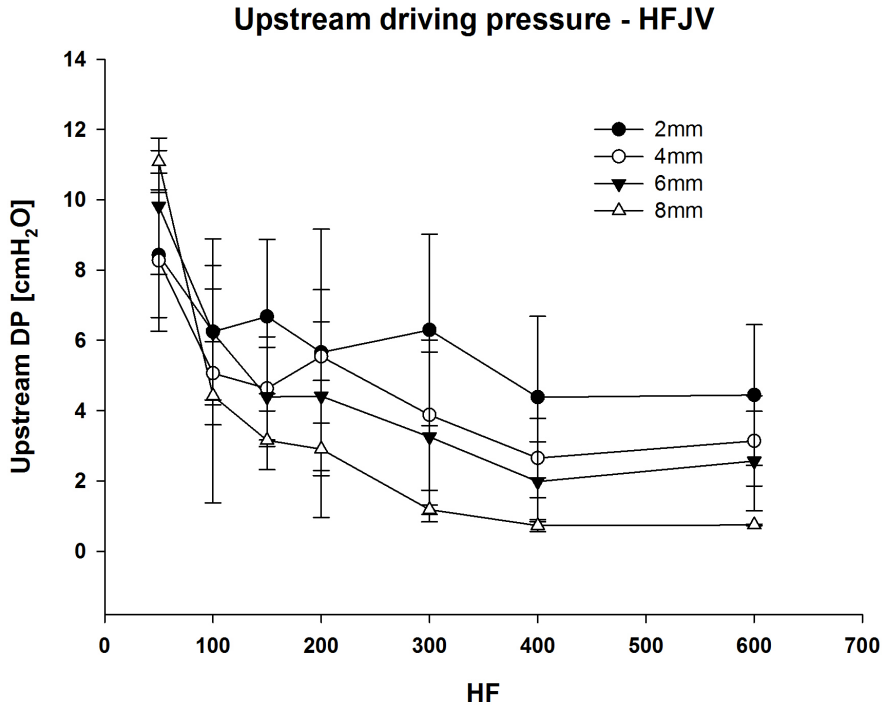

Figure 3.13: Upstream driving pressure at the different frequencies for each obstruction grade. The curves related to the largest calibers (6 and 8mm) are more frequency-dependent than the other curves.

3.3.3 Discussion

3.3.3.1 Driving Pressure

Even if the driving pressure always decreases by increasing the ventilation rate (HF), figure 3.13 shows clearly that the frequency dependence of the driving pressure increases progressively with the decrease in tracheal obstruction: in fact, the decrease in driving pressure with the increasing high frequency is more evident in the graphs related to 6 and 8 mm ID (figures 3.9(b) and 3.10).

Figure 3.14 show that the downstream driving pressure is very low in presence of the smallest ID (2 mm) being only 2.3 cmH_2O already at 50 bpm , because the obstruction uncouples the upper airways with the rest of the respiratory system and the flow below the obstruction is very low. On the contrary, with large ID (6 and 8 mm), the driving pressure reaches respectively 7.3 ± 3.76 and 11.3 ± 0.52 cmH_2O because the flow can pass through the stenosis.

In comparison with the upstream driving pressure, the progressive trend of the downstream driving pressure is completely opposite: in fact, whereas upstream the driving pressure increases as the obstruction is more severe because gases cannot move forward, downstream the driving pressure increases as much as the tracheal caliber

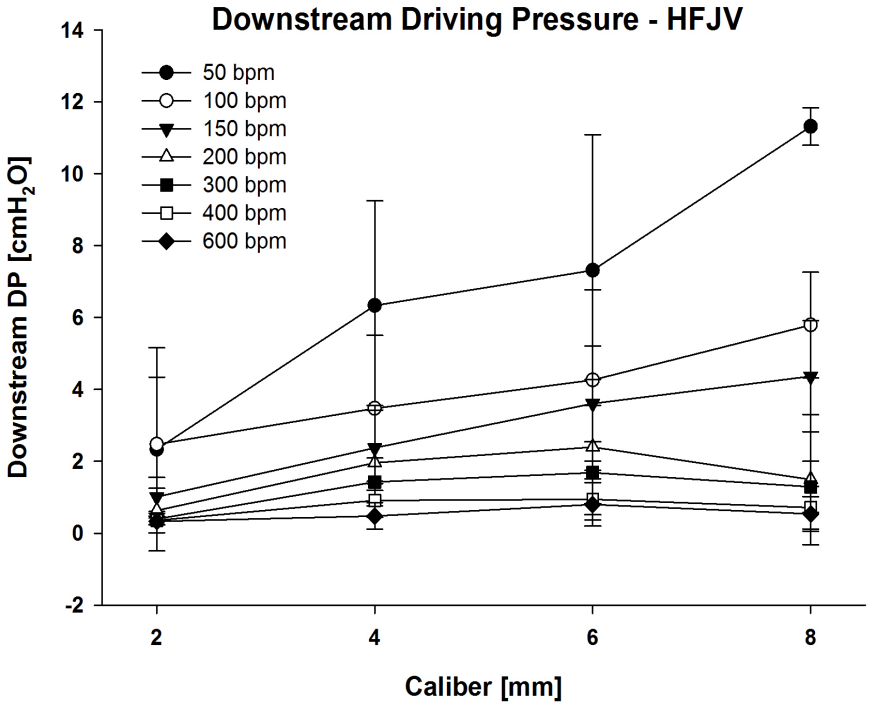

Figure 3.14: Variation of the downstream driving pressure at the different obstruction grades, for each ventilation rate. At the lowest high frequencies, the driving pressure increases as much as the caliber increases. At frequencies over than 300 bpm, no variations have been measured with any tracheal caliber.

increases and the air flows across the stenosis itself (figure 3.14).

The frequency dependence of the driving pressure is confirmed only for frequencies up to 150 bpm and for ID of 4, 6 and 8 mm, because with the most severe obstruction the downstream driving pressure is low also at 50 bpm, and for ventilation rates above 200 bpm the driving pressure is less than 1 cmH_2O for every obstruction grade.

These results are completely congruent with the tidal volume, in fact with the most severe obstruction, the lower respiratory system is uncoupled from the upper airways, therefore the flow across the stenosis is very low, leading to a low tidal volume and low driving pressure at any ventilation rate. Furthermore, the trend of the resistance's curve expressed in figure 3.1 is reflected also in the driving pressure curve: in fact, figure 3.14 shows clearly a significant difference between the 2 mm curve and the others, which are linearly differentiated.

Finally, the correlation between tidal volume and driving pressure is evident also in the frequency response of the respiratory system: in fact, the application of high frequency jet ventilation has produced the greatest tidal volume and driving pressure when the ventilation rate was lower than 150 bpm. Over this value, both tidal volume and driving pressure were very low at any obstrucion grade, therefore HFJV did not provide adequate ventilation.

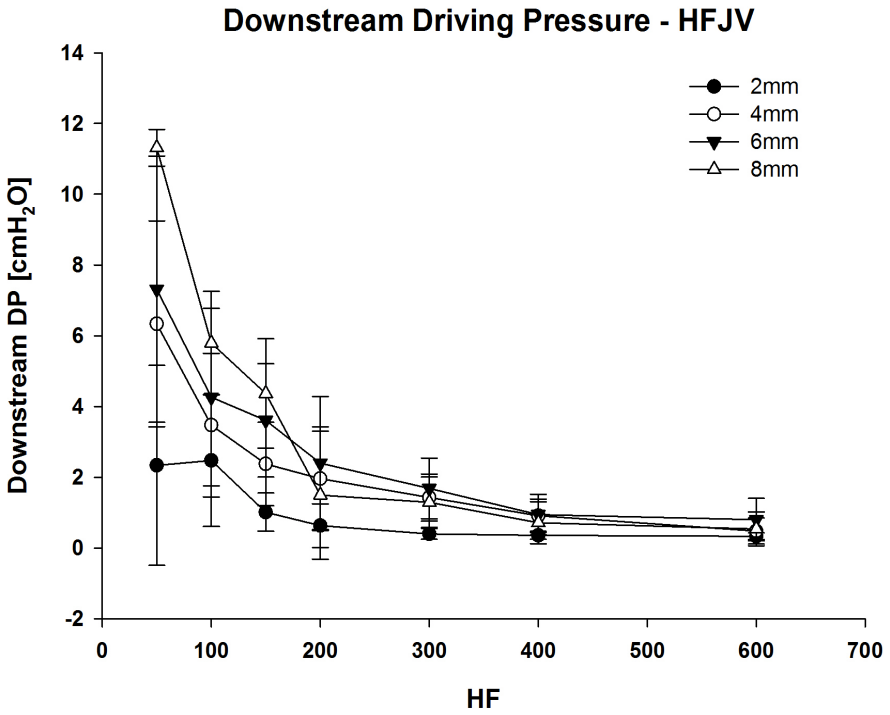

Figure 3.15: Variation of the downstream driving pressure at the different frequencies, for each tracheal caliber. This graphs confirms that the frequency dependence of the driving pressure is more evident with the larger tracheal caliber, whereas with the most severe obstruction the driving pressure is very low.

An interesting finding is that during HFJV above 200 bpm, a low-frequency signal was superposed in both pressure and volume data (figure 3.16). Being this low-frequency similar to spontaneous breathing frequency, this signal may represent the spontaneous breaths-related efforts, caused by high arterial p_{CO_2} due to inadequate ventilation. However, the presence of this signal did not affect the results.

3.3.3.2 Peak Expiratory Pressure

The peak expiratory pressure's curve represented in figures 3.11 and 3.12 provide information about the PEEP effect due to the HFJV, although data are not exactly referred to the end-expiration points as explained in paragraph 2.5.4. Data shows that PEP at the highest ventilation rate is about 4-5 cmH_2O independently on the obstruction grade. Slight differences can be found at lower frequencies, where, according to what expressed about EEV, as more severe is the obstruction, as higher is PEP. However, the statistical test did not highlight any significant difference.

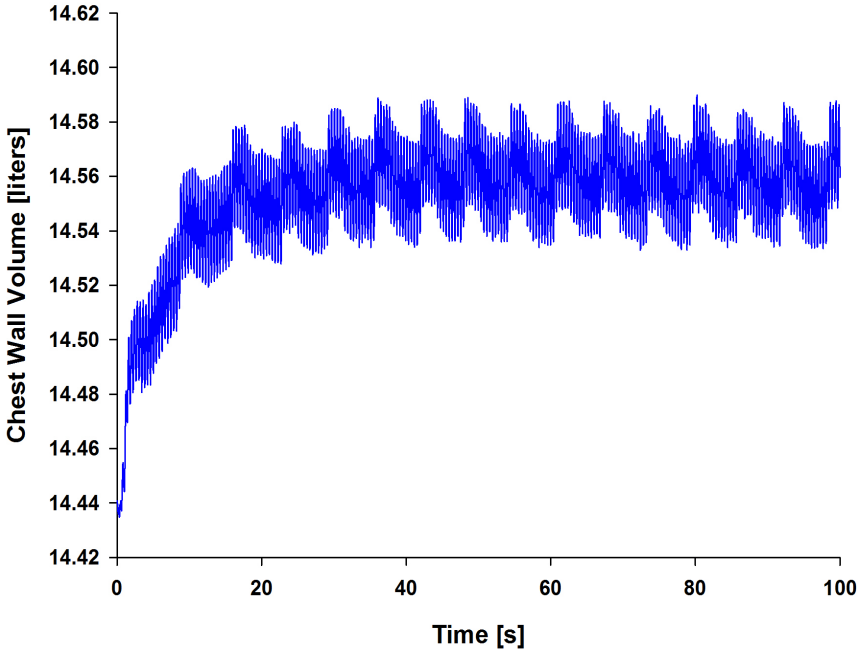

Figure 3.16: Chest-wall volume during HFJV at 400 bpm. The low frequency oscillation has a 7 second period (freq 0.14 Hz).

3.4 SHFJV - Volumes

As for HFJV, the following graphs report the variation of End-Expiration and End-Inspiration chest-wall volume in dependence on the high frequency set in the jet ventilator for each obstruction grade during SHFJV, while the graphs related to rib-cage and abdomen are reported in the Appendix I.

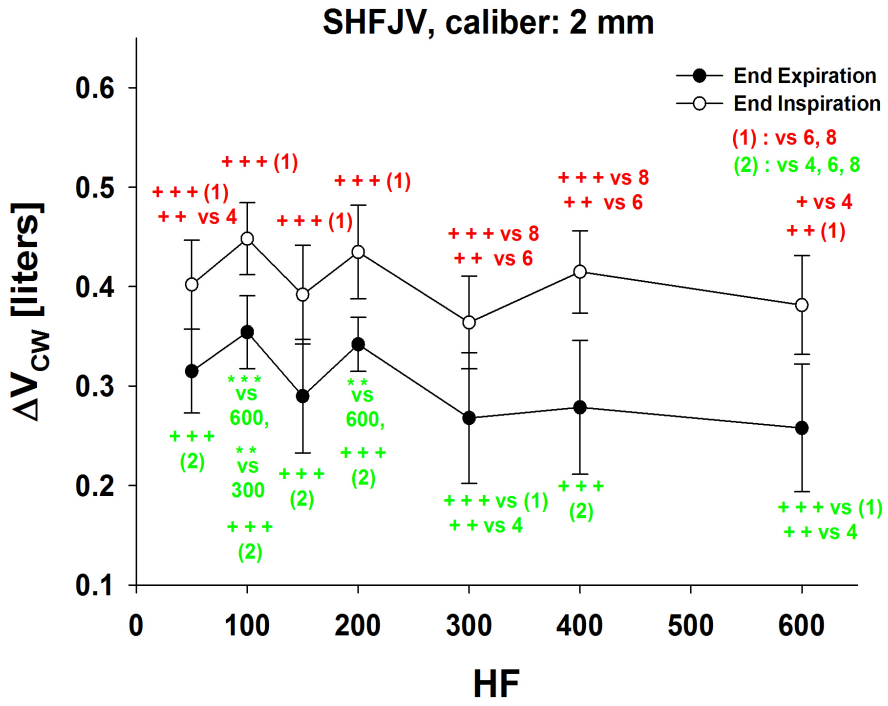

(a)

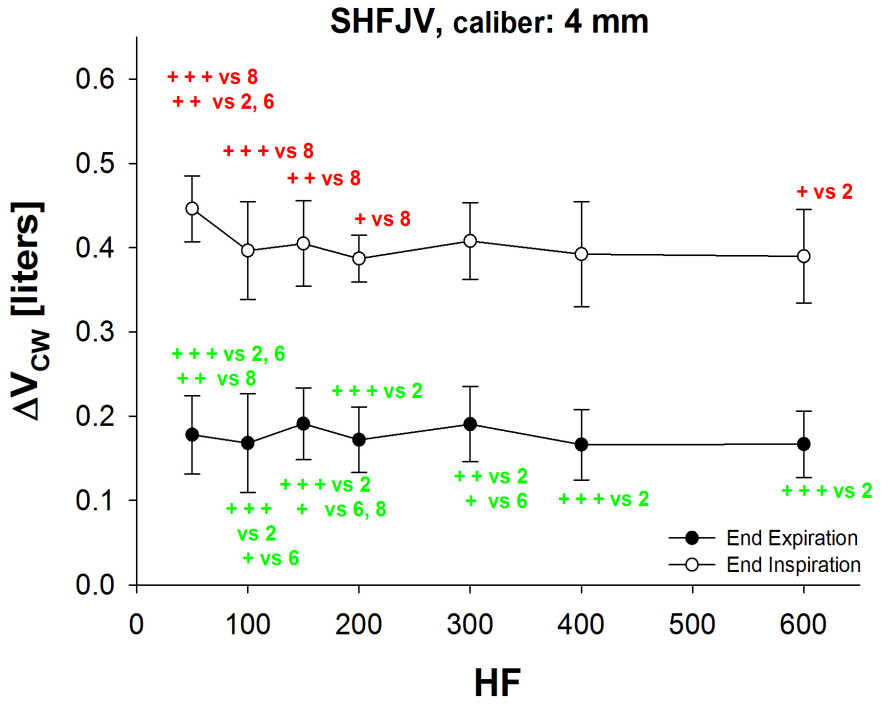

(b)

Figure 3.17: Chest-Wall volume with 2 mm (a) and 4 mm (b) tracheal caliber.

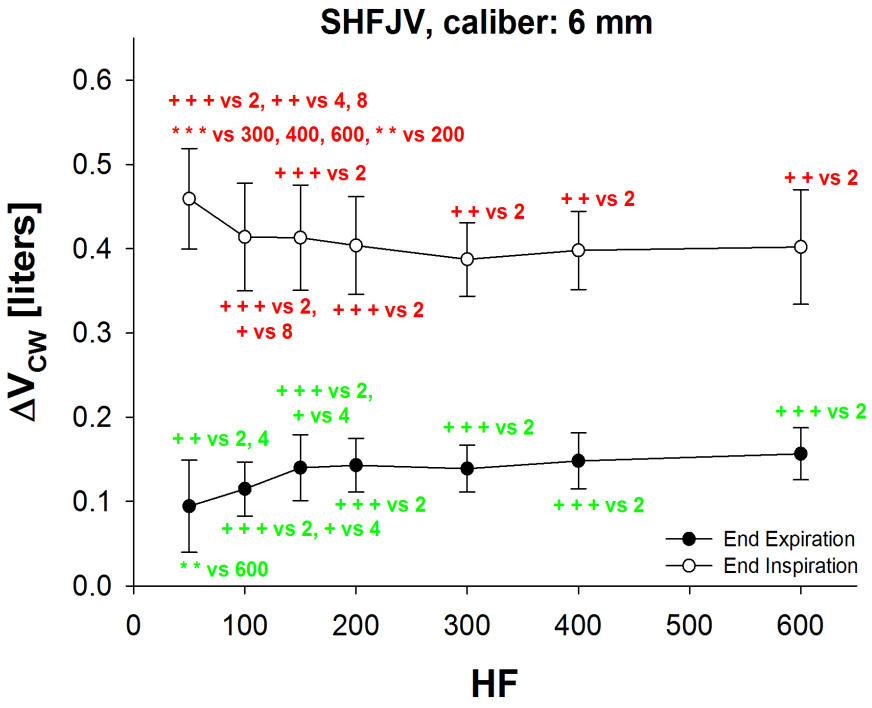

(a)

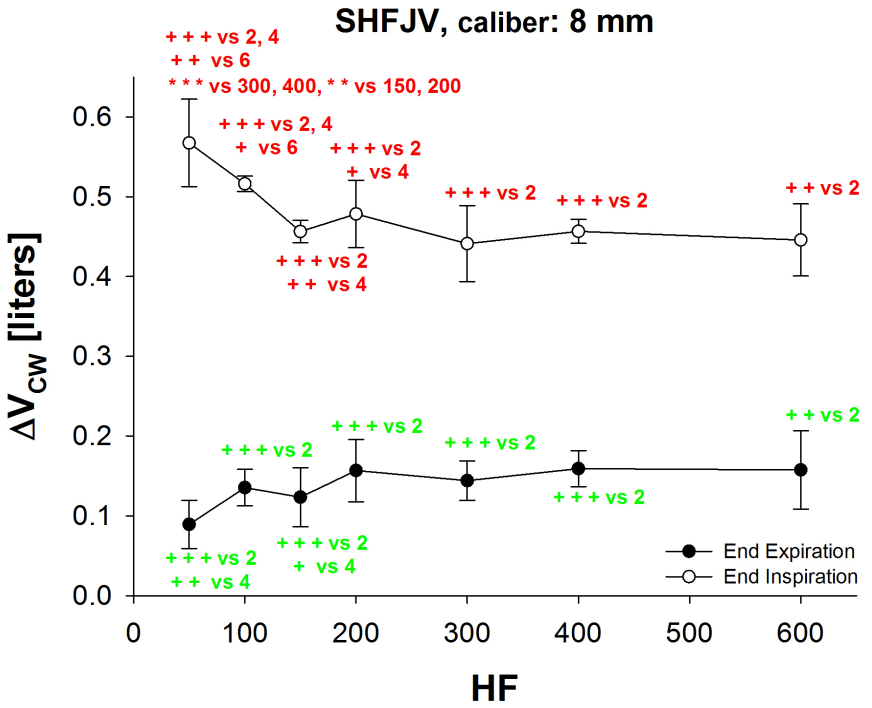

(b)

Figure 3.18: Chest-Wall volume with 6 mm (a) and 8 mm (b) tracheal caliber.

3.4.1 Discussion

3.4.1.1 Tidal Volume

Superimposed High Frequency Jet Ventilation (SHFJV) is obtained by superimposing low-frequency breaths (in this case 16 bpm) to the high frequency jet ventilation whose effects are described in the previous paragraphs. The graphs reported in figures 3.17(a), 3.18 and 3.18(b) shows that the superposition of the effects of the low- and high-frequency signals is found also in the results:

- in presence of the most severe obstruction (2 mm caliber) there is not any frequency dependence, meaning that lower respiratory system is uncoupled form the upper airways. In this conditions, during HFJV the tidal volume was very low, therefore its effects on SHFJV are not significant and the tidal volume (about 100 ml for any HF) in due only to the low-frequency component.

- for lower obstruction, the lungs and the chest-wall are no more uncoupled from the airways, therefore the non-linear relationship between chest-wall tidal volume and high frequency is due to the non-linear frequency response of a compliant system such as the respiratory system (figure 3.19). According to the results of the application of HFJV, tidal volume decreases when HF increases, being the sum of LF- and HF- related effects. However, SHFJV applied on moderate stenosis (4, 6 and 8 mm ID) provides a tidal volume of at least 214 ml even at the highest HF, since the LF component ensures adequate ventilation even though the tidal volume related to the only HF is very low. The figure shows also that the trend of the resistance's curve affects the offset of the tidal volumes related to the four calibers, confirming that the tracheal obstruction affects all the downstream variables.

- reducing the stenosis, tidal volume increases with a marked gradual trend, also for the highest frequencies, while during HFJV this trend was less defined and just for the lowest ventilation rates (figure 3.20). This suggests that the LF component-related tidal volume is caliber dependent. As already cited, the increase in tidal volume at the different obstructions reflects the trend of the resistance's curve: in the first tract, from 2 to 4 mm, the slope is higher than in the rest of the curve, where is almost linear.

- as for HFJV, tidal volume is not perfectly equally divided between rib-cage and abdomen, but abdomen has a predominant effect mostly at low obstruction and low HF.

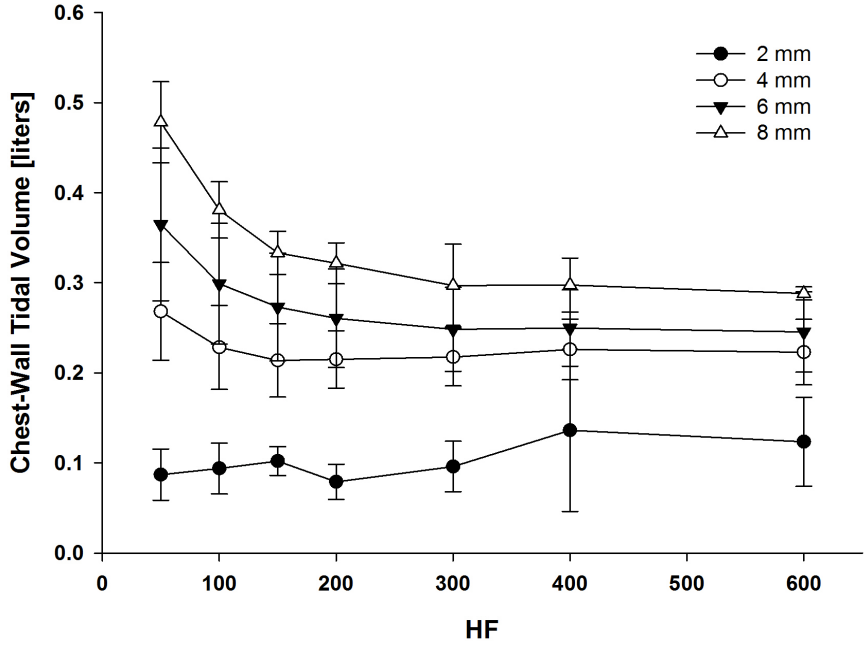

Figure 3.19: Chest-wall tidal volume at the different HF, for all calibers. It is evident the non-linear trend of the curves related to 4, 6 and 8 mm. For any HF, tidal volumes at the different obstruction grades reflects the trend of the resistance's curve: there is a big difference between 2 and 4 mm, and then a linear variation.

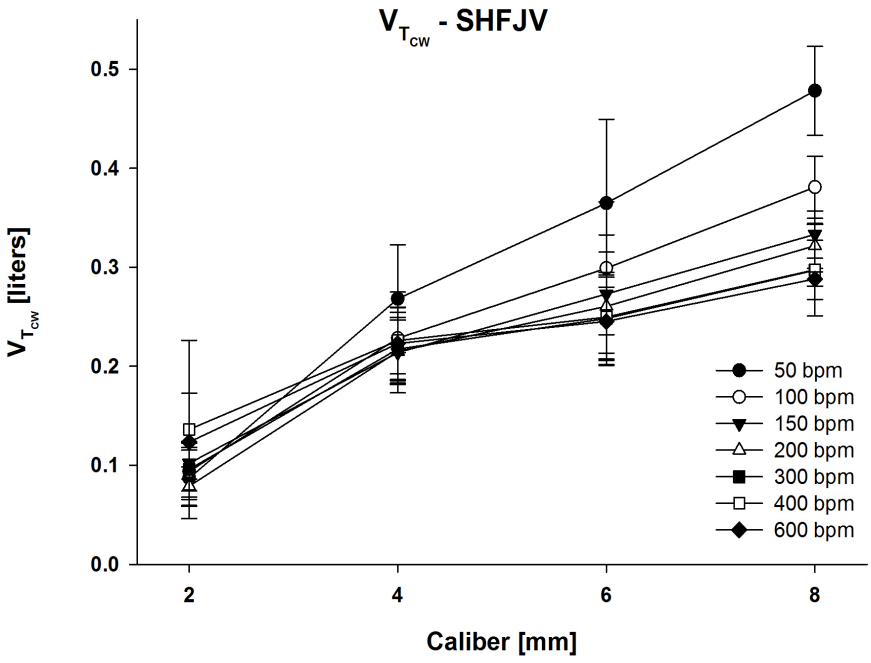

Figure 3.20: Chest-wall tidal volume at the different calibers, for all ventilation rates. The linear relationship between tidal volume and caliber is clearly visible, even if the first tract is characterized by an higher slope due to the higher slope of the resistance's curve.

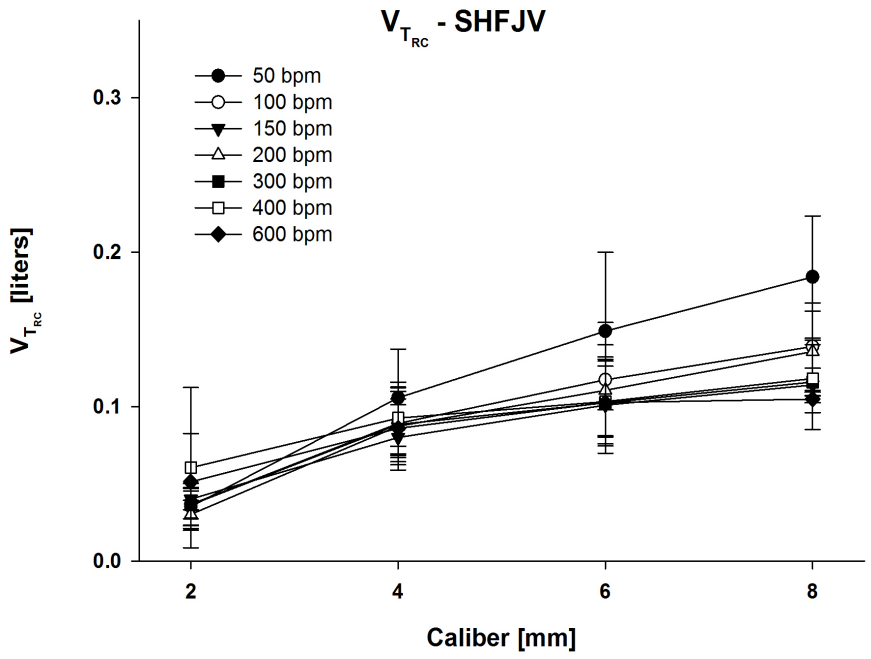

(a)

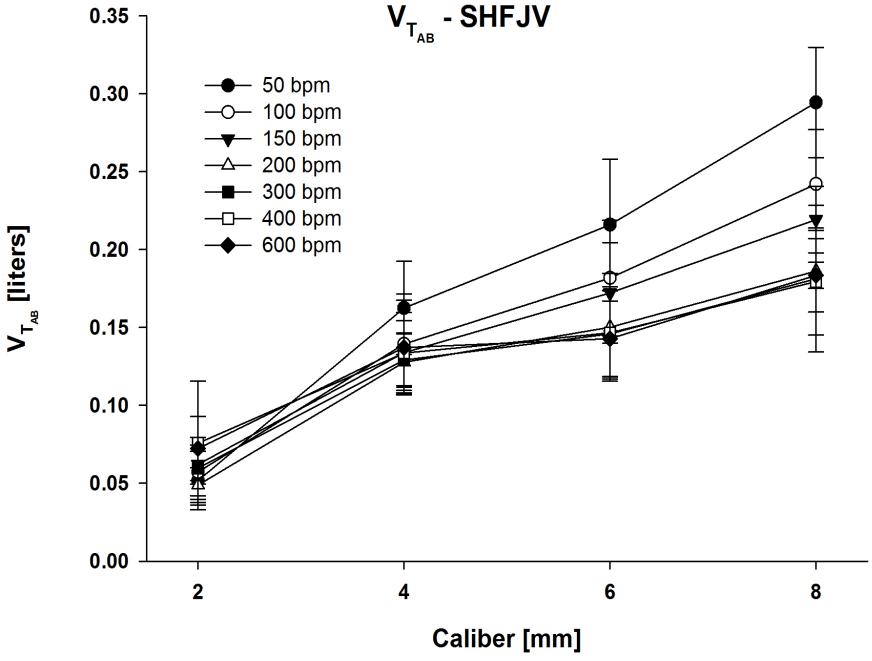

(b)

Figure 3.21: Chest-Wall volume with 4 mm (a) and 6 mm (b) tracheal caliber.

3.4.1.2 End-Expiratory Volume

The statistical analysis on the end-expiratory volume at the different obstruction grade is very important in this study because it provides information about the eventual hyperinflation of the pig, which is one of the major risks on ventilating by high frequency jet ventilation in presence of tracheal obstruction.

The application of SHFJV caused End-Expiratory Chest-Wall Volume (EECWV) similar but slightly greater than those obtained with HFJV confirming what reported in [50], remaining equally divided between abdomen and rib-cage (graphs are in Appendix A).

With the 2 mm ID stent in place, the EECWV was significantly greater than with any other obstruction, being between 258 and 354 ml for any HF set in the ventilator. At larger calibers, 6 and 8 mm the EECWV decreases to 140-160 ml for any high frequency above 200 bpm, while it is below 140 ml up to 150 bpm.

With the most severe stenosis the physiological relaxation time constant τ increased so much to lead the physiological expiration time t_E even longer than the expiration time of the LF breaths $t_{E_{LF}}$, meaning that the PEEP effect is not only due to the HF component, but to the LF component as well.

$$\tau = R_{RS}C_{RS} = 86.06\frac{cmH_20s}{L} \cdot 0.017\frac{L}{cmH_20} = 1.46s \tag{3.1a}$$

$$t_E \simeq \tau \cdot 3.5 = 5.11s \tag{3.1b}$$

$$t_{E_{LF}} = \frac{60s}{16bpm} \cdot \frac{3}{5} = 2.25s \tag{3.1c}$$

Where $\frac{3}{5}$ is due to the I:E ratio set in the jet ventilator.

The same equations can be applied for 4 (eq. 3.2) and 6 mm (eq. 3.3) ID stents (8 mm resistance value is not reliable):

$$\tau_{4mm} = R_{RS_{4mm}}C_{RS_{4mm}} = 24.46\frac{cmH_20s}{L} \cdot 0.022\frac{L}{cmH_20} = 0.54s \tag{3.2a}$$

$$t_{E_{4mm}} \simeq \tau_{4mm} \cdot 3.5 = 1.88s \tag{3.2b}$$

$$\tau_{6mm} = R_{RS_{6mm}}C_{RS_{6mm}} = 11.68\frac{cmH_20s}{L} \cdot 0.021\frac{L}{cmH_20} = 0.24s \tag{3.3a}$$

$$t_{E_{6mm}} \simeq \tau_{6mm} \cdot 3.5 = 0.85s \tag{3.3b}$$

These results show that with the 4 mm ID stent in place t_{E_4} is similar to $t_{E_{LF}}$,

thus the risk of hyperinflation should be taken in count. At greater ID, $t_{E_{LF}}$ ensures a complete exhalation of the LF-related tidal volume.

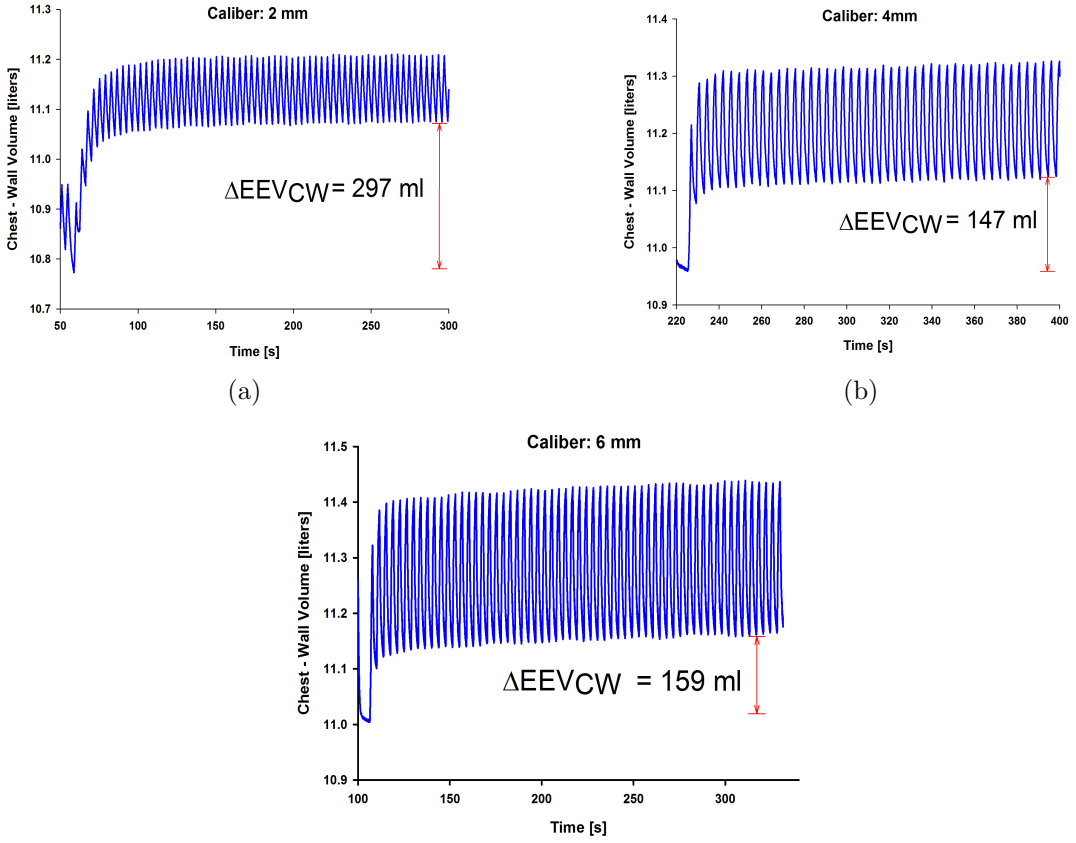

Figure 3.22: Pig 3 chest-wall volume curves during 16+400 SHFJV. The ΔEEV with the 2 mm stent in place is much greater than the others, depending also on the LF-related PEEP effect because τ got much longer. With 4 and 6 mm ID stent the ΔEEV is lower because τ is shorter.

3.5 SHFJV - Pressures

The next graphs concern upstream and downstream peak pressures measured during SHFJV. The difference between the curves represents the driving pressure, while the peak-expiratory pressure curve gives information about the PEEP effect.

3.5.1 Upstream Pressure

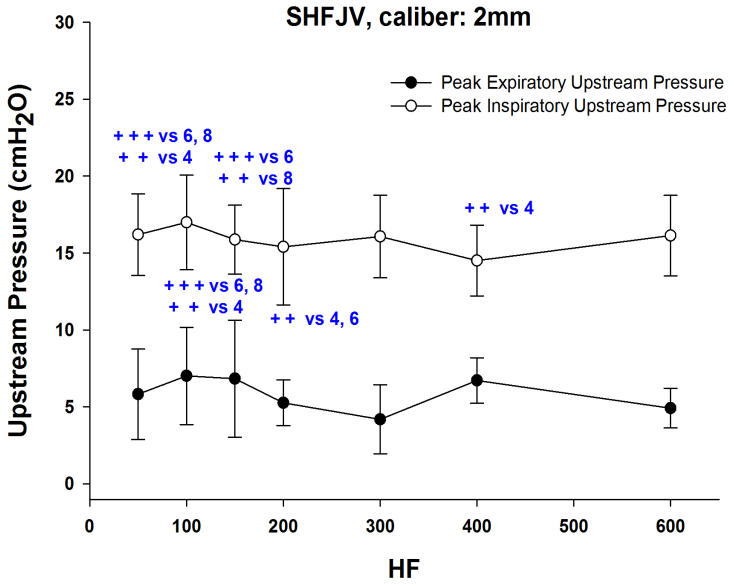

(a)

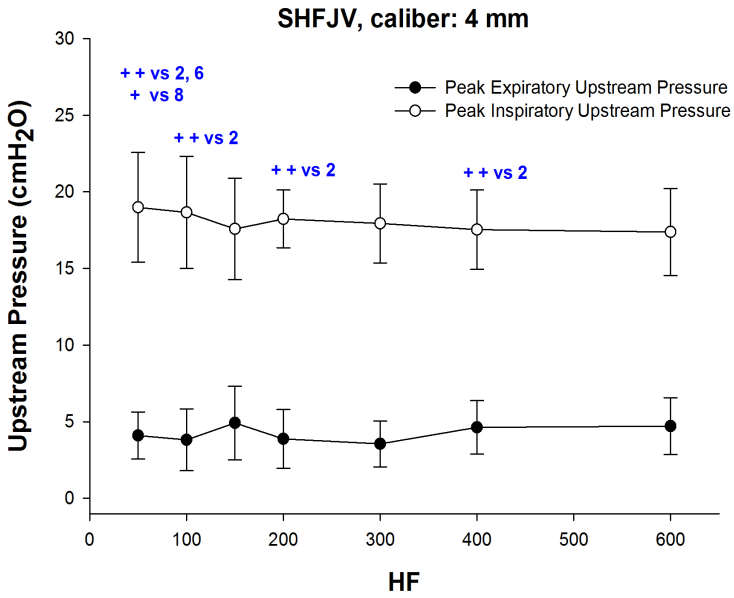

(b)

Figure 3.23: Upstream pressure with 2 mm (a) and 4 mm (b)tracheal caliber.

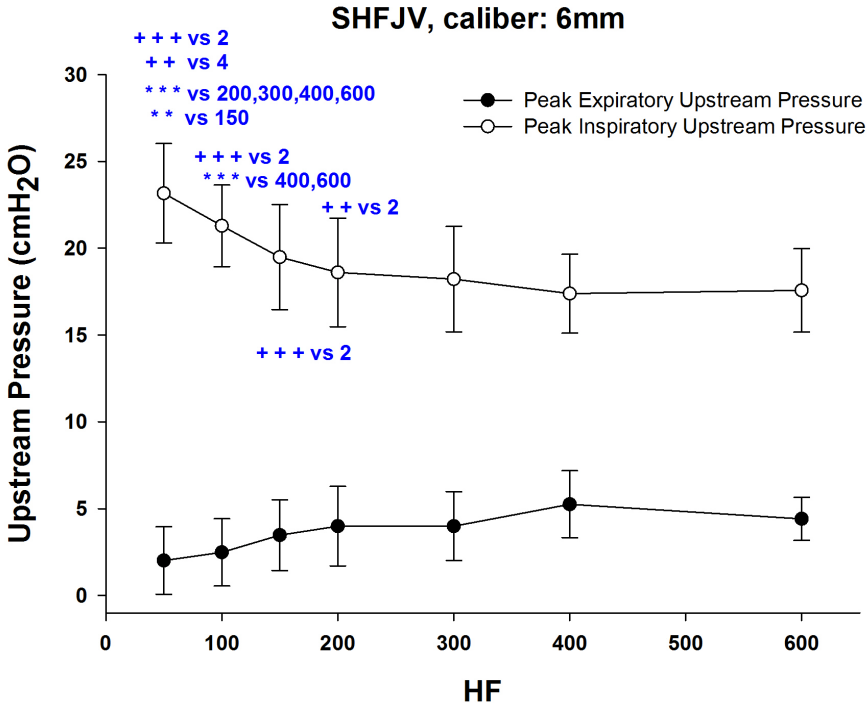

(a)

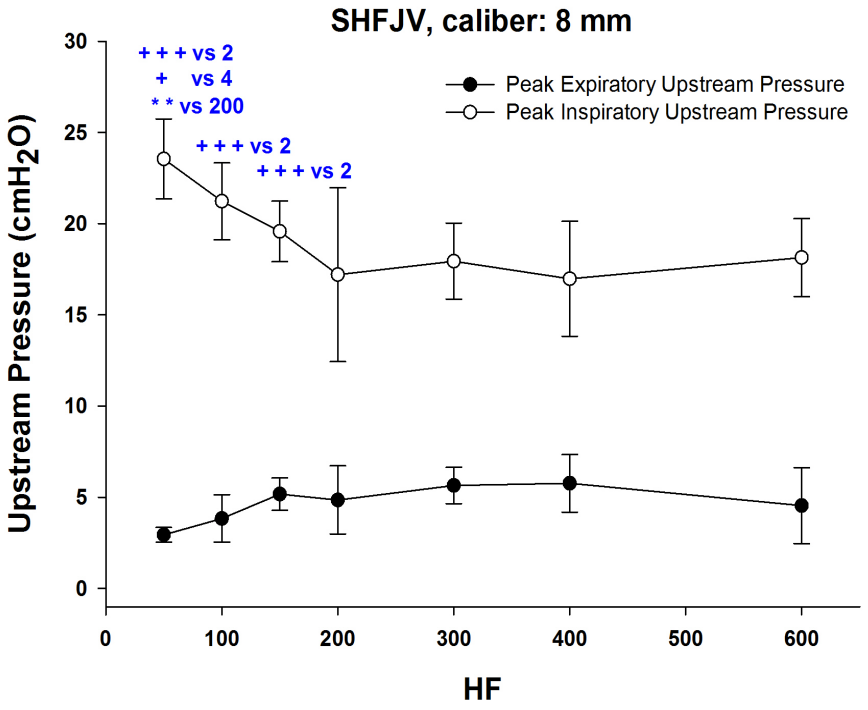

(b)

Figure 3.24: Upstream pressure with 6 mm (a) and 8 mm (b)tracheal caliber.

3.5.2 Downstream Pressure

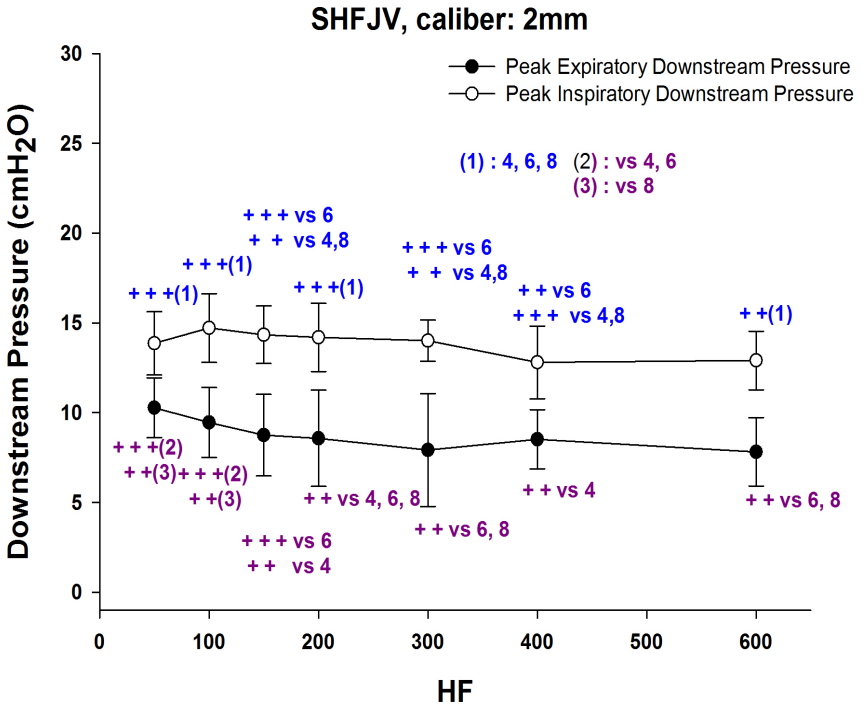

(a)

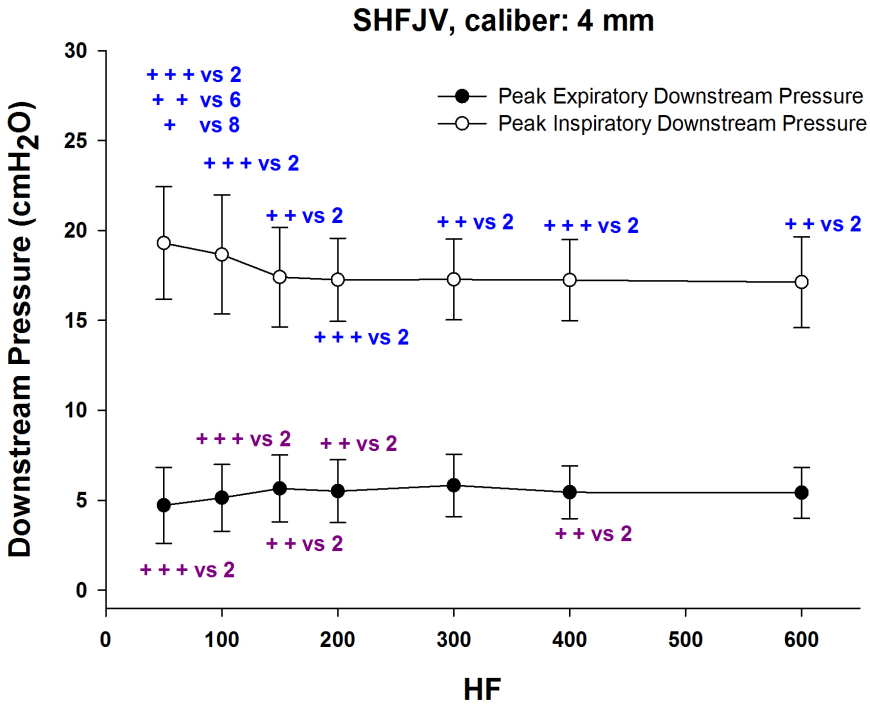

(b)

Figure 3.25: Downstream pressure with 2 mm (a) and 4 mm (b)tracheal caliber.

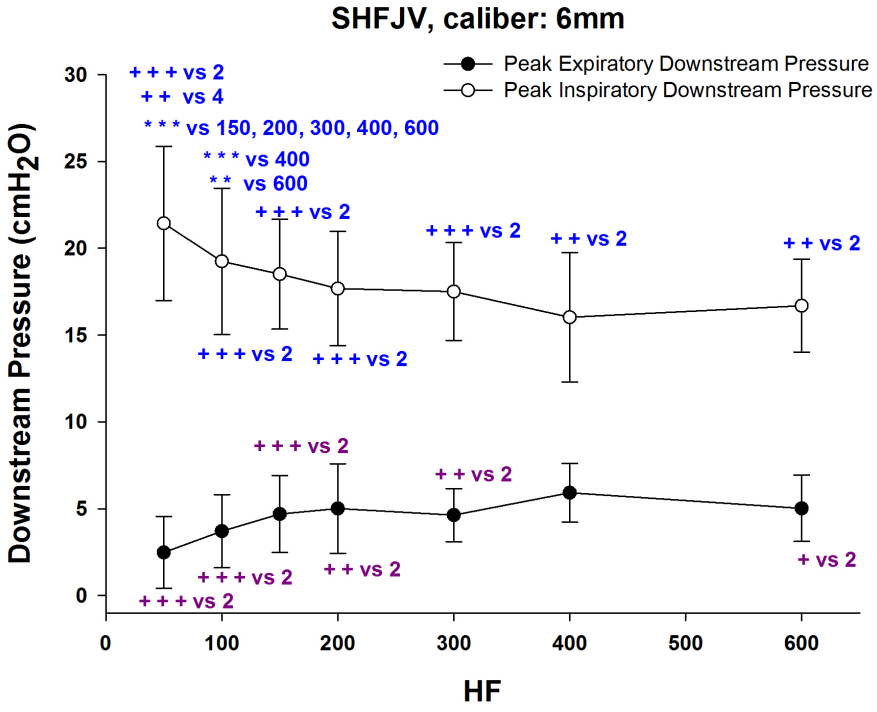

(a)

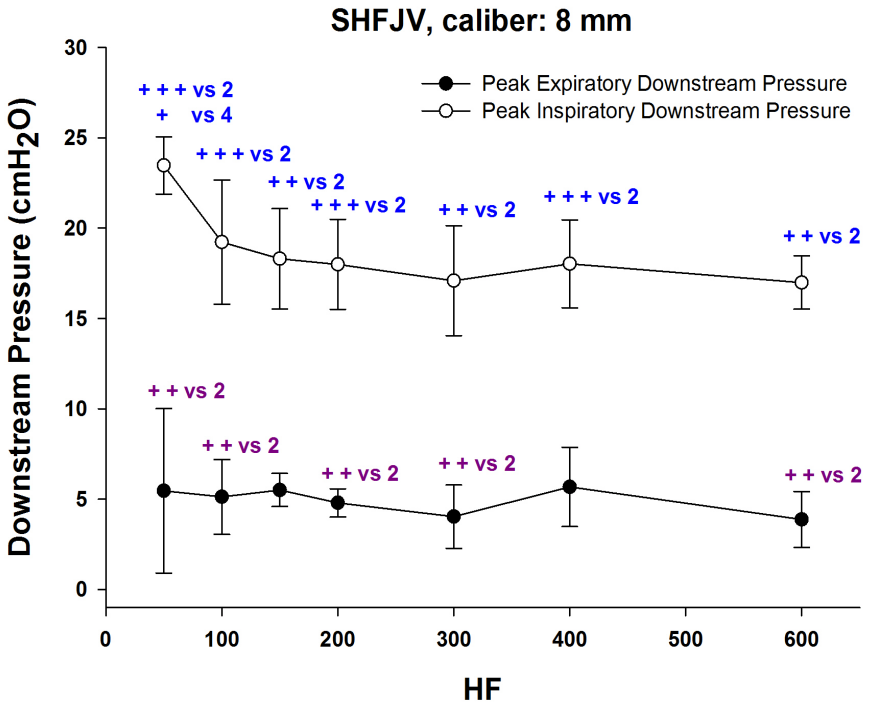

(b)

Figure 3.26: Downstream pressure with 6 mm (a) and 8 mm (b)tracheal caliber.

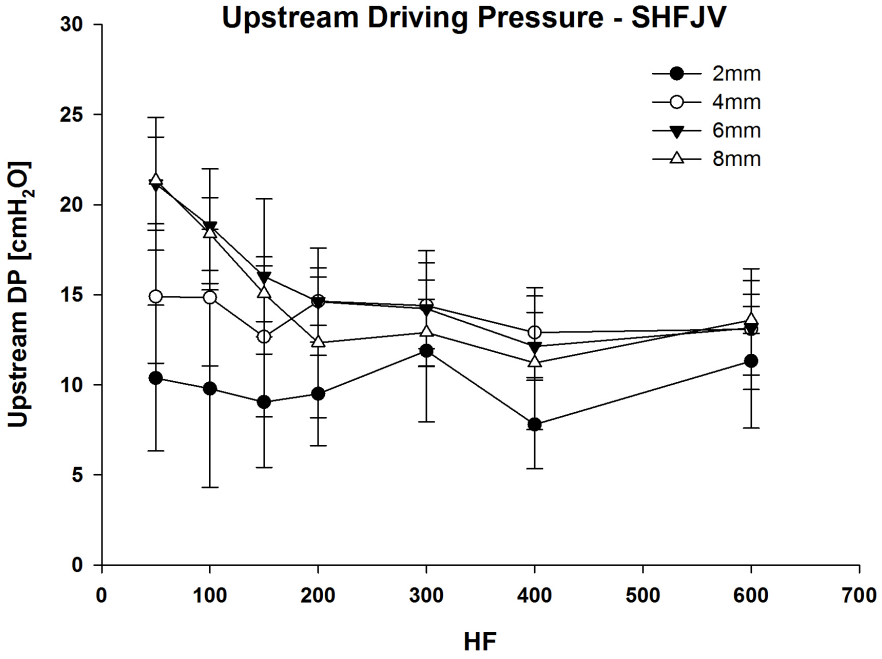

Figure 3.27: Upstream driving pressure vs HF, for each caliber. The curve related to the 2 mm caliber is almost frequency independent, whereas the others show a frequency dependence in the first tracts, then only the effects of LF breaths are evident and the frequency dependence ceases.

3.5.3 Discussion

3.5.3.1 Driving Pressure

These results confirm that the effects of the application of SHFJV can be considered as the superposition of the effect due to LFJV and HFJV both for upstream and downstream pressure. In fact, as for HFJV, the frequency dependence of the driving pressure in clearer at high calibers, such as 6 and 8 mm: at 2 mm, as well as at frequencies above 200 bpm for any other caliber, there is not any frequency dependence and the upstream driving pressure is ensured only by the low frequency component, being around 10 cmH_2O in the case of most severe stenosis and around 11-13 cmH_2O in the other cases; at lower frequencies (below 150 bpm) the LF-related driving pressure is enhanced by the driving pressure due to the HF breaths, even if the latter is caliber-dependent and has lower magnitude, since the jet ventilator was set in order to have $DP_{LF} = 1.6\ bar$ and $DP_{HF} = 0.8\ bar$. Driving pressure data are resumed in figure 3.27.

Downstream driving pressure has the same trends of the upstream DP, in fact both frequency dependence and superposition of the LF and HF effects are as evident as above the obstruction. An interesting finding is that with the 2 mm ID stent in place, the dowstream DP is significantly lower (below 6 cmH_2O) than in any other case (where

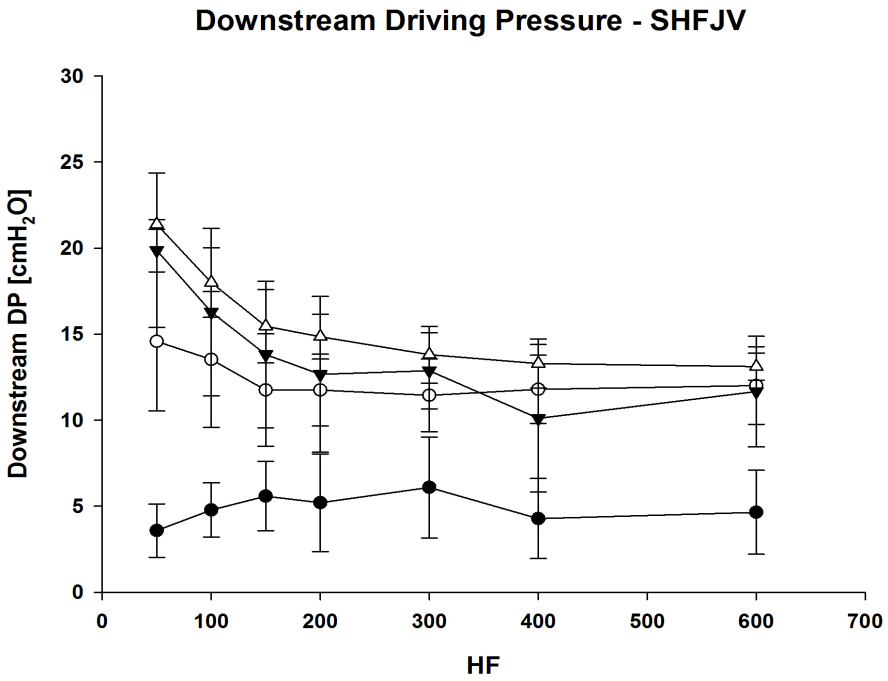

Figure 3.28: Downstream driving pressure vs HF, for each caliber. The curve related to the 2 mm caliber is almost frequency independent, whereas the others show a non-linear frequency dependence in the first tracts, then only the effects of LF are evident. However, even at HF, the 2 mm curve is separated from the others because of the uncoupling due to the severe obstruction. Please note that the distance between 2 mm curve is greater than any other, which are almost linearly distanced.

is always above 10 cmH_2O), meaning that neither the LF component is able to provide adequate ventilation in case of such a severe stenosis. Increasing the stent's ID, driving pressures improves and there are no significant differences between 4, 6 and 8 mm curves, being between 14.58 and 21.38 cmH_2O at 50 bpm and about 12 cmH_2O at 600 bpm: this is a further confirmation of the fact that the resistance's curve pattern influences any downstream variable (figure 3.28). The non-linear frequency dependence reflects the frequency response of a compliant system as the respiratory system.

As for HFJV, also in this case the results and the following conclusions about pressure completely match those about volumes and mechanical parameters, demonstrating the congruence between pressure and volume data even if the measurement systems were independent, and demonstrating that the presence of a tracheal obstruction affects all the downstream parameters, which are related each other as the equation of motion expresses.

3.5.3.2 Peak Expiratory Pressure

The peak expiratory downstream pressure is very similar among the pig with 4, 6 and 8 mm tracheal caliber, being around 5 cmH_2O, but it is significantly greater with the

most severe obstruction (2 mm caliber) reaching 10.28 cmH_2O. This confirms that with the most severe stenosis the obstruction increases dramatically the resistance and thus the physiological expiratory time constant, causing air trapping and PEEP effect even at the lowest ventilation rates employed in this study.

3.6 Blood gas analysis

Blood gas analysis has been performed during the protocol in order to evaluate the health condition of the pigs and to get information about the clinical efficacy of both SHFJV and HFJV.

With the 8 mm ID stent, SHFJV maintained P_{aO_2} above 29.4 (3.7) kPa at all frequencies, whereas with HFJV P_{aO_2} decreased progressively with increasing frequency leading to severe hypoxia (4.2 (0.8) kPa at 600 bpm). The highest P_{aCO_2} with SHFJV was 5.9 (0.9) kPa (at 600 bpm), and with HFJV 12.3 (2.1) kPa (at 600 bpm).

With decrease of stent ID both SHFJV and HFJV resulted in lower P_{aO_2} and higher P_{aCO_2} levels. At 2 mm ID, SHFJV kept P_{aO_2} above 15 (10) kPa at all frequencies. However, although HFJV at a frequency of 50 bpm gave an acceptable P_{aO_2} of 11.9 (12.3) kPa, P_{aO_2} decreased to 3.9 (1.3) kPa at frequencies above 150 bpm. P_{aCO_2} was about 12 kPa with SHFJV and about 15 kPa with HFJV for all frequencies.

The results are congruent to what expressed about volume and pressure, reporting good arterial oxygenation and adequate carbon dioxide washout only at calibers greater than 2 mm for both HFJV and SHFJV, and only frequencies below 150 bpm during HFJV.

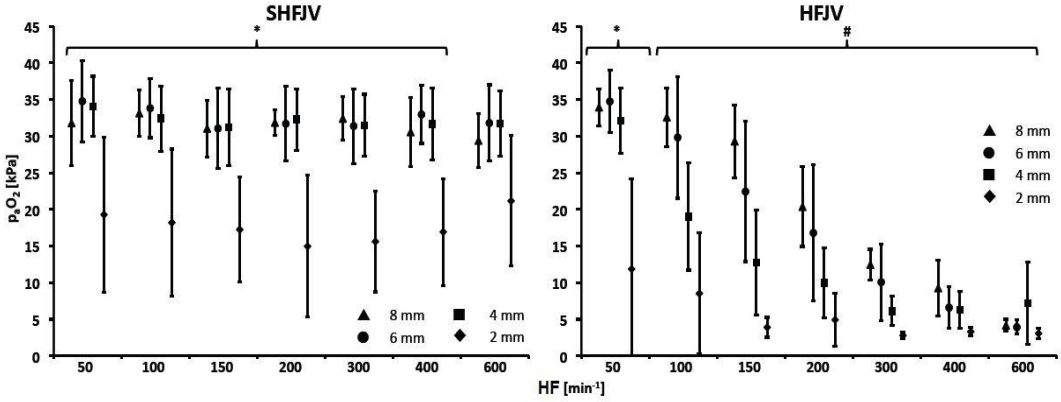

Figure 3.29: Mean (SD) of P_{aO_2} for SHFJV (left panel) and HFJV (right panel) for airway obstruction 2-8 mm ID. Asterisks indicate differences between the 2 mm obstruction compared with all other degrees of stenosis ($p<0.05$). Hash indicates significant differences of 2 mm obstruction compared with 6 and 8 mm ID ($p<0.05$).

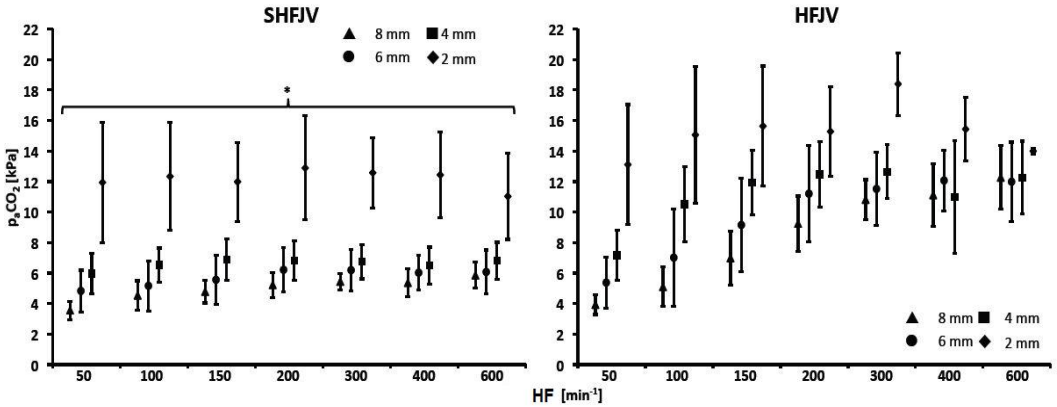

Figure 3.30: Mean (SD) of P_{aCO_2} for SHFJV (left panel) and HFJV (right panel) for airway obstruction 2-8 mm ID. Asterisks indicate differences between the 2 mm obstruction compared with all other degrees of stenosis ($p<0.05$).

3.7 Conclusions and Future Perspectives

The results presented in the previous chapter and their discussions lead to some indications about:

1. the effects of a tracheal stenosis on the mechanics of the respiratory system;
2. the interaction of an obstructed respiratory system with the jet ventilator during both HFJV and SHFJV;
3. the effects of the application of HFJV ad SHFJV in presence of tracheal stenosis;
4. the reliability of the OEP system in measuring volumes during jet ventilation.

The main results can be summarized as below:

- the compliance is unaffected by the obstruction grade, which influences only the resistance value;
- the resistance of the obstruction inserted in trachea correspond to the resistance of the whole respiratory system, meaning that its value is much higher than the normal resistance value.
- with the 2 mm ID stent the lower respiratory system can be considered uncoupled by the upper airways. Increasing the caliber from 4 mm up to 8 mm, the total resistance decreases linearly till being close to zero.
- the pattern of the *resistance vs caliber* curve reflects the trend of all downstream parameters (pressures and volumes) for both HFJV and SHFJV. This confirms

that the resistance affects directly the behaviour of the whole respiratory system acting on his physiological time constant τ.

- during HFJV, downstream driving pressures results are congruent with both resistance curve and tidal volume results, confirming that the adequate ventilation cannot be provided at frequencies greater than 150 bpm or with such a severe obstruction as the case of the 2 mm caliber.

- during both HFJV and SHFJV the total chest-wall tidal volume is mainly due to the abdominal compartment.

- during both HFJV and SHFJV with 2 mm ID stent, the EEV and PEP were greater then in any other case already at 50 bpm, indicating hyperinflation due to the fact that τ got longer than the expiration time.

- during SHFJV, a tidal volume of greater than 200 ml was ensured by the LF component for calibers of 4-6-8 mm even at the highest HF, and the direct relationship between tidal volume and caliber was enhanced for every superposed HF, reflecting the resistance curve's trend and meaning a caliber-dependence of the LF-related tidal volume. With the 2 mm ID the tidal volume was lower and frequency independent, confirming the uncoupling between airways and lower respiratory system.

- also for SHFJV, pressure's results are congruent with tidal volume and resistance curve's trend: adequate ventilation is not provided if the tracheal caliber is reduced to 2 mm and, for higher calibers, the direct relationship between driving pressure and caliber is much clearer than during HFJV for any HF.

- finally, the congruency between pressures, volumes, arterial P_{O_2} and P_{CO_2} confirms the reliability of the OEP system for measurements of respiratory volumes even during mechanical ventilation performed by jet ventilation.

Therefore, in conclusion the tracheal obstruction highly affected all downstream parameters and the expiration time constant. The most effective ventilation mode is SHFJV, providing always much greater tidal volume and driving pressure than HFJV, which is effective only up to 150 bpm at mild airway obstruction.

With SHFJV, both V_T and DP are caliber dependent, however there is no risk of hyperinflation or inadvertent PEEP in case of tracheal caliber reduced up to 4 mm. In case of extremely obstructed trachea, even SHFJV is not effective due to the complete uncoupling with the lower part of the respiratory system, and hyperinflation and inadvertent PEEP may occur.

It would be interesting to continue this study with future investigations about the applicability of HFJV and SHFJV on patients characterized by different obstructive pathologies, in order to verify if the results obtained on the animal model are confirmed also in humans.

Appendix A

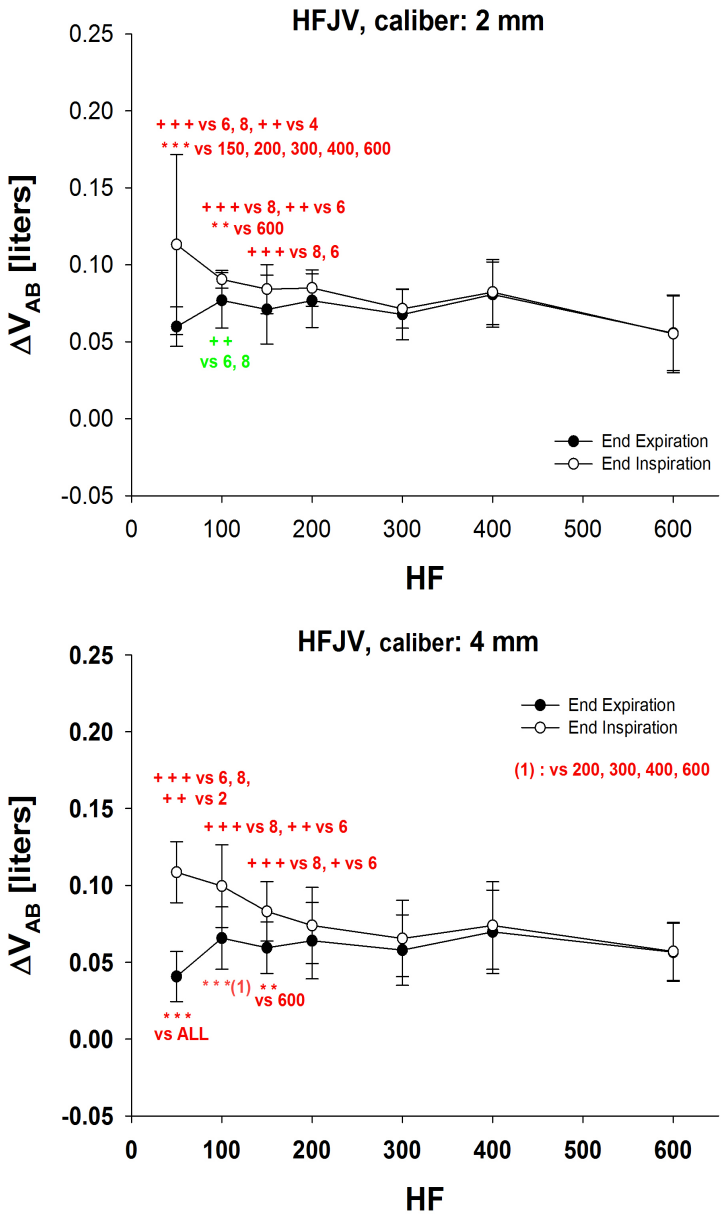

Figure 3.31: Vab with 2 mm (a) and 4 mm (b)tracheal caliber during HFJV.

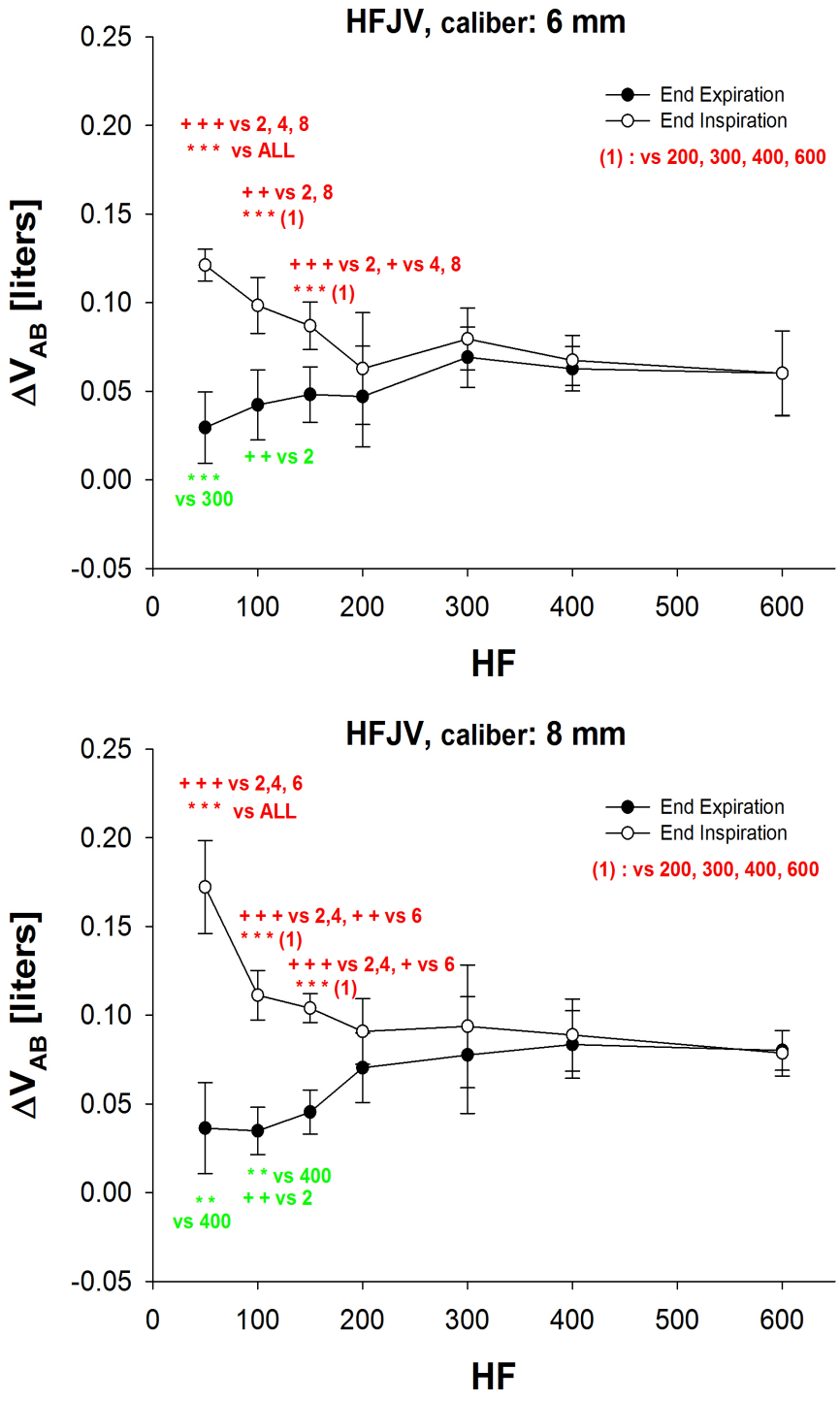

Figure 3.32: Vab with 6 mm (a) and 8 mm (b)tracheal caliber during HFJV.

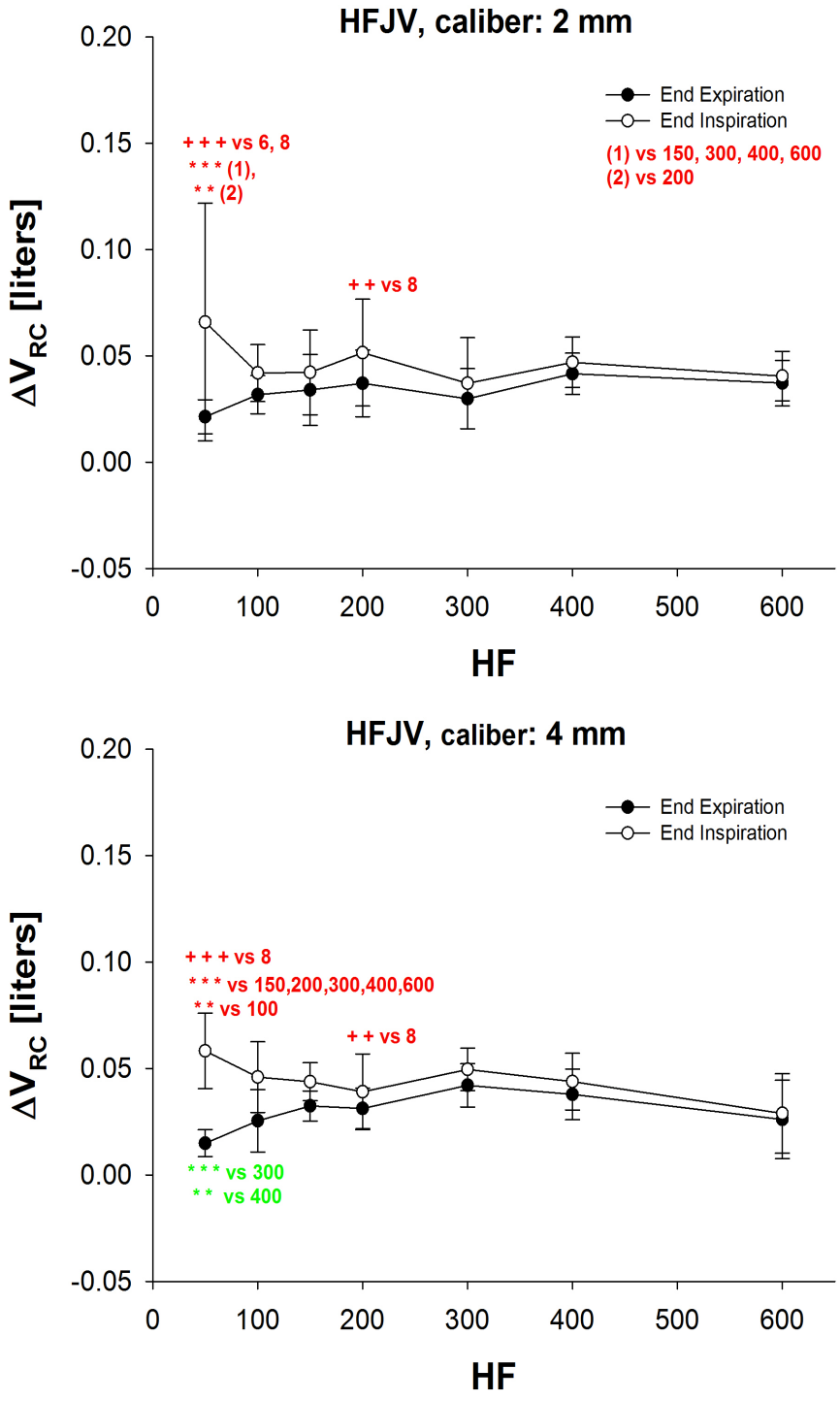

Figure 3.33: Vrc with 2 mm (a) and 4 mm (b)tracheal caliber during HFJV.

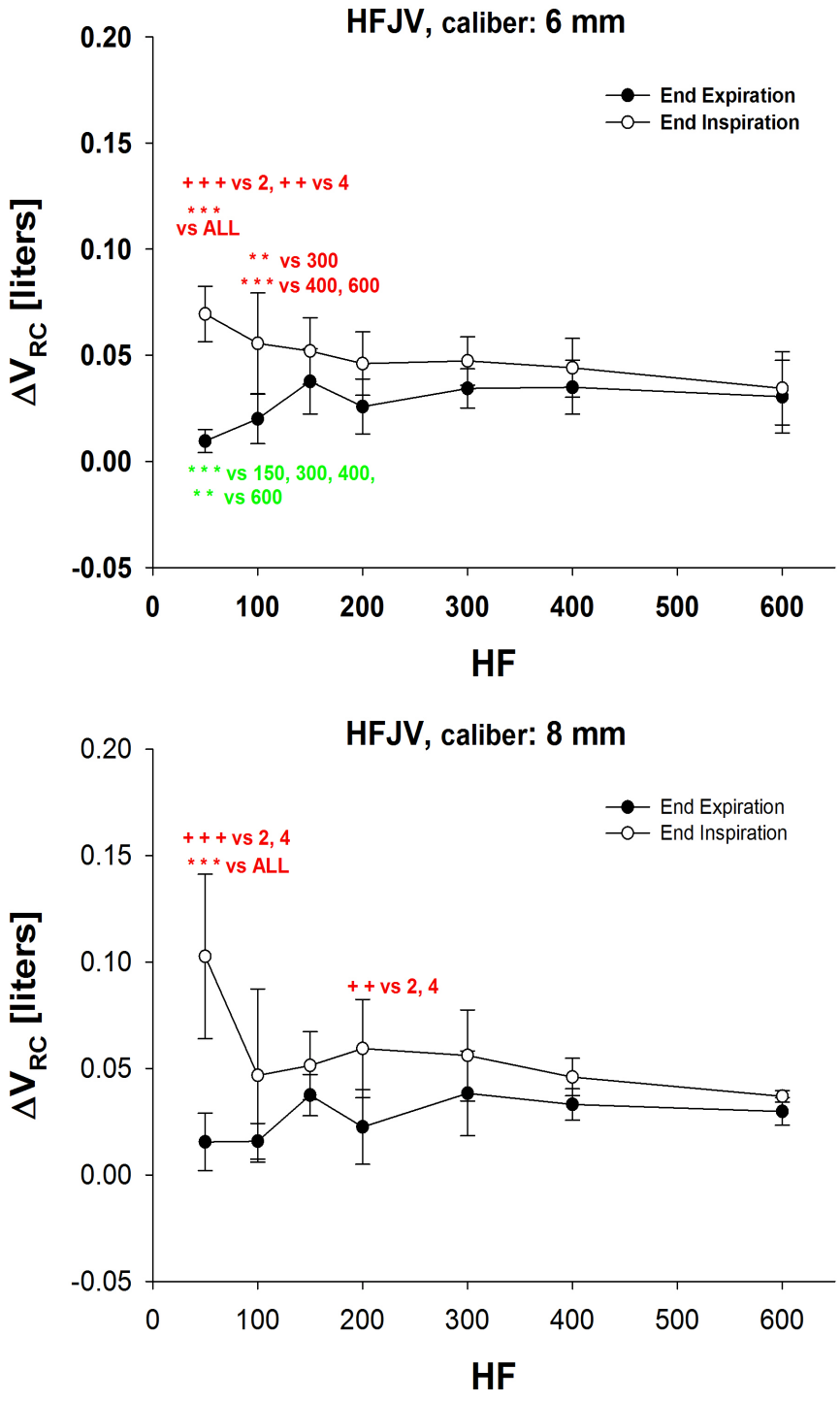

Figure 3.34: Vrc with 6 mm (a) and 8 mm (b)tracheal caliber during HFJV.

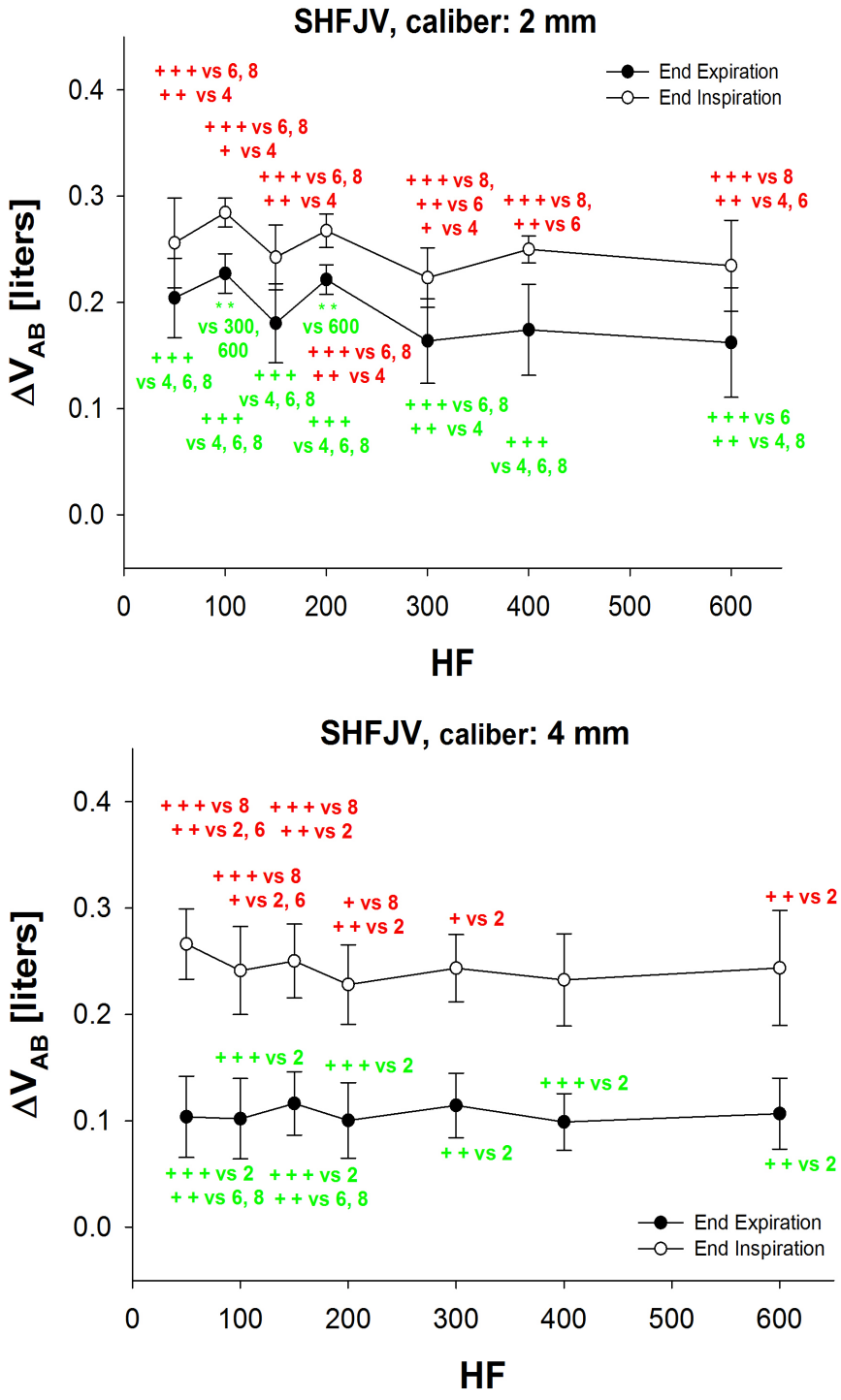

Figure 3.35: Vab with 2 mm (a) and 4 mm (b)tracheal caliber during SHFJV.

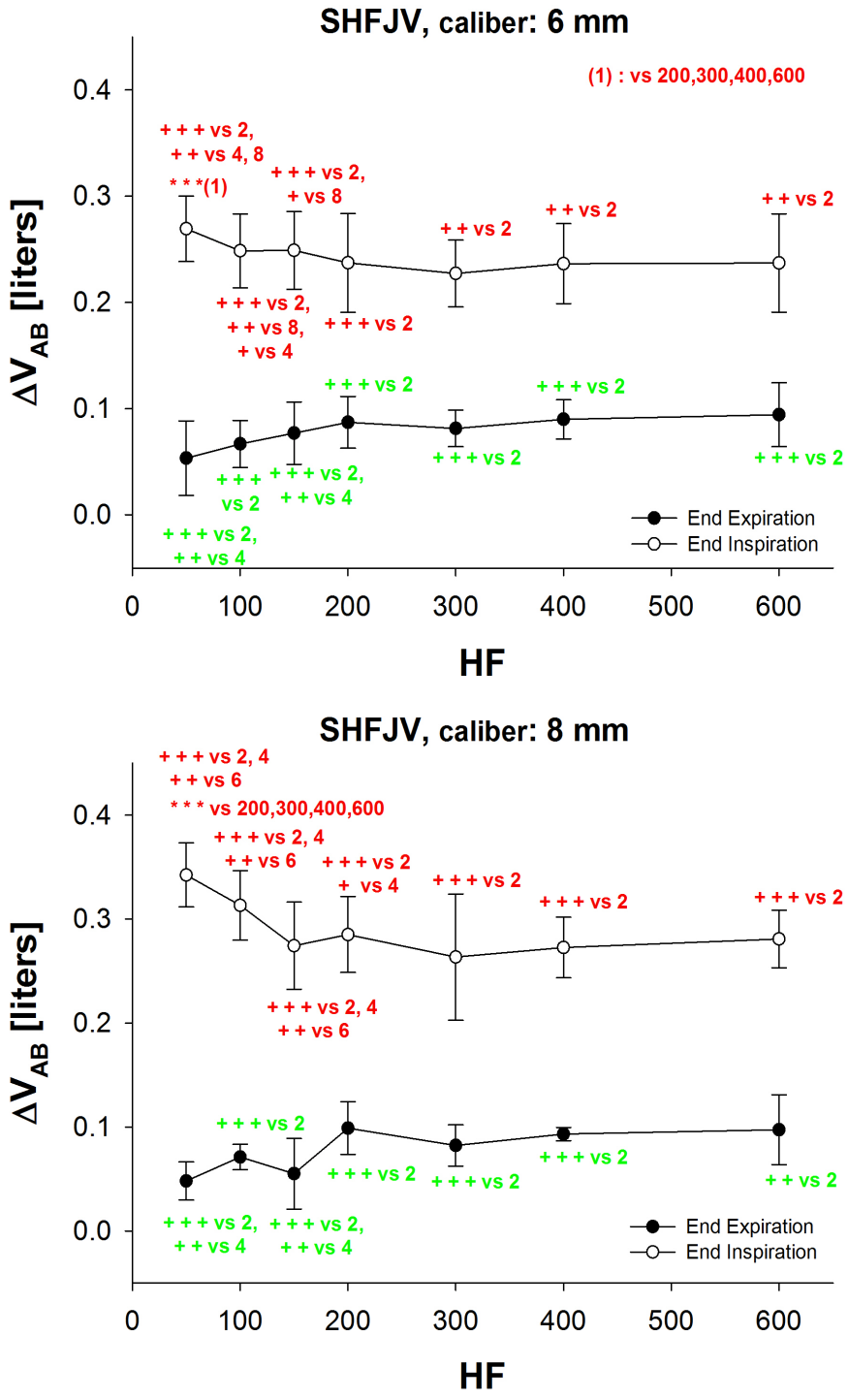

Figure 3.36: Vab with 6 mm (a) and 8 mm (b)tracheal caliber during SHFJV.

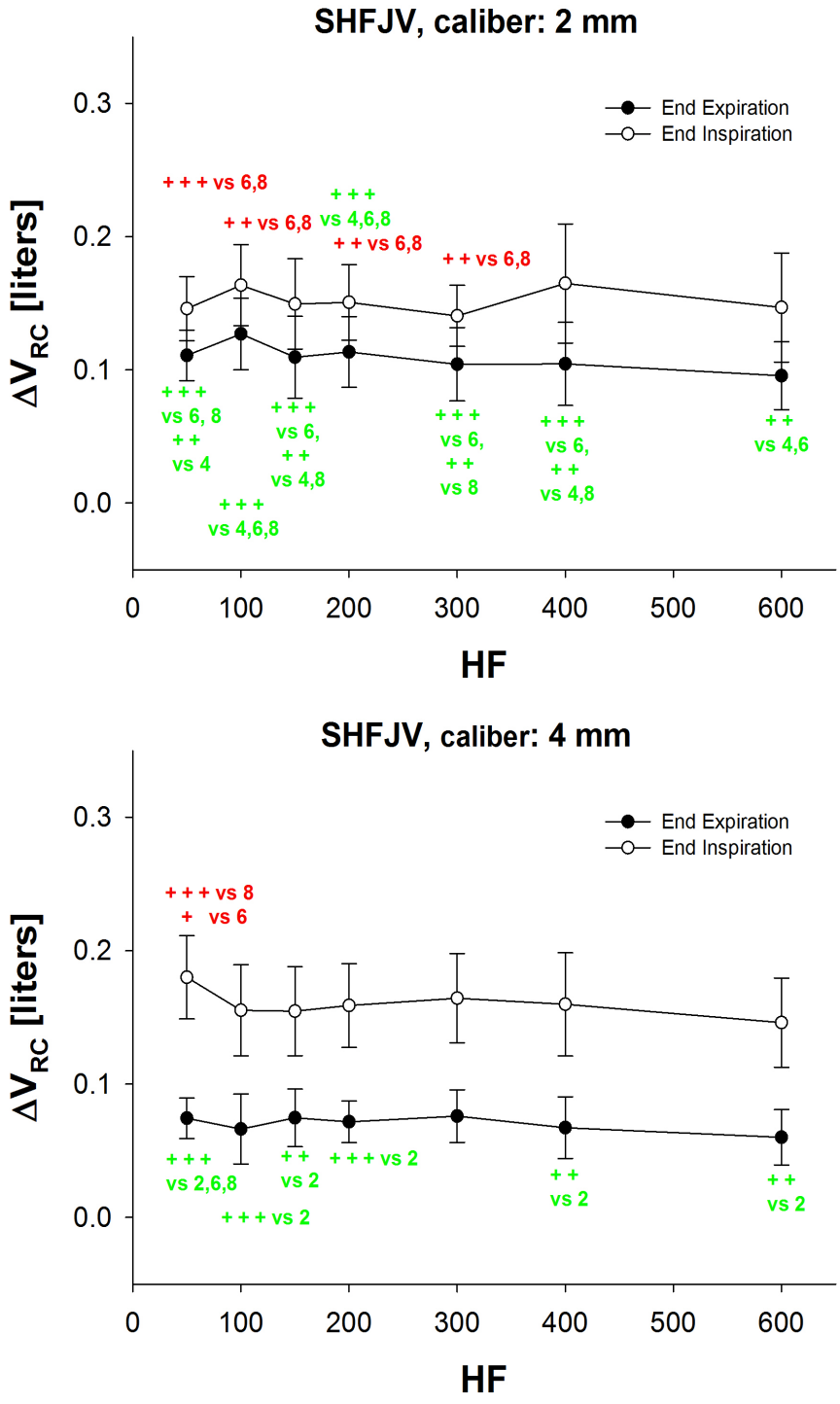

Figure 3.37: Vrc with 2 mm (a) and 4 mm (b)tracheal caliber during SHFJV.

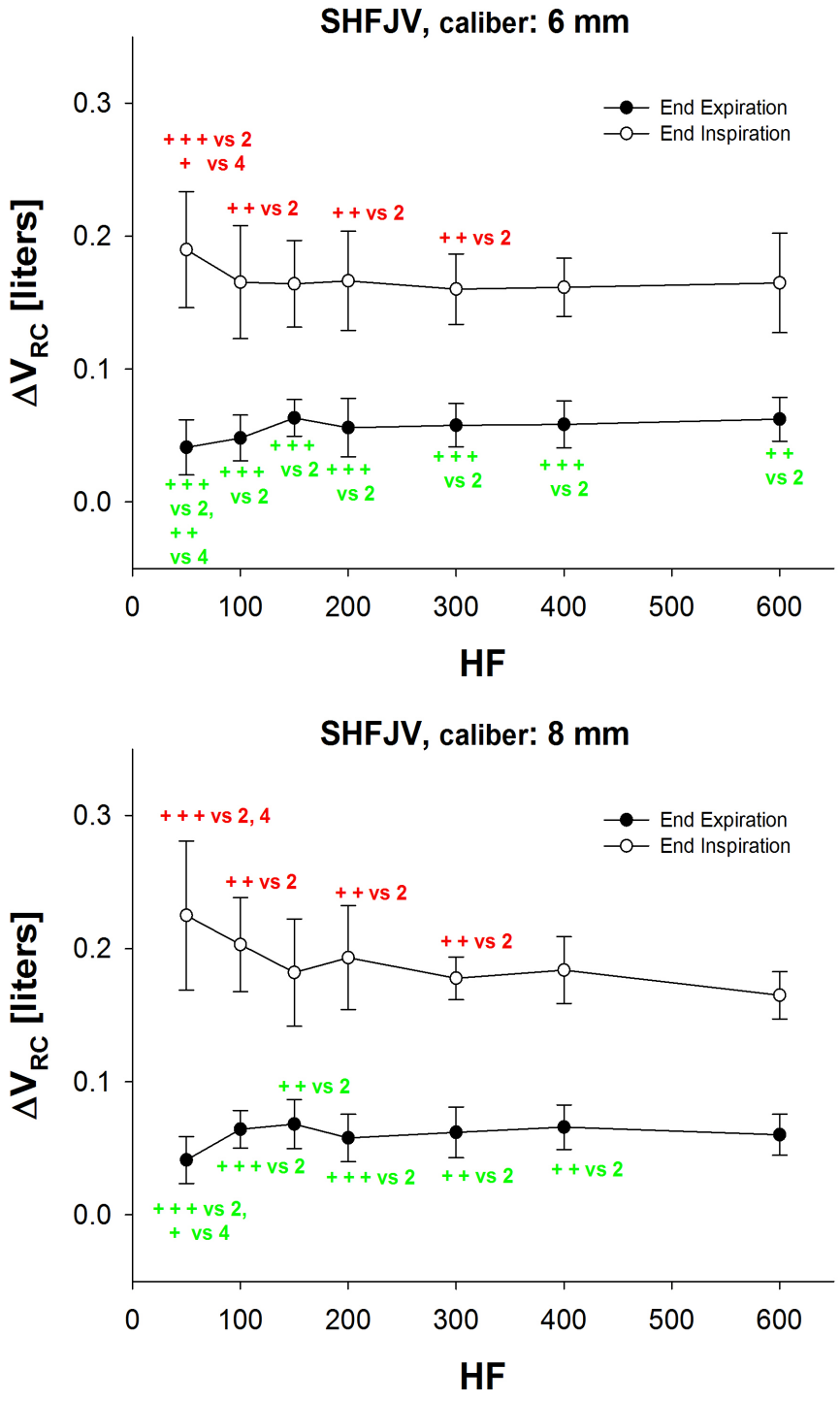

Figure 3.38: Vrc with 6 mm (a) and 8 mm (b)tracheal caliber during SHFJV.

Appendix B

In this appendix all numeric results are reported grouped by caliber and ventilation mode. For each parameter, the first column refers to the mean value over the population, and the second column refers to the standard deviation. Volumes are in Liters, Pressures in cmH_2O, P_{aO_2} and P_{aCO_2} in kPa.

HFJV - 2 mm

HF	ΔEEV_{RC}		ΔEEV_{AB}		ΔEEV_{CW}		ΔEIV_{RC}		ΔEIV_{AB}		ΔEIV_{CW}	
50	0.021	0.008	0.060	0.013	0.081	0.020	0.066	0.056	0.113	0.059	0.179	0.114
100	0.032	0.009	0.077	0.018	0.109	0.020	0.042	0.013	0.091	0.006	0.132	0.013
150	0.034	0.017	0.071	0.022	0.105	0.026	0.042	0.020	0.084	0.016	0.126	0.031
200	0.037	0.016	0.077	0.017	0.114	0.020	0.051	0.025	0.085	0.012	0.136	0.014
300	0.030	0.014	0.068	0.017	0.098	0.021	0.037	0.021	0.071	0.013	0.108	0.021
400	0.042	0.010	0.081	0.021	0.122	0.025	0.047	0.012	0.082	0.021	0.129	0.023
600	0.037	0.011	0.056	0.024	0.093	0.025	0.040	0.012	0.055	0.025	0.096	0.024

HF	VT_{RC}		VT_{AB}		VT_{CW}	
50	0.045	0.050	0.053	0.054	0.098	0.104
100	0.010	0.007	0.014	0.012	0.024	0.019
150	0.008	0.008	0.013	0.023	0.021	0.030
200	0.014	0.021	0.008	0.008	0.023	0.028
300	0.007	0.010	0.004	0.004	0.011	0.014
400	0.005	0.007	0.002	0.001	0.007	0.008
600	0.003	0.002	0.000	0.001	0.003	0.001

HF	PEI_{UP}		PEE_{UP}		DP_{UP}		PEI_{DOWN}		PEE_{DOWN}		DP_{DOWN}	
50.000	9.65	1.50	1.22	0.81	8.43	1.78	5.95	1.41	3.61	1.64	2.33	2.83
100.000	9.00	2.40	2.75	1.51	6.25	2.65	6.61	0.65	4.14	1.66	2.47	1.87
150.000	8.64	1.58	1.96	1.35	6.68	2.19	5.55	0.87	4.54	1.18	1.01	0.54
200.000	9.47	2.99	3.18	1.03	5.66	3.50	5.68	1.06	5.29	1.00	0.63	0.62
300.000	8.30	1.97	2.00	1.17	6.30	2.72	5.36	0.89	4.96	1.01	0.40	0.16
400.000	7.22	1.40	2.84	1.31	4.39	2.30	4.90	0.81	4.54	0.73	0.36	0.11
600.000	7.73	1.80	2.94	0.89	4.45	2.00	5.24	1.16	4.94	1.15	0.33	0.09

HF	P_{aO_2}		P_{aCO_2}	
50	11.86	12.31	13.11	3.93
100	8.52	8.30	15.06	4.50
150	3.90	1.35	15.63	3.94
200	4.91	3.62	15.28	2.96
300	2.79	0.49	18.40	2.05
400	3.29	0.56	15.43	2.08
600	3.06	0.72	14.00	0.18

HFJV - 4 mm

HF	ΔEEV_{RC}		ΔEEV_{AB}		ΔEEV_{CW}		ΔEIV_{RC}		ΔEIV_{AB}		ΔEIV_{CW}	
50	0.015	0.006	0.041	0.016	0.053	0.017	0.058	0.018	0.109	0.020	0.167	0.022
100	0.025	0.015	0.066	0.020	0.091	0.025	0.046	0.017	0.100	0.027	0.146	0.031
150	0.032	0.007	0.060	0.017	0.092	0.017	0.044	0.009	0.083	0.019	0.127	0.020
200	0.031	0.010	0.064	0.025	0.091	0.038	0.039	0.018	0.074	0.025	0.113	0.039
300	0.042	0.010	0.058	0.023	0.100	0.023	0.050	0.010	0.066	0.025	0.115	0.024
400	0.038	0.012	0.070	0.027	0.108	0.033	0.044	0.013	0.074	0.029	0.118	0.034
600	0.026	0.018	0.057	0.019	0.083	0.021	0.029	0.019	0.057	0.019	0.086	0.020

HF	VT_{RC}		VT_{AB}		VT_{CW}	
50	0.043	0.016	0.068	0.015	0.114	0.027
100	0.021	0.007	0.034	0.011	0.054	0.015
150	0.012	0.006	0.024	0.007	0.035	0.010
200	0.008	0.006	0.010	0.003	0.022	0.007
300	0.008	0.003	0.008	0.004	0.015	0.005
400	0.006	0.003	0.004	0.002	0.010	0.003
600	0.003	0.001	0.000	0.001	0.003	0.001

HF	PEI_{UP}		PEE_{UP}		DP_{UP}		PEI_{DOWN}		PEE_{DOWN}		DP_{DOWN}	
50	9.94	1.34	1.78	1.01	8.27	2.01	8.97	1.71	2.66	1.02	6.34	2.91
100	7.43	1.31	2.37	1.30	5.07	0.90	6.76	1.52	3.29	1.31	3.47	2.03
150	7.44	1.21	3.21	1.08	4.63	1.47	6.21	1.31	3.84	1.00	2.37	1.18
200	7.34	1.80	2.23	1.40	5.54	1.90	5.32	1.56	3.58	0.85	1.96	1.46
300	7.19	1.64	3.31	1.29	3.88	2.14	5.92	1.15	4.50	0.80	1.42	0.67
400	6.80	1.33	4.15	1.23	2.65	1.13	5.45	0.83	4.54	0.81	0.91	0.47
600	6.84	1.41	3.70	1.19	3.14	1.29	5.27	1.31	4.79	1.18	0.48	0.37

HF	P_{aO_2}		P_{aCO_2}	
50	32.12	4.44	7.17	1.62
100	19.01	7.30	10.51	2.44
150	10.56	2.94	12.37	1.77
200	9.95	4.79	12.47	2.15
300	6.11	2.00	12.64	1.77
400	6.27	2.55	10.99	3.68
600	7.17	5.64	12.26	2.39

HFJV - 6 mm

HF	ΔEEV_{RC}		ΔEEV_{AB}		ΔEEV_{CW}		ΔEIV_{RC}		ΔEIV_{AB}		ΔEIV_{CW}	
50	0.010	0.005	0.030	0.020	0.039	0.023	0.069	0.013	0.121	0.009	0.191	0.013
100	0.020	0.012	0.042	0.020	0.062	0.024	0.056	0.024	0.098	0.016	0.154	0.027
150	0.038	0.015	0.048	0.016	0.086	0.028	0.052	0.016	0.087	0.013	0.139	0.027
200	0.026	0.013	0.047	0.028	0.073	0.034	0.046	0.015	0.063	0.032	0.109	0.033
300	0.034	0.009	0.069	0.017	0.104	0.013	0.047	0.011	0.080	0.017	0.127	0.008
400	0.035	0.013	0.063	0.013	0.098	0.021	0.044	0.014	0.067	0.014	0.112	0.023
600	0.031	0.017	0.060	0.024	0.091	0.034	0.034	0.017	0.060	0.024	0.095	0.033

HF	VT_{RC}		VT_{AB}		VT_{CW}	
50	0.060	0.026	0.092	0.020	0.152	0.003
100	0.036	0.015	0.056	0.013	0.092	0.002
150	0.014	0.010	0.039	0.011	0.053	0.002
200	0.020	0.010	0.016	0.006	0.036	0.002
300	0.013	0.007	0.010	0.003	0.023	0.002
400	0.009	0.004	0.005	0.004	0.014	0.002
600	0.004	0.001	0.000	0.001	0.004	0.002

HF	PEI_{UP}		PEE_{UP}		DP_{UP}		PEI_{DOWN}		PEE_{DOWN}		DP_{DOWN}	
50	11.00	1.79	1.11	0.78	9.82	1.94	9.35	2.54	1.86	1.49	7.31	3.76
100	8.24	1.58	2.36	1.30	6.22	1.91	7.33	1.58	3.51	1.34	4.26	2.51
150	7.36	1.36	2.94	1.26	4.39	1.41	6.65	1.03	3.05	1.44	3.61	1.60
200	7.48	1.60	3.06	1.91	4.41	2.11	6.19	1.30	3.80	1.40	2.40	1.88
300	6.56	1.61	3.31	1.57	3.25	2.42	5.87	1.02	4.18	1.16	1.68	0.86
400	6.28	1.70	4.30	1.12	1.98	1.13	5.00	1.61	4.06	1.39	0.94	0.57
600	6.28	1.49	3.71	1.13	2.57	1.41	5.01	1.09	4.21	0.88	0.80	0.60

HF	P_{aO_2}		P_{aCO_2}	
50	34.74	4.26	5.37	1.66
100	29.83	8.30	7.01	3.18
150	22.43	9.56	9.15	3.08
200	16.79	9.32	11.20	3.17
300	10.07	5.22	11.52	2.39
400	6.58	2.86	12.07	1.98
600	3.91	0.97	11.99	2.60

HFJV - 8 mm

HF	ΔEEV_{RC}		ΔEEV_{AB}		ΔEEV_{CW}		ΔEIV_{RC}		ΔEIV_{AB}		ΔEIV_{CW}	
50	0.015	0.014	0.036	0.026	0.052	0.039	0.103	0.039	0.172	0.026	0.275	0.065
100	0.016	0.008	0.035	0.013	0.037	0.014	0.047	0.041	0.111	0.014	0.158	0.029
150	0.038	0.010	0.045	0.012	0.083	0.011	0.051	0.016	0.104	0.008	0.155	0.014
200	0.023	0.018	0.070	0.020	0.093	0.028	0.059	0.023	0.091	0.019	0.150	0.024
300	0.038	0.020	0.078	0.033	0.116	0.026	0.056	0.021	0.094	0.035	0.150	0.021
400	0.033	0.007	0.084	0.019	0.117	0.016	0.046	0.009	0.089	0.020	0.135	0.015
600	0.030	0.006	0.080	0.011	0.111	0.017	0.037	0.003	0.079	0.013	0.121	0.008

HF	VT_{RC}		VT_{AB}		VT_{CW}	
50	0.087	0.027	0.136	0.004	0.223	0.029
100	0.031	0.018	0.077	0.004	0.121	0.018
150	0.014	0.007	0.059	0.006	0.072	0.012
200	0.037	0.012	0.020	0.004	0.057	0.012
300	0.018	0.007	0.016	0.004	0.034	0.006
400	0.013	0.004	0.005	0.002	0.018	0.003
600	0.007	0.004	-0.002	0.002	0.011	0.009

HF	PEI_{UP}		PEE_{UP}		DP_{UP}		PEI_{DOWN}		PEE_{DOWN}		DP_{DOWN}	
50	11.743	0.998	1.125	0.267	11.082	0.320	12.196	0.494	0.883	0.029	11.314	0.523
100	7.611	1.582	3.220	0.811	4.421	3.047	8.075	1.024	2.657	0.345	5.790	1.470
150	7.245	0.734	4.345	0.654	3.158	0.835	6.561	1.243	3.701	0.583	4.367	1.548
200	6.811	1.498	4.191	0.282	2.908	1.952	6.039	1.358	4.658	1.203	1.494	1.811
300	5.993	1.011	5.222	0.639	1.184	0.136	5.731	0.990	4.763	0.221	1.291	0.711
400	5.713	1.213	4.983	1.382	0.730	0.170	5.423	0.819	4.712	1.314	0.711	0.593
600	5.101	1.764	4.353	1.787	0.748	0.022	5.557	2.237	5.020	2.719	0.537	0.482

HF	P_{aO_2}		P_{aCO_2}	
50	33.94	2.52	3.93	0.65
100	32.58	3.97	5.10	1.29
150	29.29	4.98	6.98	1.79
200	20.37	5.44	9.24	1.80
300	12.45	2.11	10.82	1.31
400	9.25	3.79	11.11	2.04
600	4.17	0.83	12.27	2.08

SHFJV - 2 mm

HF	ΔEEV_{RC}		ΔEEV_{AB}		ΔEEV_{CW}		ΔEIV_{RC}		ΔEIV_{AB}		ΔEIV_{CW}	
50.000	0.111	0.019	0.204	0.037	0.315	0.042	0.146	0.024	0.256	0.042	0.402	0.045
100.000	0.127	0.027	0.227	0.019	0.354	0.037	0.164	0.031	0.285	0.014	0.448	0.036
150.000	0.109	0.031	0.180	0.037	0.290	0.057	0.150	0.034	0.242	0.031	0.392	0.050
200.000	0.114	0.027	0.222	0.014	0.342	0.027	0.151	0.028	0.268	0.016	0.435	0.047
300.000	0.104	0.028	0.164	0.040	0.268	0.066	0.141	0.023	0.223	0.028	0.364	0.047
400.000	0.105	0.031	0.174	0.043	0.279	0.067	0.165	0.045	0.250	0.013	0.415	0.041
600.000	0.096	0.026	0.162	0.052	0.258	0.064	0.147	0.041	0.235	0.043	0.381	0.050

HF	VT_{RC}		VT_{AB}		VT_{CW}	
50.000	0.035	0.012	0.052	0.019	0.087	0.028
100.000	0.037	0.014	0.057	0.015	0.094	0.028
150.000	0.040	0.007	0.062	0.013	0.102	0.016
200.000	0.030	0.009	0.049	0.011	0.079	0.019
300.000	0.036	0.009	0.060	0.020	0.096	0.028
400.000	0.060	0.052	0.076	0.040	0.136	0.090
600.000	0.051	0.031	0.072	0.021	0.124	0.049

HF	PEI_{UP}		PEE_{UP}		DP_{UP}		PEI_{DOWN}		PEE_{DOWN}		DP_{DOWN}	
50.0	16.19	2.66	5.83	2.94	10.37	4.05	13.86	1.77	10.28	1.66	3.58	1.54
100.0	16.99	3.07	7.02	3.16	9.79	5.48	14.72	1.91	9.45	1.95	4.78	1.58
150.0	15.87	2.23	6.83	3.81	9.04	3.62	14.34	1.60	8.75	2.27	5.59	2.01
200.0	15.41	3.78	5.27	1.48	9.49	2.88	14.20	1.90	8.57	2.68	5.20	2.83
300.0	16.08	2.68	4.20	2.24	11.88	3.94	14.01	1.15	7.92	3.14	6.09	2.94
400.0	14.51	2.30	6.72	1.48	7.79	2.45	12.80	2.02	8.52	1.65	4.28	2.32
600.0	16.13	2.61	4.92	1.29	11.31	3.71	12.90	1.63	7.82	1.90	4.65	2.45

HF	P_{aO_2}		P_{aCO_2}	
50	19.28	10.57	11.95	3.94
100	18.19	10.05	12.33	3.54
150	17.23	7.15	11.98	2.59
200	14.97	9.69	12.89	3.41
300	15.59	6.85	12.58	2.30
400	16.92	7.30	12.44	2.82
600	21.16	8.91	11.03	2.82

SHFJV - 4 mm

HF	ΔEEV_{RC}		ΔEEV_{AB}		ΔEEV_{CW}		ΔEIV_{RC}		ΔEIV_{AB}		ΔEIV_{CW}	
50	0.074	0.015	0.104	0.038	0.178	0.046	0.180	0.031	0.266	0.033	0.446	0.039
100	0.066	0.026	0.102	0.038	0.168	0.059	0.155	0.034	0.241	0.041	0.397	0.058
150	0.075	0.022	0.116	0.030	0.191	0.043	0.155	0.033	0.250	0.035	0.405	0.051
200	0.072	0.016	0.100	0.036	0.172	0.039	0.159	0.032	0.228	0.037	0.387	0.028
300	0.076	0.020	0.115	0.030	0.191	0.045	0.164	0.033	0.244	0.032	0.408	0.046
400	0.067	0.023	0.099	0.027	0.166	0.042	0.160	0.039	0.233	0.043	0.392	0.063
600	0.060	0.021	0.107	0.033	0.167	0.040	0.146	0.033	0.244	0.054	0.390	0.055

HF	VT_{RC}		VT_{AB}		VT_{CW}	
50	0.106	0.032	0.163	0.030	0.268	0.054
100	0.089	0.021	0.139	0.032	0.228	0.047
150	0.080	0.021	0.134	0.026	0.214	0.041
200	0.087	0.025	0.128	0.018	0.215	0.032
300	0.088	0.024	0.129	0.017	0.217	0.032
400	0.093	0.023	0.134	0.021	0.226	0.034
600	0.086	0.019	0.137	0.030	0.223	0.036

HF	PEI_{UP}		PEE_{UP}		DP_{UP}		PEI_{DOWN}		PEE_{DOWN}		DP_{DOWN}	
50	18.987	3.579	4.098	1.534	14.888	3.688	19.299	3.129	4.720	2.113	14.579	4.039
100	18.658	3.657	3.821	2.017	14.837	3.795	18.659	3.309	5.136	1.858	13.523	3.944
150	17.580	3.316	4.916	2.392	12.664	4.439	17.407	2.766	5.656	1.862	11.751	3.264
200	18.232	1.885	3.877	1.920	14.639	1.336	17.252	2.315	5.504	1.749	11.749	2.087
300	17.943	2.579	3.554	1.496	14.389	2.385	17.272	2.248	5.825	1.725	11.447	2.107
400	17.537	2.592	4.634	1.746	12.903	2.499	17.237	2.249	5.445	1.462	11.792	1.978
600	17.377	2.831	4.710	1.858	13.088	3.352	17.123	2.533	5.418	1.406	12.015	2.260

HF	P_{aO_2}		P_{aCO_2}	
50	34.05	4.13	5.97	1.31
100	32.41	4.45	6.52	1.12
150	31.22	5.24	6.87	1.35
200	32.29	4.20	6.82	1.29
300	31.48	4.25	6.74	1.12
400	31.69	4.92	6.49	1.22
600	31.71	4.45	6.81	1.21

SHFJV - 6 mm

HF	ΔEEV_{RC}		ΔEEV_{AB}		ΔEEV_{CW}		ΔEIV_{RC}		ΔEIV_{AB}		ΔEIV_{CW}	
50	0.041	0.021	0.053	0.035	0.094	0.055	0.190	0.044	0.269	0.031	0.459	0.060
100	0.048	0.017	0.067	0.022	0.115	0.032	0.165	0.043	0.249	0.035	0.414	0.064
150	0.063	0.014	0.077	0.029	0.140	0.039	0.164	0.033	0.249	0.037	0.413	0.063
200	0.056	0.022	0.087	0.024	0.143	0.032	0.166	0.037	0.237	0.047	0.404	0.058
300	0.058	0.016	0.081	0.017	0.139	0.028	0.160	0.027	0.227	0.031	0.387	0.044
400	0.058	0.018	0.090	0.018	0.148	0.033	0.162	0.022	0.236	0.038	0.398	0.047
600	0.062	0.017	0.094	0.030	0.157	0.031	0.165	0.038	0.237	0.046	0.402	0.068

HF	VT_{RC}		VT_{AB}		VT_{CW}	
50	0.149	0.051	0.216	0.042	0.365	0.085
100	0.117	0.037	0.182	0.037	0.299	0.067
150	0.101	0.031	0.172	0.032	0.273	0.060
200	0.111	0.029	0.150	0.035	0.261	0.055
300	0.102	0.028	0.146	0.028	0.248	0.047
400	0.103	0.023	0.147	0.030	0.250	0.042
600	0.103	0.027	0.143	0.024	0.245	0.045

HF	PEI_{UP}		PEE_{UP}		DP_{UP}		PEI_{DOWN}		PEE_{DOWN}		DP_{DOWN}	
50	23.16	2.86	2.01	1.94	21.15	3.69	21.43	4.43	2.48	2.07	19.87	4.49
100	21.29	2.35	2.49	1.93	18.80	3.17	19.24	4.22	3.70	2.11	16.29	4.87
150	19.49	3.02	3.48	2.03	16.01	4.31	18.51	3.17	4.70	2.21	13.81	4.26
200	18.60	3.12	3.99	2.30	14.61	2.97	17.67	3.29	5.01	2.58	12.66	4.52
300	18.22	3.04	3.99	1.98	14.22	3.22	17.50	2.81	4.63	1.53	12.88	2.22
400	17.38	2.27	5.25	1.93	12.13	1.88	16.02	3.72	5.91	1.68	10.11	4.28
600	17.57	2.40	4.41	1.24	13.16	2.62	16.68	2.67	5.02	1.91	11.67	3.21

HF	P_{aO_2}		P_{aCO_2}	
50	34.77	5.53	4.83	1.36
100	33.81	4.02	5.16	1.64
150	31.06	5.50	5.56	1.59
200	31.69	5.09	6.21	1.45
300	31.38	5.12	6.19	1.35
400	32.96	3.94	6.02	1.15
600	31.79	5.22	6.07	1.44

SHFJV - 8 mm

HF	ΔEEV_{RC}		ΔEEV_{AB}		ΔEEV_{CW}		ΔEIV_{RC}		ΔEIV_{AB}		ΔEIV_{CW}	
50	0.041	0.018	0.048	0.018	0.089	0.030	0.225	0.056	0.342	0.031	0.567	0.055
100	0.064	0.014	0.071	0.012	0.135	0.023	0.203	0.035	0.313	0.033	0.516	0.010
150	0.068	0.018	0.055	0.034	0.123	0.037	0.182	0.040	0.274	0.042	0.456	0.014
200	0.058	0.018	0.099	0.026	0.157	0.039	0.193	0.039	0.285	0.037	0.478	0.042
300	0.062	0.019	0.082	0.020	0.144	0.025	0.178	0.016	0.264	0.061	0.441	0.048
400	0.066	0.017	0.093	0.006	0.159	0.023	0.184	0.025	0.273	0.029	0.457	0.015
600	0.060	0.015	0.097	0.034	0.158	0.049	0.165	0.018	0.281	0.028	0.446	0.045

HF	VT_{RC}		VT_{AB}		VT_{CW}	
50	0.184	0.040	0.294	0.035	0.478	0.045
100	0.139	0.028	0.242	0.035	0.381	0.031
150	0.114	0.029	0.219	0.021	0.333	0.024
200	0.136	0.026	0.186	0.026	0.322	0.023
300	0.116	0.009	0.181	0.047	0.297	0.046
400	0.118	0.022	0.179	0.034	0.298	0.030
600	0.105	0.002	0.183	0.008	0.288	0.007

HF	PEI_{UP}		PEE_{UP}		DP_{UP}		PEI_{DOWN}		PEE_{DOWN}		DP_{DOWN}	
50	23.551	2.192	2.944	0.401	21.343	2.407	23.468	1.586	5.462	4.548	21.380	0.286
100	21.226	2.107	3.838	1.303	18.372	2.016	19.223	3.438	5.127	2.067	17.998	2.024
150	19.574	1.665	5.172	0.882	15.057	1.545	18.306	2.779	5.508	0.912	15.455	2.134
200	17.203	4.771	4.851	1.868	12.330	4.154	17.995	2.490	4.794	0.780	14.848	1.302
300	17.941	2.088	5.645	0.998	12.896	1.850	17.093	3.037	4.032	1.755	13.803	1.645
400	16.979	3.152	5.764	1.582	11.215	3.708	18.026	2.431	5.678	2.193	13.292	1.426
600	18.139	2.132	4.541	2.078	13.598	0.748	16.987	1.476	3.878	1.549	13.109	0.787

HF	P_{aO_2}		P_{aCO_2}	
50	31.78	5.82	3.56	0.60
100	33.13	3.14	4.53	0.96
150	31.03	3.85	4.78	0.74
200	31.85	1.78	5.23	0.82
300	32.41	2.96	5.44	0.54
400	30.57	4.67	5.37	0.92
600	29.38	3.66	5.86	0.85

Bibliography

[1] A.C Guyton, J.E. Hall. *Fisiologia Medica*. Edises. 2007

[2] A. Aliverti. Slides of *Bioingegneria del Sistema Respiratorio*. TBMlab, Department of Bioengineering, Politecnico di Milano.

[3] D.R. Johnson. *Introductory Anatomy: Respiratory System*. Faculty of Biological System, University of Leeds.

[4] J.G. Webster. *Medical Instrumentation, Application and Design*. Chapter 9. Hoepli. 2009

[5] J.H.T. Bates. *Lung Mechanics. An inverse modeling approach*. Cambridge University Press. 2009

[6] A. Aliverti. Notes of *Bioingegneria del Sistema Respiratorio*. TBMlab, Department of Bioengineering, Politecnico di Milano.

[7] Priori R. *Chest wall mechanics during jet ventilation in pig and humans*. Department of Bioengineering, Politecnico di Milano. 2010.

[8] R.S. Harris. *Pressure Volume Curves of the Respiratory System*. Respiratory Care, 50(1): 78-99. 2005.

[9] P. Navalesi, S.M. Maggiore. *Positive End-Expiratory Pressure*. In Martin J. Tobin, Principles and Practice of Mechanical Ventilation, volume 1, chapter 11. McGraw-Hill. 2006

[10] C.S.H. Sassoon. *Intermittent Mandatory Ventilation*. In Martin J. Tobin, Principles and Practice of Mechanical Ventilation, volume 1, chapter 8. McGraw-Hill. 2006

[11] R.L. Chatburn. *Classification of ventilator modes: update and proposal for implementation*. Respiratory Care, Vol . 52 No. 3: 301-323, 2007.

[12] R.L. Chatburn. *Fundamentals of mechanical ventilation.* Chapter 1. Mandu Press, 2003

[13] R.L. Chatburn. *Fundamentals of mechanical ventilation.* Chapter 2. Mandu Press, 2003

[14] G.F. Franklin, J.D. Powell, A. Emami Naeini. *Feedback control of dynamic systems.* Prentice Hall, 2002

[15] A. Dourado. Slides of *Algoritmos de diagnostico e de Auto-Regulação.* Faculty of Sciences and Technology, University of Coimbra, Portugal.

[16] R.L Chatburn. *Computer Control of mechanical Ventilation.* Respiratory Care, volume49, (5):507–515. 2004

[17] J. Henriques. Slides of *Computação Neuronal e Sistemas Difusos.* Faculty of Sciences and Technology, University of Coimbra, Portugal.

[18] J. Schaublin, M. Derighetti, P. Feigenwinter, S. Petersen-Felix, A.M. Zbinden. *Fuzzy logic control of mechanical ventilation during anaesthesia.* British journal of anaesthesia, (77): 636-641. 1996

[19] M. Amato, J.Marini. *Pressure-Controlled and Inverse-Ratio Ventilation.* In Martin J. Tobin, Principles and Practice of Mechanical Ventilation, volume 1, chapter 10. McGraw-Hill. 2006

[20] J. Mancebo. *Assist Control Ventilation.* In Martin J. Tobin, Principles and Practice of Mechanical Ventilation, volume 1, chapter 7. McGraw-Hill. 2006

[21] A. Esteban, A. Anzueto, I. Alia, F. Gordo, C. Apezteguia, F. Palizas, D. Cide, R. Goldsawer, L. Soto, G. Bugedo, C. Rodrigo, J. Pimentel, G. Raimondi, M. J. Tobin. *How is mechanical Ventilation employed in intensive care unit?* American Journal of respiratory and critical care medicine. Vol.161. 2000

[22] L. Brochard, F. Lellouche. *Pressure-Support Ventilation.* In Martin J. Tobin, Principles and Practice of Mechanical Ventilation, volume 1, chapter 9. McGraw-Hill. 2006

[23] E. Mireles-Cabodevila, E. Diaz-Guzman, G. Heresi, R.L. Chatburn. *Alternative modes of mechanical ventilation: a review for the hospitalists.* Cleveland Clinic Journal of Medicine, Volume 76, (7): 417-430. 2009

[24] C.F. Sulzer, R. Chiolero, P.G. Chassot, X.M. Mueller, J.P. Revelly. *Adaptive Support Ventilation for fast extubation after cardiac surgery.* Anesthesiology, Volume 95, (6):1339-1345. 2001

[25] N. Ambrosino, A. Rossi. *Proportional assist ventilation (PAV): a significant advance or a futile struggle between logic and practice?* Thorax, (57): 272-276. 2002

[26] A.B. Froese. *High Frequency Ventilation.* In Martin J. Tobin, Principles and Practice of Mechanical Ventilation, volume 1, chapter 20. McGraw-Hill. 2006

[27] M.K. Sykes. *High Frequency Ventilation.* Thorax, Volume 40:161-165. 1985

[28] R.B. Smith, U.H. Sjostrand, M.F. Babinski. *Technical Considerations Using High Frequency Positive Pressure Ventilation and High Frequency Jet Ventilation.*International anesthesiology clinics 21(3): 183-200.1983

[29] J.C. Bouchut, J. Godard, O. Claris. *High-frequency Oscillatory Ventilation.* Anesthesiology, (100):1007–1012. 2004

[30] R.B. Smith, M. Klain. *Experimental High Frequency Jet Ventilation.* International anesthesiology clinics. 21(3): 33-47. 1983

[31] G.C. Carlon, W.S. Howland. *Clinical Experience with High Frequency Jet Ventilation.*International anesthesiology clinics 21(3): 99-120. 1983

[32] P. Kraincuk, A. Kepka, G. Ihra, C. Schabernig, A. Aloy. *A new prototype of an electronic jet-ventilator and its humidification system.* Critical Care, (3): 101–110. 1999

[33] G. Ihra, A. Aloy. *On the use of Venturi's principle to describe entrainment during Jet Ventilation.* Journal of Clinic Anaesthesiology. (12): 417-419. 2000

[34] J.J. Rouby, G. Simonneau, D. Benhamou, R. Sartene, F. Sardnal, H. Deriaz, P. Doroux, P. Viars. *Factors Influencing Pulmonary Volumes and $C0_2$ elimination during High Frequency Jet Ventilation.* Anesthesiology, 63: 473-482. 1985

[35] M.K. Skyes. *Gas exchange during high frequency jet ventilation.* Acta Anaesthesiologica Scandinavica. (90): 32-33. 1989

[36] J.J. Rouby, J. Fusciardi, J.L. Bourgain, P. Viars. *High-Frequency Jet Ventilation in postoperative respiratory failure: Determinants of oxygenation.* Anesthesiology (59): 281-287. 1983

[37] J. R. Johnston, D. L. Coppel, J. J. Wilson, B.F. McLaughlin, P. J. Hildebrand. *High Frequency Jet Ventilation.* Anaesthesia, Volume 39:163-166. 1984

[38] R.B. Smith, M.F. Babinski. *Clinical High Frequency Jet Ventilation.* International anesthesiology clinics 21(3): 89-97. 1983

[39] G. C. Carlon, W. S. Howland, C. Ray, S. Miodownik, J. P. Griffin, J. S. Groeger. *High Frequency Jet Ventilation. A prospective randomized evaluation.* Chest 84:551-559. 1983

[40] A. Aloy, M. Schachner, W. Cancura. *Tubeless translaryngeal superimposed jet ventilation.* European Archives Otorhinolaryngology, 248:475-478. 1991

[41] A. Bacher, K. Pichler, A. Aloy. *Supraglottic combined frequency jet ventilation versus subglottic monofrequent jet ventilation in patients udergoing microlaryngeal surgery.* Anesthesia Analgesia 90:460-465. 2000

[42] E. Lanzenberger-Schragl, A. Donner, M.C. Grasl, M. Zimpfer, A. Aloy. *Superimposed high frequency jet ventilation for laryngeal and tracheal surgery.* Archives Otolaryngology Head Neck Surgery. 126:40-44. 2000

[43] A. Bacher, T. Lang, J. Weber, A. Aloy. *Respiratory Efficacy of Subglottic Low-Frequency, Subglottic Combined-Frequency, and Supraglottic Combined-Frequency Jet Ventilation During Microlaryngeal Surgery.* Anesthesia Analgesia 91:1506–1512. 2000

[44] A. Rezaie-Majd, W. Bigenzhan, D.M. Denk, M. Burian, J. Kornfehl, M. C. Grasl, G. Ihra, A. Aloy. *Superimposed high-frequency jet ventilation (SHFJV) for endoscopic laryngotracheal surgery in more than 1500 patients.* British Journal Anaesthesia 96: 650–659. 2006

[45] A. Aliverti, A. Pedotti. *Opto-electonic Plethysmography.* Mechanics of Breathing, chapter 5.

[46] G.C. Carlon, C.Jr Ray, J. Griffin, S. Midownik. *Tidal volume and airway pressure on high frequency jet ventilation.* Critical care medicine, 11 (2): 83 - 86. 1983

[47] G. Ferrigno, P.Carnevali, A. Aliverti, F. Molteni, G. Beulcke, A. Pedotti. *Three-Dimensional optical analysis of the chest wall motion.* 1994

[48] G. Santambrogio. Notes of *Tecnologie per la Virtualizzazione Motoria.* Department of Bioengineering, Politecnico di Milano.

[49] A. Aliverti, R. Dellacà, P. Pelosi, D. Chiumello, L. Gattinoni, A. Pedotti. *Compartmental analysis of breathing in the supine and prone positions by optoelectronic plethysmography.* Annals of Biomedical Engineering. 29:60-70. 2001

[50] R. Leiter, A. Aliverti, R. Priori, P. Staun, A. Lo Mauro, A. Larsson, P. Frykholm. *Comparison of superimposed high-frequency jet ventilation with conventional jet ventilation for laryngeal surgery.* British Journal of Anaesthesia 108 (4): 690–7. 2012

[51] C. Guerin, F. Bayle, S. Debord, J.C. Poupelin, M. Badet, S. Lemasson, J. C. Richard. *Viscoelastic properties of lung and thoracic wall of anesthetized mechanically ventilated piglets.* Veterinary Anaesthesia and Analgesia (34): 331-338. 2007